2011-09

Investigation of transitional flows on compressor blades in cascade

Holihan, Michael L.

Monterey, California. Naval Postgraduate School

NAVAL POSTGRADUATE SCHOOL

MONTEREY, CALIFORNIA

THESIS

INVESTIGATION OF TRANSITIONAL FLOWS ON COMPRESSOR BLADES IN CASCADE

by

Michael L. Holihan

September 2011

Thesis Advisor:	Garth V. Hobson
Second Reader:	Anthony J. Gannon

Approved for public release; distribution is unlimited

THIS PAGE INTENTIONALLY LEFT BLANK

REPORT DOCUMENTATION PAGE			Form Approved OMB No. 0704–0188
Public reporting burden for this collection of information is estimated to average 1 hour per response, including the time for reviewing instruction, searching existing data sources, gathering and maintaining the data needed, and completing and reviewing the collection of information. Send comments regarding this burden estimate or any other aspect of this collection of information, including suggestions for reducing this burden, to Washington headquarters Services, Directorate for Information Operations and Reports, 1215 Jefferson Davis Highway, Suite 1204, Arlington, VA 22202–4302, and to the Office of Management and Budget, Paperwork Reduction Project (0704–0188) Washington DC 20503.			
1. AGENCY USE ONLY *(Leave blank)*	**2. REPORT DATE** September 2011	**3. REPORT TYPE AND DATES COVERED** Master's Thesis	
4. TITLE AND SUBTITLE Investigation of Transitional Flows on Compressor Blades in Cascade		**5. FUNDING NUMBERS**	
6. AUTHOR(S) Michael L. Holihan			
7. PERFORMING ORGANIZATION NAME(S) AND ADDRESS(ES) Naval Postgraduate School Monterey, CA 93943–5000		**8. PERFORMING ORGANIZATION REPORT NUMBER**	
9. SPONSORING /MONITORING AGENCY NAME(S) AND ADDRESS(ES) N/A		**10. SPONSORING/MONITORING AGENCY REPORT NUMBER**	
11. SUPPLEMENTARY NOTES The views expressed in this thesis are those of the author and do not reflect the official policy or position of the Department of Defense or the U.S. Government. IRB Protocol number N.A.			
12a. DISTRIBUTION / AVAILABILITY STATEMENT Approved for public release; distribution is unlimited		**12b. DISTRIBUTION CODE** A	

13. ABSTRACT (maximum 200 words)

Flow around polished second-generation controlled-diffusion blades in cascade set at their design inlet flow angle was investigated at various Reynolds numbers using static pressure measurements, five-hole probe surveys, two-component laser Doppler velocimetry (LDV), computational fluid dynamics and flow visualization. A suction-side separation bubble formed at Reynolds number, based on chord length, of 203,000 and collapsed by a Reynolds number of 393,000. Five-hole probe surveys characterized the blade-row inlet and outlet flow and showed the loss coefficient had a maximum value of 0.030 at a Reynolds number of 203,000 and a minimum of 0.012 at a Reynolds number of 400,000. The suction-side separation bubble was completely documented with LDV. The boundary layer was found to undergo laminar separation at 55 percent axial chord, transitioned in the boundary layer and re-attached turbulent by 67 percent axial chord. A quasi three-dimensional, Reynolds-Averaged Navier-Stokes, computational fluid dynamics model was created and accurately predicted the suction-side separation bubble and boundary layer transition inside the bubble. Flow visualization verified the transitional behavior of the separation bubble and showed the separation point was steady while the reattachment point was turbulent.

14. SUBJECT TERMS Controlled-Diffusion, Cascade, Compressor, Separation, Laser Doppler Velocimetry, Computational Fluid Dynamics			**15. NUMBER OF PAGES** 111
			16. PRICE CODE
17. SECURITY CLASSIFICATION OF REPORT Unclassified	**18. SECURITY CLASSIFICATION OF THIS PAGE** Unclassified	**19. SECURITY CLASSIFICATION OF ABSTRACT** Unclassified	**20. LIMITATION OF ABSTRACT** UU

NSN 7540–01–280–5500

Standard Form 298 (Rev. 2–89)
Prescribed by ANSI Std. 239–18

THIS PAGE INTENTIONALLY LEFT BLANK

Approved for public release; distribution is unlimited

INVESTIGATION OF TRANSITIONAL FLOWS ON COMPRESSOR BLADES IN CASCADE

Michael L. Holihan
Lieutenant, United States Navy
B.S., North Carolina State University, 2003

Submitted in partial fulfillment of the
requirements for the degree of

MASTER OF SCIENCE IN MECHANICAL ENGINEERING

from the

NAVAL POSTGRADUATE SCHOOL
September 2011

Author: Michael L. Holihan

Approved by: Dr. Garth V. Hobson
Thesis Advisor

Dr. Anthony J. Gannon
Second Reader

Dr. Knox T. Millsaps
Chair, Department of Mechanical and Aerospace Engineering

THIS PAGE INTENTIONALLY LEFT BLANK

ABSTRACT

Flow around polished second-generation controlled-diffusion blades in cascade set at their design inlet flow angle was investigated at various Reynolds numbers using static pressure measurements, five-hole probe surveys, two-component laser Doppler velocimetry (LDV), computational fluid dynamics and flow visualization. A suction-side separation bubble formed at Reynolds number, based on chord length, of 203,000 and collapsed by a Reynolds number of 393,000. Five-hole probe surveys characterized the blade-row inlet and outlet flow and showed the loss coefficient had a maximum value of 0.030 at a Reynolds number of 203,000 and a minimum of 0.012 at a Reynolds number of 400,000. The suction-side separation bubble was completely documented with LDV. The boundary layer was found to undergo laminar separation at 55 percent axial chord, transitioned in the boundary layer and re-attached turbulent by 67 percent axial chord. A quasi three-dimensional, Reynolds-Averaged Navier-Stokes, computational fluid dynamics model was created and accurately predicted the suction-side separation bubble and boundary layer transition inside the bubble. Flow visualization verified the transitional behavior of the separation bubble and showed the separation point was steady while the reattachment point was turbulent.

THIS PAGE INTENTIONALLY LEFT BLANK

TABLE OF CONTENTS

LIST OF FIGURES

LIST OF TABLES

THIS PAGE INTENTIONALLY LEFT BLANK

LIST OF SYMBOLS

β	Non-dimensional stagnation pressure ratio
β_1	Test section inlet flow angle
β_2	Test section outlet flow angle
$\beta_{5\text{-Hole}}$	Setting angle of 5-hole probe with respect to vertical
C	Blade chord
C_{ac}	Axial chord location
$C_{ps,ds}$	Downstream coefficient of static pressure
$C_{ps,us}$	Upstream coefficient of static pressure
$C_{pt,ds}$	Downstream coefficient of total pressure
$C_{pt,us}$	Upstream coefficient of total pressure
$\frac{d}{C}$	Perpendicular distance from blade surface with respect to blade chord
K_{ds}	5-hole probe downstream reference flow function
K_{us}	5-hole probe upstream reference flow function
δ	Non-dimensional pitch pressure ratio
δ_{bl}	Limit of integration denoting the edge of the boundary layer
δ^*	Displacement thickness
γ	Non-Dimensional yaw pressure ratio
θ	Momentum thickness
φ	Pitchwise difference between inlet flow angle and 5-hole probe setting
H	Shape factor
P_{bar}	Barometric pressure
P_{loc}	Local pressure as read from fully instrumented blade static pressure ports
P_{stag}	Stagnation pressure as read from upstream Prandtl probe
P_{stat}	Static pressure as read from upstream Prandtl probe
Re	Reynolds number based on chord length
Ti	Turbulence intensity
T_0	Stagnation temperature
Tu	Horizontal turbulence intensity
Tv	Axial turbulence intensity
u	Horizontal velocity component
v	Axial velocity component
W	Magnitude of total velocity vector
ω	Loss coefficient
X	Non-dimensional velocity
x	Axial length along the blade chord, or axial distance through the cascade
V_{ref}	Reference velocity
y	Pitchwise distance across the cascade

THIS PAGE INTENTIONALLY LEFT BLANK

ACKNOWLEDGMENT

I would like to thank Dr. Garth V. Hobson and Dr. Anthony Gannon for their enthusiasm and guidance throughout this process. The atmosphere they have cultivated at the NPS Turbopropulsion Laboratory has made this a worthwhile academic experience, which I will always remember fondly. I would also like to thank the Turbopropulsion laboratory engineering technician, John Gibson, whose technical competence and trouble shooting ability saved me countless hours. Finally, and most importantly, I want to thank my beautiful wife, Natalie. Thank you for your patience and understanding over these last few months.

THIS PAGE INTENTIONALLY LEFT BLANK

I. INTRODUCTION

A. BACKGROUND

The current trend in turbofan design for the propulsion of subsonic aircraft is to slow the fan down substantially using gearbox drives. This has been shown to significantly reduce overall fuel consumption especially during takeoff and climb. As a result of slowing down the fan rotor the Reynolds number (Re), based on chord length, of the blades are reduced to levels, which may delay the transition of the boundary layer to turbulent flow. High altitude, low speed flight will also reduce the Re of the flow due to density effects [1]. The predominantly laminar flow over the airfoils will decrease the stagnation pressure losses, but may reduce stall margin as a result of the likelihood of a laminar boundary layer to separate more easily than one that is turbulent.

The Turbopropulsion Laboratory within the Department of Mechanical and Aerospace Engineering at the Naval Postgraduate School (NPS) has a unique Low Speed Cascade Wind Tunnel (LSCWT) for the testing of fan-compressor and turbine blades. For a theoretical discussion on Cascade Aerodynamics see Gostelow [2]. The LSCWT is configured with ten second-generation Controlled-Diffusion (CD) compressor blades for flow field measurements. See Hansen [3] for a description on the evolution of the CD blade from the NACA-65 to those used in the current study, the 67B. Additionally, the 67B blades within the LSCWT have recently been polished to a roughness value, Ra, of 0.38 μm, making them ideal candidates for the study of transitional flow over airfoil sections.

Numerous studies have been conducted at the NPS LSCWT on the same blade design that this study was performed on. Hansen [3] installed the 67B midspan blade sections in the LSCWT, characterized the boundary layers and losses at a design incidence of 36.3° and a Re = 640,000 using static pressure, five-hole probe and Laser Doppler Velocimetry (LDV) measurements. Hansen concluded that despite the 67B CD design, boundary layer separation still occurred at design conditions. Schnorenberg [4]

conducted static pressure, LDV and flow visualization experiments at an off-design inlet flow angle of 38 degrees and also studied the effect Re variation had on flow separation. Nicholls [5] studied the flow characteristics over and around the test section using multiple techniques after installation of the currently installed blower motor and found a moderate increase in free-stream turbulence due to the new motor. Carlson [6] investigated the three-dimensionality of the test-section flow caused by end-wall flow interactions. Caruso [7] conducted off design upstream and downstream three-component LDV surveys and confirmed the existence of secondary vortices produced by end-wall flows. Fitzgerald [8] studied the flow around the blades at stall for various Re. Urban [9] conducted detailed pitch-wise and span-wise pressure surveys upstream and downstream of the test section and calculated the total pressure loss distribution across the blades. Brown [10] investigated downstream vortex shedding at various inlet flow angles and Re and determined vortex shedding was a leading edge phenomenon and that the shedding frequency depended on Re. Choon [11] used static pressure measurements, two-component LDV and hotwire anemometry to study vortex shedding at various off-design inlet flow angles and Re.

B. PURPOSE

The purpose of this study was to refurbish the cascade Inlet Guide Vanes (IGVs), install 67B test section blades that had been polished to a roughness value of less than 0.38 μm, and to instrument and automate the data acquisition system in the cascade with more accurate Digital Sensor Arrays (DSAs) for pressure measurements. Measurements were done at the design inlet flow angle (IFA) of 36 degrees and at Reynolds numbers spanning the transitional range of flow. Detailed flow field measurements have been performed at various Reynolds numbers to characterize the flow field through the polished blade row. Specifically, blade surface pressure measurements were conducted at Re spanning the transitional range of flow. Five-hole probe measurements were performed ahead of and downstream of the blade row to determine the Axial Velocity Density Ratio (AVDR) and stagnation pressure losses through the cascade. LDV was performed on the blades at a Re of 203,000 to fully document the transitional suction-side

boundary layer. A quasi three-dimensional Reynolds Averaged Navier-Stokes (RANS) Computational Fluid Dynamics (CFD) analysis of the 67B CD compressor blade was performed and validated with the LDV data. Flow visualization was performed on the suction side of the blade to study the separation bubble. With recently polished blades it was an ideal opportunity to create a CFD model and validate it with experimental data acquired in the study.

THIS PAGE INTENTIONALLY LEFT BLANK

II. TEST FACILITY AND INSTRUMENTATION

A. LOW-SPEED CASCADE WIND TUNNEL

The NPS LSCWT is a variable-speed, open-loop wind tunnel capable of testing flows up to Mach 0.4 and Re based on chord length of up to $1x10^6$. The flow path and main components of the LSCWT are shown in Figure 1. The facility is unique in that it is capable of testing flows at Re that span the range of conditions a typical compressor will experience in operation by varying the blower motor's intake mass flow. A schematic of the test section is shown in Figure 2.

B. TEST SECTION

The test blade geometry, locations and installation were thoroughly documented by Hansen [3]. The blade stagger angle and inlet-sidewall angle were both adjusted to the design inlet-flow angle of 36.3 ± 0.1 degrees using a digital inclinometer with an accuracy of ± 0.1 degrees. The cascade test section characteristics are listed in Table 1. To attain uniform inlet-flow the tunnel was brought to Re = 640K (See Section III.A for Re calculations) and the IGVs were adjusted until all upstream static-pressure water-manometer readings agreed to within 124 Pa (0.5 inches of water) (Figure 3). To attain a uniform exit-flow angle, the tailboard sections were adjusted until the downstream static-pressure water-manometer readings agreed to within 0.5 inches of water. Therefore, the tunnel was set for the design conditions of the test blades. See Figure 2 for the sidewall angle settings of the LSCWT. Prior to this study, all IGV trailing edges were machined down to a uniform thickness, re-pinned as needed, re-shimmed for clearance and their shafts were greased and covered with Teflon tape to prevent binding. A new pressure data acquisition system (Figure 4) was installed and the test blades were polished to a roughness value of less than 0.38 μm.

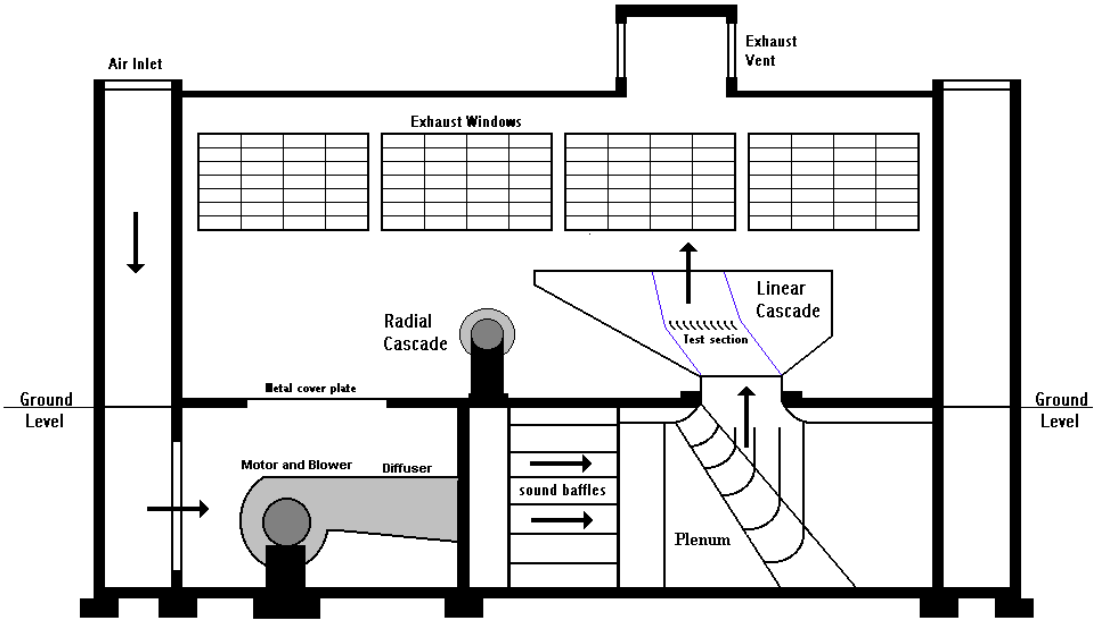

Figure 1. LSCWT building layout

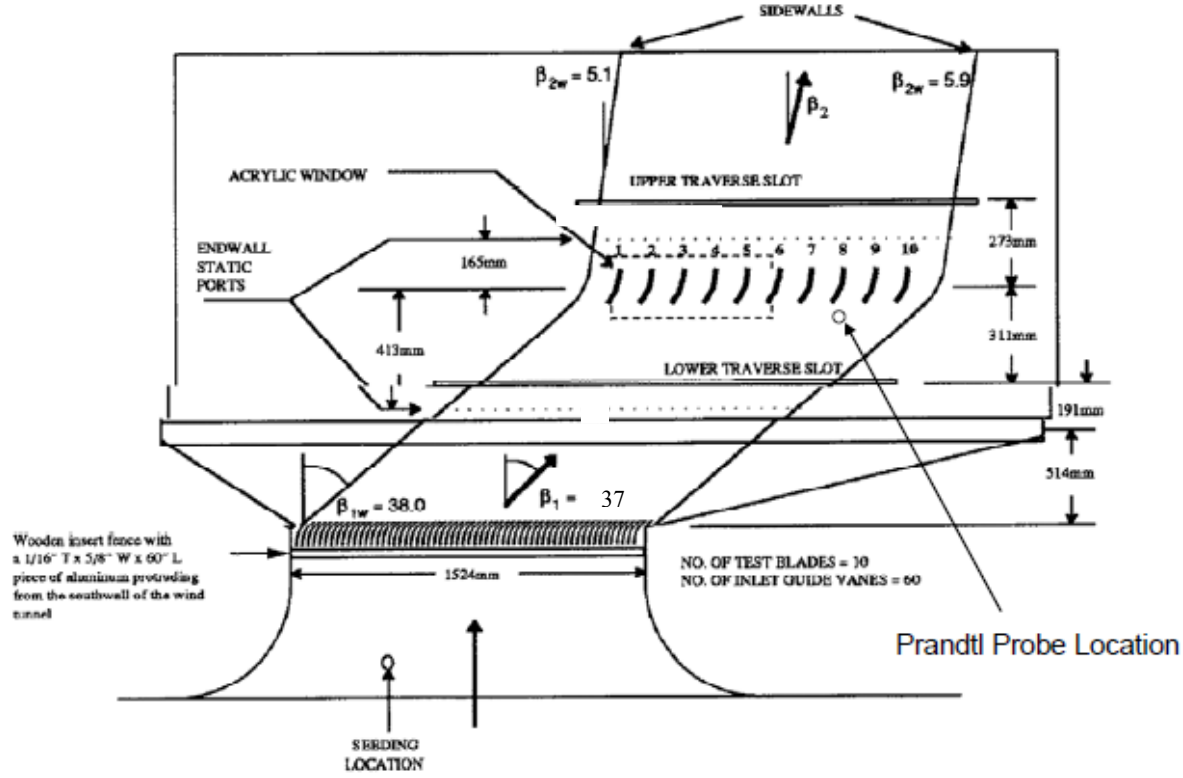

Figure 2. LSCWT test section

Type	Stator 67B Controlled-Diffusion
Number of Blades	10
Spacing	152.4 mm
Chord	127.14 mm
Solidity	0.834
Thickness/Chord	0.05
Setting Angle	16.3 deg
Span	254.0 mm

Table 1. Cascade test section characteristics

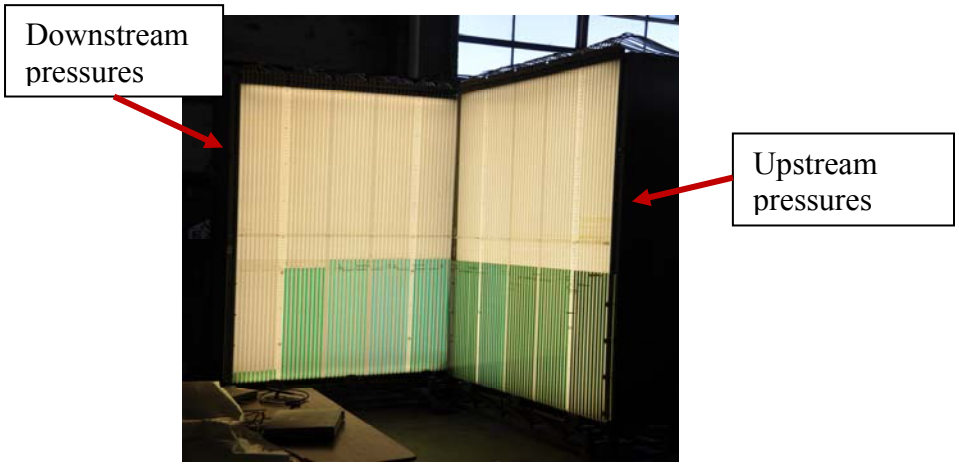

Figure 3. Water manometer banks

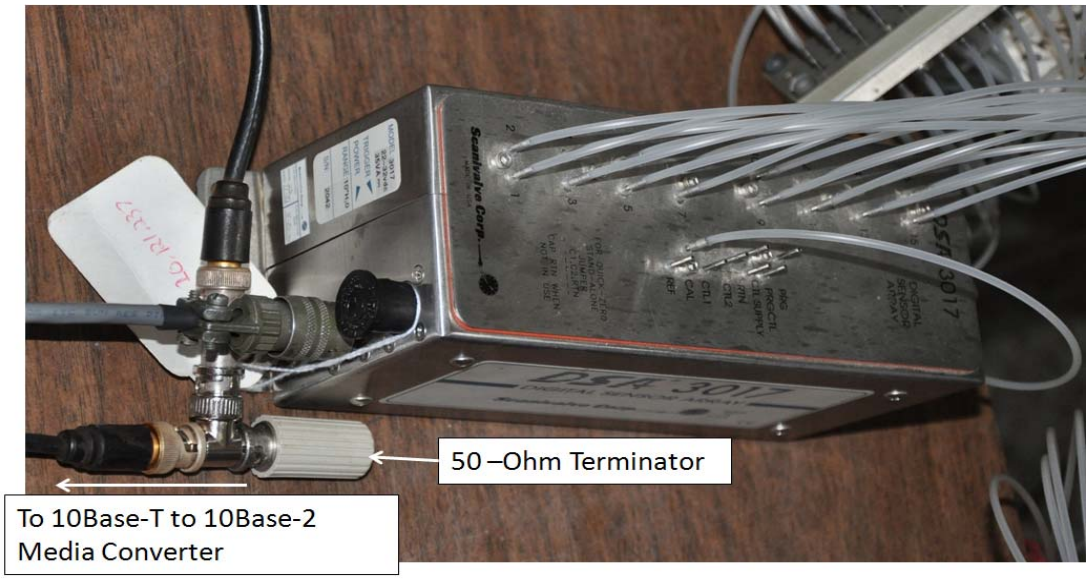

Figure 4. DSA Model 3017 termination and signal conversion

C. INSTRUMENTATION AND PRESSURE DATA ACQUISITION

The fully instrumented blade 5 and the partially instrumented blade 9 were connected via Tygon tubing to one 2.5-PSID and two 10-inches of water Scanivalve model 3017 Digital Sensor Arrays (Figure 4). The partially instrumented blade 2, the Prandtl probe and five-hole probe were connected via Tygon tubing to a 2.5-PSID Scanivalve model 3217 DSA. The pressure ports exposed to the highest pressures during testing were attached to the 2.5 PSID DSAs to avoid over pressurization. The three older 3017 DSAs were connected in series via BNC cables to a Transition Networks 10Base-T to 10Base-2 Media Converter. The first DSA in the series was singly terminated with a 50-Ohm terminator. The third DSA in series, which was connected to the 10Base-T to 10Base-2 Media Converter, was also terminated at its "T" with a 50-Ohm terminator for the data acquisition system to recognize any of the 3017 DSAs. See Figure 4 for BNC connections and terminations. The model 3217 DSA and output of the 10Base-T to 10Base-2 Media Converter were connected to a 3Com OfficeConnect Dual Speed Hub 8, which provided the Ethernet communications link to a personal computer for data acquisition, storage and processing.

For all pressure surveys, the pressures were read via DSAs vice the rotary-style pneumatic pressure-scanning systems that had been used in previous LSCWT studies. Prior to operation, all DSAs had to have their IP addresses changed to be recognized by the personal computer. See Appendix A for a description of DSA IP addressing. The DSAs, pressures and plenum thermocouple were read by and the traverse mechanism was controlled by an Agilent VEE Pro program. Urban [9] installed and documented the operation of the traverse mechanism control. For pressure distribution surveys "ScanBrick.vee" read each DSA. The program iteratively read all pressures and wrote them to a tab-delimited text file for post processing in Microsoft EXCEL. The signal flow from pressure measurement location, to DSA port, to VEE Pro program was documented in Table 2. The DSAs were indexed from 1 while VEE Pro indexed from zero.

The VEE Pro program "5Hole.vee" was used for five-hole probe surveys. This program automatically controlled the instruments, recorded the data and performed the calculations described in section III.D. Figure 5 shows the signal flow in "5Hole.vee" and Figure 6 shows its HPVEE front panel. Vertical arrows denote execution flow while horizontal arrows denote data flow. "Raw.txt" was populated with the pitch-wise sample locations, pressures, and temperatures. "S9bgd.txt" was populated with the values of γ, β and δ, which were used for pitch, yaw and non-dimensional velocity calculations.

Channel (Patch Panel A/C)	Brick IP (last 3)	Brick Port#	VeePro Port#	Pressure Tap Location
1	235	1	0	Atm
2	235	2	1	18P
3	235	3	2	17P
4	235	4	3	16P
5	235	5	4	15P
6	235	6	5	14P
7	235	7	6	13P
8	235	8	7	12P
9	235	9	8	11P
10	235	10	9	10P
11	235	11	10	9P
12	235	12	11	8P
13	235	13	12	7P
14	235	14	13	6P
15	235	15	14	5P
16	235	16	15	4P
17	236	1	0	3P
18	236	2	1	2P
19	236	3	2	1P
20	236	4	3	LE
21	236	5	4	1S
22	236	6	5	2S
23	236	7	6	3S
24	236	8	7	4S
25	236	9	8	5S
26	236	10	9	6S
27	236	11	10	7S
28	236	12	11	8S
29	236	13	12	9S
30	236	14	13	10S
31	236	15	14	11S
32	236	16	15	12S
33 / 16	237	16	15	13S
34 / 15	237	15	14	14S
35 / 14	237	14	13	15S
36 / 13	237	13	12	16S
37 / 12	237	12	11	17S
38 / 11	237	11	10	18S
39 / 10	237	10	9	19S
40 / 9	237	9	8	20S
41 / 8	237	8	7	TE
42 / 7	237	7	6	Blade 9 P1
43 / 6	237	6	5	Blade 9 P2
44 / 5	237	5	4	Blade 9 S1
45 / 4	237	4	3	Blade 9 S2
46 / 3	237	3	2	Blade 9 S3
47 / 2	237	2	1	Blade 9 S4
48 / 1	237	1	0	Blade 9 S5

Channel (Patch Panel B)	Brick IP	Brick Port#	VeePro Port#	Pressure Tap Location
1	233	1	0	(5-hole Probe) 1
2	233	2	1	(5-hole Probe) 2
3	233	3	2	(5-hole Probe) 3
4	233	4	3	(5-hole Probe) 4
5	233	5	4	(5-hole Probe) 5
6	233	6	5	Blade 2 1S
7	233	7	6	Blade 2 2S
8	233	8	7	Blade 2 4S
9	233	9	8	Blade 2 5S
10	233	10	9	Blade 2 1P
11	233	11	10	Pitot Static
12	233	12	11	Pitot Stag
13	233	13	12	Plenum

note: Patch Panel C is quick disconnect

Brick Pressure Ranges	
236	2.5 psid
235	10"
237	10"
233	2.5 psid

Table 2. DSA pressure port connection information

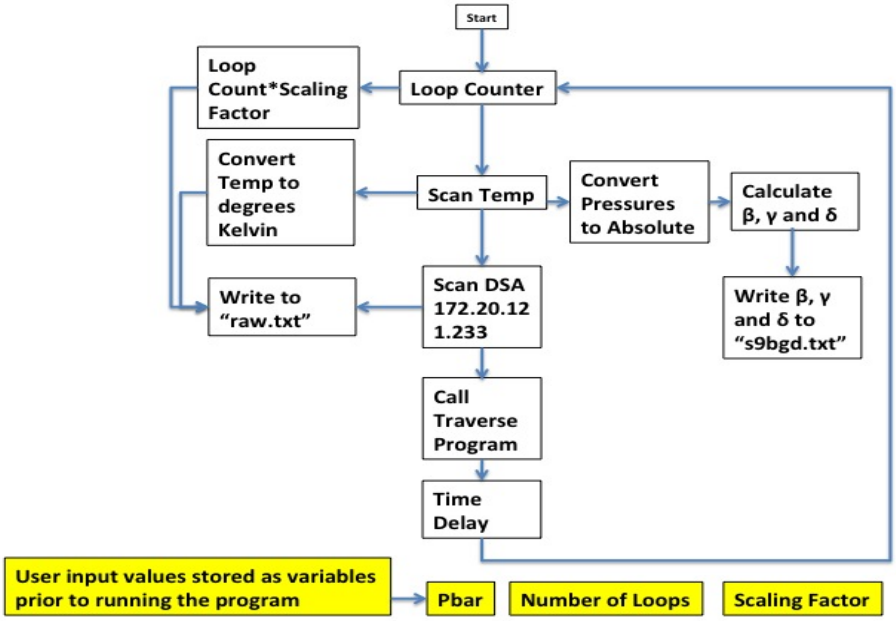

Figure 5. 5Hole.vee flow chart

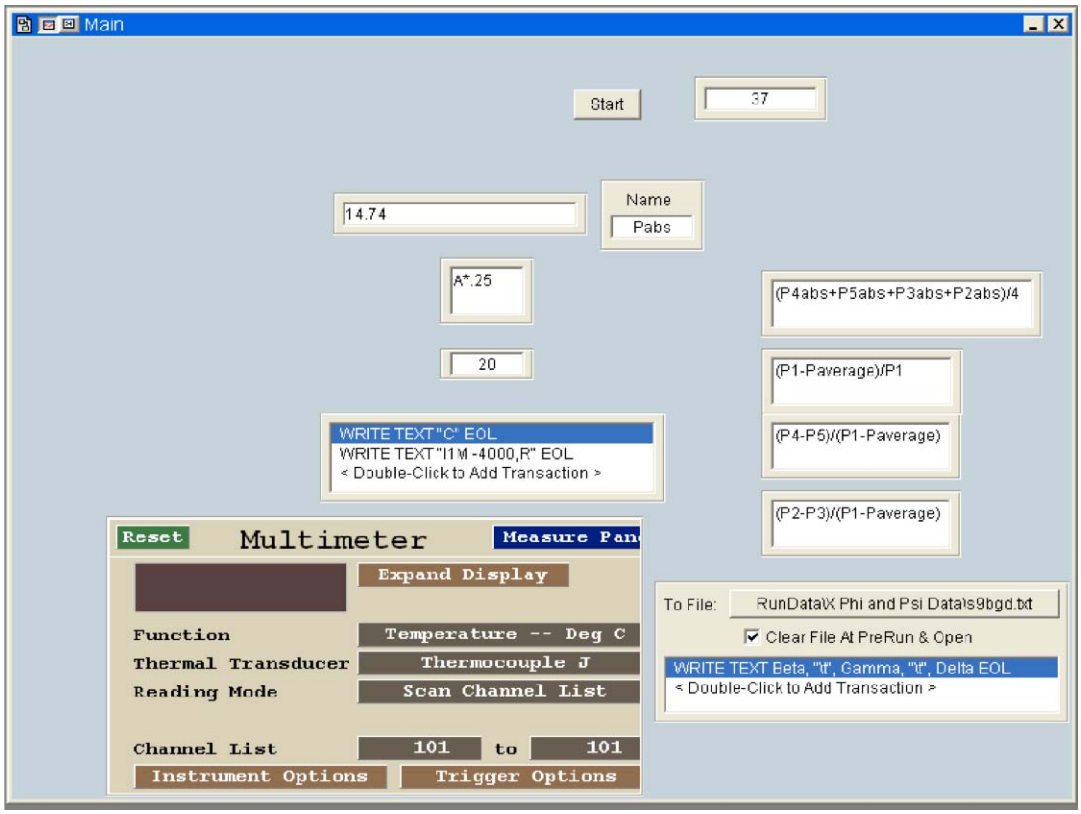

Figure 6. 5Hole.vee front panel

D. LDV SURVEYS

Fitzgerald [8] documented the laser optics, data acquisition, traverse table and particle seeding. Hansen [3] documented the laser alignment tool and alignment procedure. Prior to this study the model 9230 ColorLink-Plus Multicolor Receiver and LDV probe were sent to the manufacturer for refurbishment. The blue beams were assigned to channel two and oriented vertically to measure the axial (vertical) velocity component. The green beams measured the pitch-wise (horizontal) velocity component. For boundary layer surveys the LDV probe was pitched five degrees toward the blade to attain measurements as close to the blade surface as possible and minimize interference from the end of the blade while maintaining the highest data rate. Data were recorded at a survey location until one thousand coincident seed particle measurements were received or three hundred seconds elapsed.

III. EXPERIMENTAL PROCEDURE

A. REYNOLDS NUMBER CALCULATION

Cascade flow analysis was performed at five different Re based on the chord length of 0.1724 m. To calculate the Re, an Hp 3456A Digital Voltmeter connected to a thermocouple, located in the plenum, read temperature. Barometric pressure was manually read via a Wallace and Tiernan stand-alone barometer. The bulk fluid pressure was measured via the static port of an upstream Prandtl probe. The density of the flow entering the test section was computed from the equation of state ($P = \rho RT$):

$$\rho = \frac{(P_{bar} + P_{stat})}{287 \frac{J}{kg \bullet K} * T}$$

The bulk flow velocity V_{ref} entering the blade row was calculated from the upstream static and stagnation Pressures as:

$$V_{ref} = \sqrt{\frac{2}{\rho}(P_{stag} - P_{stat})}$$

Where P_{stag} is the stagnation pressure recorded by the upstream Prandtl probe.

During all data runs the plenum temperature was 20 degrees C, plus or minus 2 degrees C, therefore the dynamic viscosity was taken as a constant .000018 $\frac{(N \cdot s)}{m^2}$.

The Re based chord length was then calculated as:

$$Re = \frac{\rho \frac{kg}{m^3} \cdot V_{ref} \frac{m}{s} \cdot 0.12714m}{.000018 \frac{(N \cdot s)}{m^2}}$$

B. BLADE PRESSURE DISTRIBUTIONS

The Coefficient of Pressure (Cp) for each of the Reynolds numbers of interest were calculated using fully instrumented Blade 5 (Figure 2). First, the DSAs were calibrated about zero using the "calz" command from the DSA link program and then the tunnel was started and brought up to speed. The tunnel velocity was set via plenum pressure as read from the inlet-plenum water-manometer (Figure 3). The Agilent VEE Pro program "ScanBrick.vee" was initialized and all pressures were sampled ten times in three-second sample intervals via the DSAs. ScanBrick.vee wrote all pressures to the text file "testv4.txt." The VEE Pro Program "ScanTemp.vee" was initialized to read the plenum temperature. "Testv4.txt" and the plenum temperature were copied into a Microsoft Excel spreadsheet for post processing. The Cp was calculated as:

$$Cp = \frac{P_{loc} - P_{stat}}{P_{stag} - P_{stat}}$$

where P_{stag} and P_{stat} were the upstream stagnation and static pressures measured by the Prandtl probe and P_{loc} was the local pressure measured on the fully instrumented blade.

C. 5-HOLE PROBE SURVEYS

The traverse mechanism was initially mounted downstream of the cascade in the in the acrylic window (Figure 2) on the North side of the tunnel and the vernier was set to 90 degrees, which made the 5-hole probe point vertically downward into the flow. The probe was traversed to the leading edge of blade three. The tunnel was started and brought up to the desired inlet plenum pressure, which was read from the water manometer. The VEE Pro program "5Hole.vee" was started and the probe sampled over a range of 154 mm (6.06 inches) to capture one complete blade pitch. Samples were performed at 1.5875 mm (0.0625 inches) intervals with a 28 second pause between samples to allow the pressures in the 5-hole probe to stabilize. A total of 97 samples per survey were conducted. When the survey was completed the traverse was returned to the

zero position. The tunnel was adjusted to the next inlet plenum pressure of interest to change the inlet-flow speed and the survey process was repeated until samples at all plenum pressures were complete.

After completing the downstream survey the traverse mechanism and 5-hole probe were removed and mounted in the lower traverse slot upstream of the blade row (Figure 2) located on the south side of the tunnel. The five-hole probe was set to approximately the inlet flow angle of 37 degrees. All upstream surveys were completed at the Re settings as described in the previous paragraph. Blades three and four were surveyed to facilitate comparison to LDV measurements.

D. AVDR AND LOSS COEFFICIENT

The Axial Velocity Density Ratio (AVDR) and loss coefficient were computed using the equations from Hansen [3] for X_{ref}, K, $AVDR$, C_{pt}, C_{ps} and ω. To compute X and φ the five-hole probe calibration coefficient files were used in conjunction with the MATLAB program "s9.m" (Grubb et al. [12]). The five-hole probe data was processed during collection by the same VEE Pro program that automated the 5-hole probe surveys (See Section III.C) to produce a text file called "s9bgd.txt" containing β, γ and δ values at each survey location. S9.m read in the calibration coefficient files "C.WK1," "D.WK1" and "E.WK1" and the s9bgd.txt text file and produced values for X and φ at every pitchwise sample location. For the upstream data $\beta_1 = \varphi + \beta_{5-hole}$, where β_{5-hole} was 37 degrees as mentioned earlier. For the downstream data, β_2 was equal to φ because the 5-hole probe was zero degrees relative to vertical. Upstream and

downstream data was copied into Microsoft Excel spreadsheets and numerically integrated to determine the loss and AVDR. AVDR was calculated as:

$$AVDR = \frac{\int_0^S K_{ds}\,dx}{\int_0^S K_{us}\,dx}$$

where K_{ds} and K_{us} were the downstream and upstream five-hole probe reference flow functions as defined by Hansen [3].

The AVDR was then used to calculate the loss coefficient:

$$\omega = \frac{\int_0^S C_{pt,us}K_{us}\,dx - \frac{1}{AVDR}\int_0^S C_{pt,ds}K_{ds}\,dx}{\int_0^S C_{pt,us}K_{us}\,dx - \int_0^S C_{ps,us}K_{us}\,dx}$$

where C_{pt} and C_{ps} were the total and static pressure ratios at either the upstream or downstream location, respectively. The trapezoidal rule was used for all numerical integrations.

E. LDV SURVEYS

LDV surveys were performed at Re = 203K to fully document this test case, specifically the suction-side separation bubble. Plenum temperature was read using "ScanTemp.vee" and recorded into an EXCEL spreadsheet so the non-dimensional velocity, X, could be computed and compared to the five-hole probe X distributions. For the LDV data X was computed as:

$$X = \frac{W}{\sqrt{2C_pT_0}}$$

where W was the resultant velocity measured by the two-component LDV, C_p is the specific heat capacity of air at constant pressure and T_0 was the plenum stagnation temperature.

LDV data sets were also non-dimensionalized with respect to V_{ref}, whose calculation was described in section III.A. Tabulated measurements and calculated reference velocities are listed in Table 3. "Scanbrick.vee" was iterated 100 times with a 15 second pause between each iteration to get a sample of Prandtl probe pressures that spanned the duration of the applicable LDV sample. The pressures were averaged for use in the density and velocity calculations (Section III.A).

Re/1000	Location	Survey Size	Pplen (in H20)	Tplen (K)	Density (kg/m^3)	Vref (m/s)
203	Upstream	coarse	1.3	293.61	1.20	24.70
203	Downstream	coarse	1.4	295.11	1.20	25.88
203	Downstream	fine	1.4	295.15	1.20	26.07
395	Upstream	coarse	4.4	294.75	1.20	46.93
203	Station 8 bl	na	1.3	293.17	1.20	24.91
203	Station 7.75 bl	na	1.3	295.17	1.19	24.96
203	Station 7.25 bl	na	1.3	295.73	1.19	24.88
203	Station 7.0 bl	na	1.3	295.45	1.20	24.17
203	Station 6.75 bl	na	1.3	292.93	1.21	24.57

Table 3. LDV survey computed reference velocities

1. Upstream and Downstream Surveys

Prior to each upstream and downstream survey the LDV probe volume was aligned as in Hansen [3] section III.C. Test section inlet and exit-flow surveys were performed at Re = 203K across a pitch-wise distance of 158.75 mm at 6.35 mm intervals, which resulted in 25 survey points. The surveys were performed at stations 1 and 13 (Figure 7). A fine wake survey was performed at station 13 across blade 3 for wake characterization and comparison to the five-hole probe data. The survey was done at 1.587 mm intervals at twenty-six survey locations for a total span of 41.274 mm.

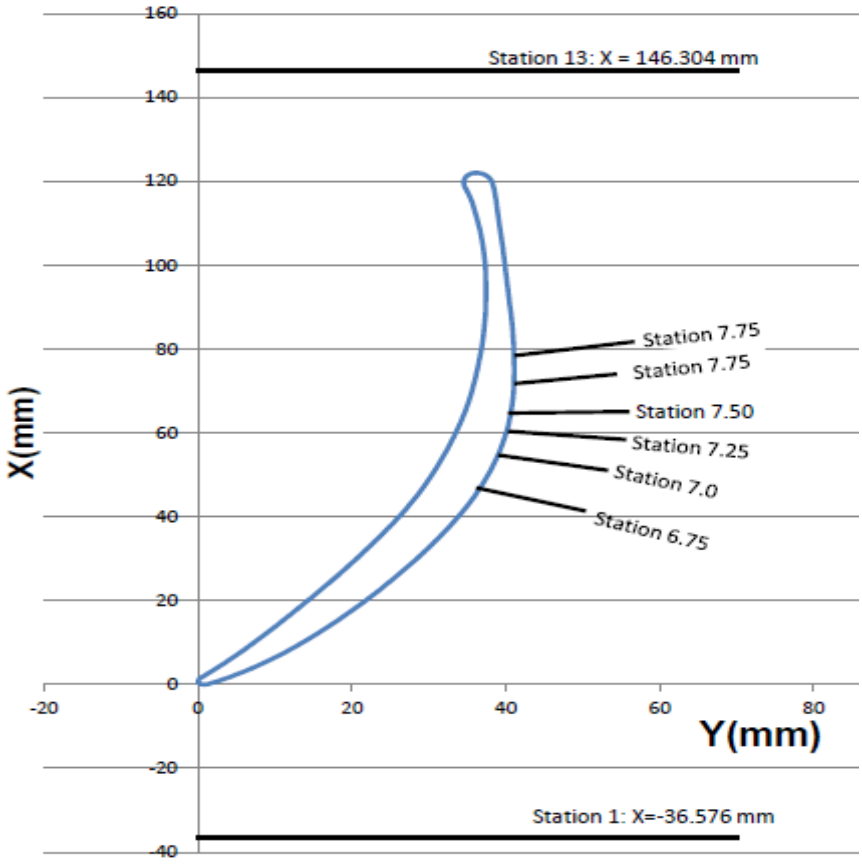

Figure 7. LDV survey locations

2. Boundary Layer Surveys

Boundary Layer surveys were performed at Re = 203K at stations 6.75, 7, 7.25, 7.5, 7.75 and 8 (Figure 7). The intent was to describe the axial chord locations (C_{ac}) where the boundary layer separated and re-attached and whether the boundary layer was laminar or turbulent at those locations. Boundary layer surveys were performed along a line perpendicular to the blade surface at the applicable station. Before each survey the probe volume was verified to be on the blade surface at mid-span, as indicated by all four beams converging to a single turquoise dot at the midspan of the blade. The probe volume was then traversed into the free-stream and settings were adjusted in the TSI Find software to attain the best data rate. Surveys were performed from the free-stream to the blade surface. Once the survey in the free-stream to blade direction was completed the

probe volume was traversed into the boundary layer and the TSI Find settings were re-adjusted to maximize data rate. A survey was then done along the same perpendicular but in the wall to the free-stream direction. The two surveys were combined to create one curve at that survey station. At least 179 data points were required at a survey point for that data point to be included in the plot as a valid measurement.

To further characterize and compare the boundary layers momentum integral approximation methods were used. The displacement thickness (δ^*) was computed as:

$$\delta^* = \int_0^{\delta_{bl}} (1 - \frac{w}{W}) d\left(\frac{y}{c}\right)$$

where w was the mean total velocity vector at that survey location, δ the boundary layer thickness and W was the maximum total velocity vector for a given boundary layer survey. The location of the free-stream was taken as the location of maximum W in a given survey. The momentum thickness (θ) was computed as:

$$\theta = \int_0^{\delta_{bl}} \frac{w}{W}(1 - \frac{w}{W}) d\left(\frac{y}{c}\right)$$

The shape factor (H) was computed as:

$$H = \frac{\delta^*}{\theta}$$

All numerical integrations were performed using the trapezoidal rule.

F. FLOW VISUALIZATION

The LSCWT was brought to a plenum pressure of 1.3 inches of water and the blower motor was secured, which maintained the tunnel setting but stopped the airflow. The acrylic window was removed and a mixture of Day-Glo Corp's "Saturn Yellow" pigment and diesel fuel was brushed onto the suction side of blade three. The window was rapidly reinstalled and the blower motor energized. Flow features were recorded and photographed using a Nikon D90 digital camera.

IV. COMPUTATIONAL FLUID DYNAMICS

A. GEOMETRY AND MESHING

A Re=203K was used as the CFD test case for this study. The 67B compressor blade profile was modeled in SolidWorks 2010 using the 343 machine coordinates. The domain encompassed one complete blade pitch of 152.4 mm and was extended one axial chord of 122 mm forward from the leading edge and one axial chord back from the trailing edge. The inlet section of the domain is canted at 16 degrees, which was the blade stagger angle in the experiment (Figure 8).

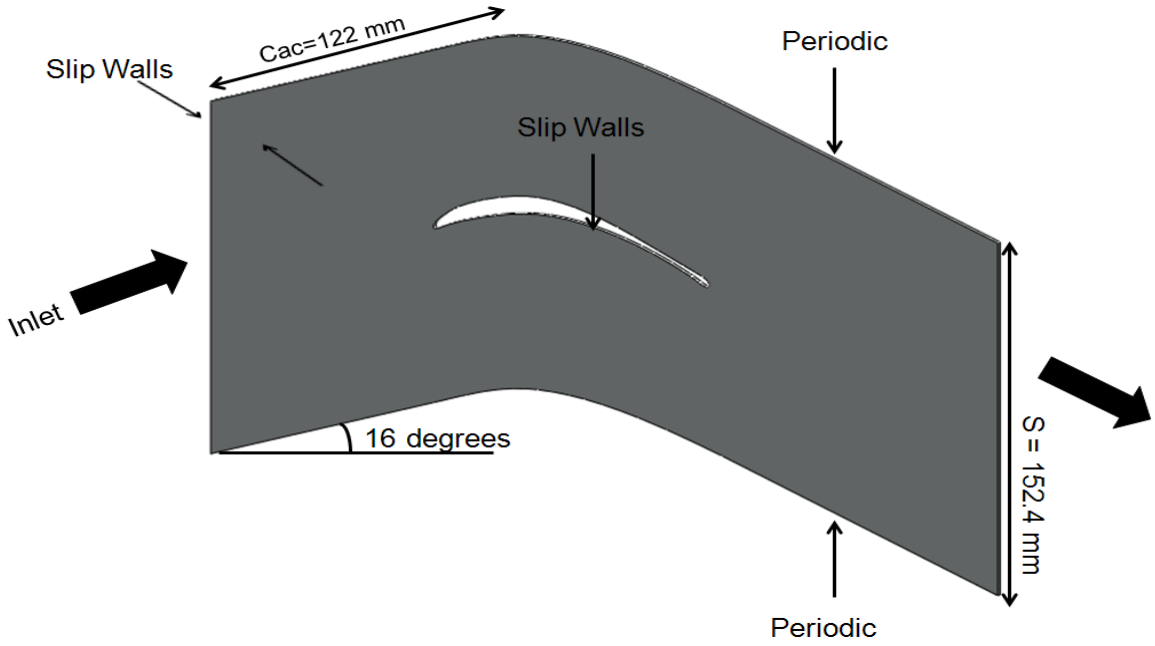

Figure 8. CFD domain and boundary conditions

It was desired to have a fine mesh around the surface, but a coarser mesh in the free stream where the flow was more uniform. The mesh was refined by adjusting the number of divisions in the "Edge Sizing" menu and the growth rate in the "sizing" section of the CFX Mesher. The mesh was generated with five sweeps across the domain in the pitch-wise direction and an edge sizing refinement of 15,400 around the blade. It

was determined that a better mesh could be achieved by letting CFX determine the "Min Size," "Max Size" and "Max Face Size" and refining the mesh through growth rate, curvature normal angle and edge sizing rather than manually adjusting the sizing options (Figure 9).

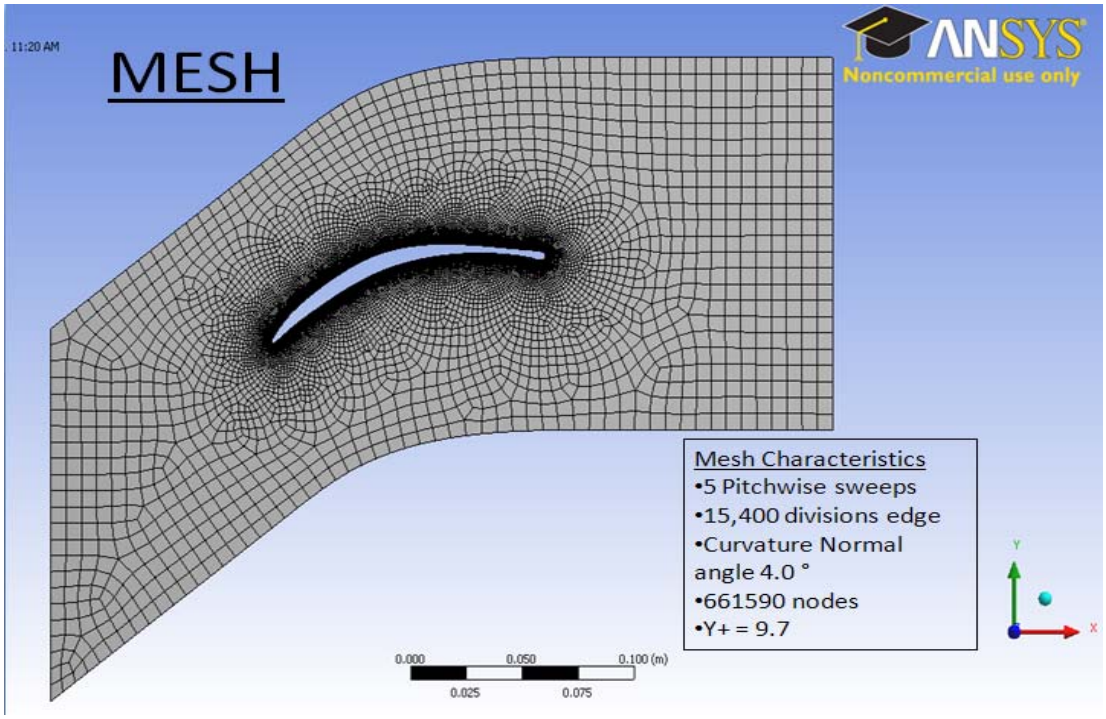

Figure 9. CFD mesh with statistics

B. SETUP

Axial Velocity Density Ratio (AVDR) was modeled as a linear area contraction in the stream-wise direction. To incorporate AVDR the 2-D solid-model domain was extruded from 1.0 mm to a width of 1.1377 mm in the pitch-wise direction, which equaled the magnitude of the AVDR at Re = 203K that was determined with the five-hole probe (Figure 10). Two extruded cuts were made at a 0.0939 degrees from vertical in the axial direction 0.5 mm from the centerline making the inlet to outlet surface-area ratios of the domain match the computed area contraction due to side-wall boundary layer growth.

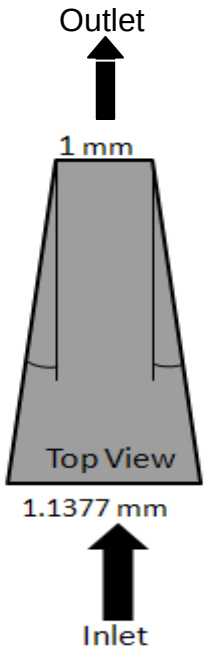

Figure 10. CFD AVDR streamwise area contraction

The domain boundaries in the pitch-wise direction were no longer symmetrical so those boundary conditions had to be changed from symmetry to slip-free walls. To verify this boundary condition was valid, two test cases were performed on models that had no area contraction i.e., the pitch-wise boundaries were still symmetrical. The first used free-slip walls while the second used symmetry as the pitch-wise domain boundaries. The *Cp* plots were over plotted and were identical, which verified the free-slip wall boundary condition for the AVDR case.

The flow-field physics were modeled as adiabatic air at 25 degrees Celsius. Transition was modeled using the gamma-theta model and turbulence was modeled using the shear-stress-transport (SST) model. The turbulent kinetic energy was initialized with a value of 0.6 $\frac{m^2}{s^2}$ to match the free-stream turbulence intensity measured during the LDV inlet survey A steady-state simulation was run first with 200 time-steps and a convergence criteria of $1x10^{-7}$ and used to initialize the flow field for the transient run.

The transient run had a convergence criteria of $1x10^{-4}$ and employed time-steps of $5x10^{-4}$ seconds for a total duration of 0.1 seconds. This resulted in a Root Mean Square (RMS) Courant number of 155.

V. RESULTS AND DISCUSSIONS

A. BLADE PRESSURE DISTRIBUTIONS

Surface pressure measurements were taken from the fully instrumented blade 5 at Reynolds numbers of 203,000, 286,000, 393,000, 537,000 and 639,000. The results were presented as the blades' Coefficient of pressure (Cp) plotted versus x/c (Figure 11). The Cp plots showed that the flow behavior on the pressure side of the blade was insensitive to Re. On the suction side of the blade a laminar separation bubble was evident at the lower two Re from $0.55489 < x/C_{ac} < 0.690619$. As the Re increased above the lowest two the separation bubble collapsed and was not present at all at the highest Re. Five-hole probe data showed that β_1 varied from 43 degrees at Re = 203,000 to 37 degrees at Re = 639,000 (Figure 13). The design angle of attack for the 67B compressor blade was 36 degrees so suction side blade unloading due to off design angle of attack could contribute to flow separation. The location and magnitude of the separation bubble agreed with Schnorenberg's [4] results. At different Re the pressure side pressure distributions were indistinguishable, which contradicted some variation observed in Reference 4. This pressure side variation could be due to the blade polishing or that Schnorenberg's measurements were done at off-design angles of attack. The plots also indicated there were several pressure ports around which included the leading edge that became partially blocked during testing. All pressure-sensing lines were blown out with compressed nitrogen but the blockages remained.

B. 5-HOLE PROBE SURVEYS

1. Periodicity and Inlet Flow Angle

$C_{pt,ds}$ was plotted for blades 3 and 4 and then superimposed at three Re. At low Re the wake surveys were largely asymmetrical but identical when plotted on top of each other showing flow periodicity existed (Figure 12). As the Re was increased the flow periodicity diminished, resulting in the wakes at blades 3 and 4 not plotting on top of

each other. To verify that the results were not due to surveys that were not sufficiently fine, 0.79375 mm surveys were performed at the lowest and highest Re and then plotted with the 1.5875 mm surveys.

At low Re a 6 degree deviation from the design IFA was observed (Figure 13). A significant deviation from IFA was observed until Re = 380K, at which point the IFAs converged on 37 degrees.

2. AVDR

Table 4 shows the computed AVDR at all Re. The AVDR was a maximum of 1.138 at Re = 203K, had a minimum of 1.048 at Re = 400K and then slowly increased at the last two Re.

Re # (k)	AVDR
221	1.138
310	1.070
400	1.048
538	1.052
674	1.055

Table 4. AVDR v. Reynolds number

3. Loss Calculations

The loss calculations showed a maximum loss of 0.030, which occurred at Re = 203K with the minimum loss of 0.012 occurring at Re = 393K and the losses increasing from Re = 393K to 639K (Figure 15). The maximum loss at low Re was caused by the presence of the separation bubble and large deviation from the design inlet flow angle. The decrease in loss from Re = 203K to Re = 393K correlated to a decreasing separation bubble observed on the *Cp* plots for Re = 203K through Re = 393K (Figure 11). From

Re = 203K to Re = 393K a thinning of the wake (Figure 14) occurred, which lessened the loss. At Re = 393K the *Cp* plot indicated that the separation bubble had collapsed and the boundary layer had re-attached.

The increase in loss from 0.012 to 0.014 between Re = 393K and Re = 639K correlated to a sharp rise in wake deficit between these points (Figures 14). This indicated that the polished 67B compressor blades had an optimal Reynolds number of 400K at the design inlet flow angle.

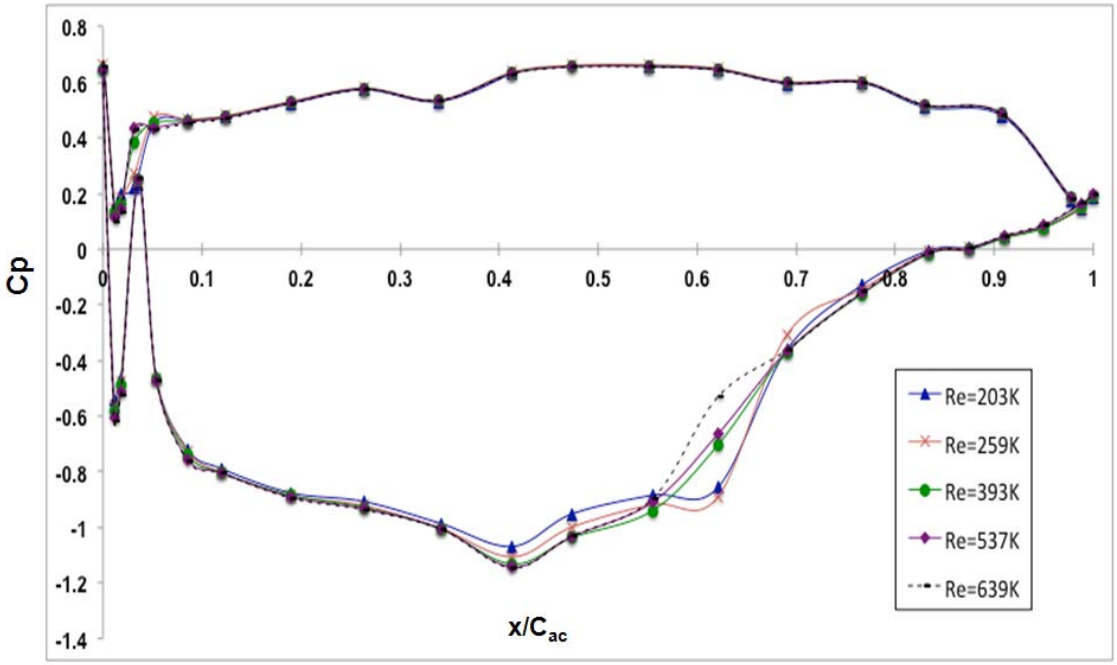

Figure 11. Blade surface pressure distributions for all Reynolds numbers

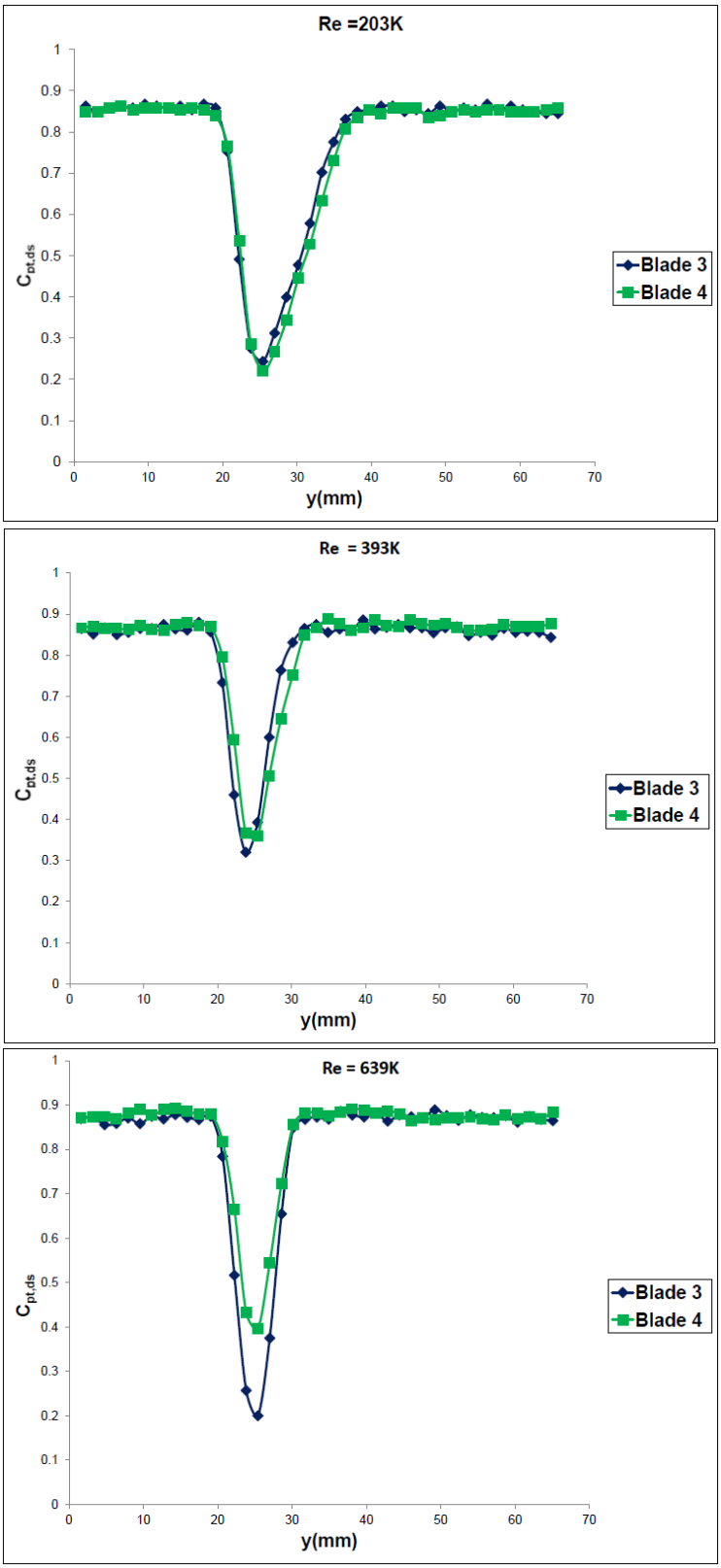

Figure 12. Blade 3 and blade 4 $C_{pt,ds}$ overplots

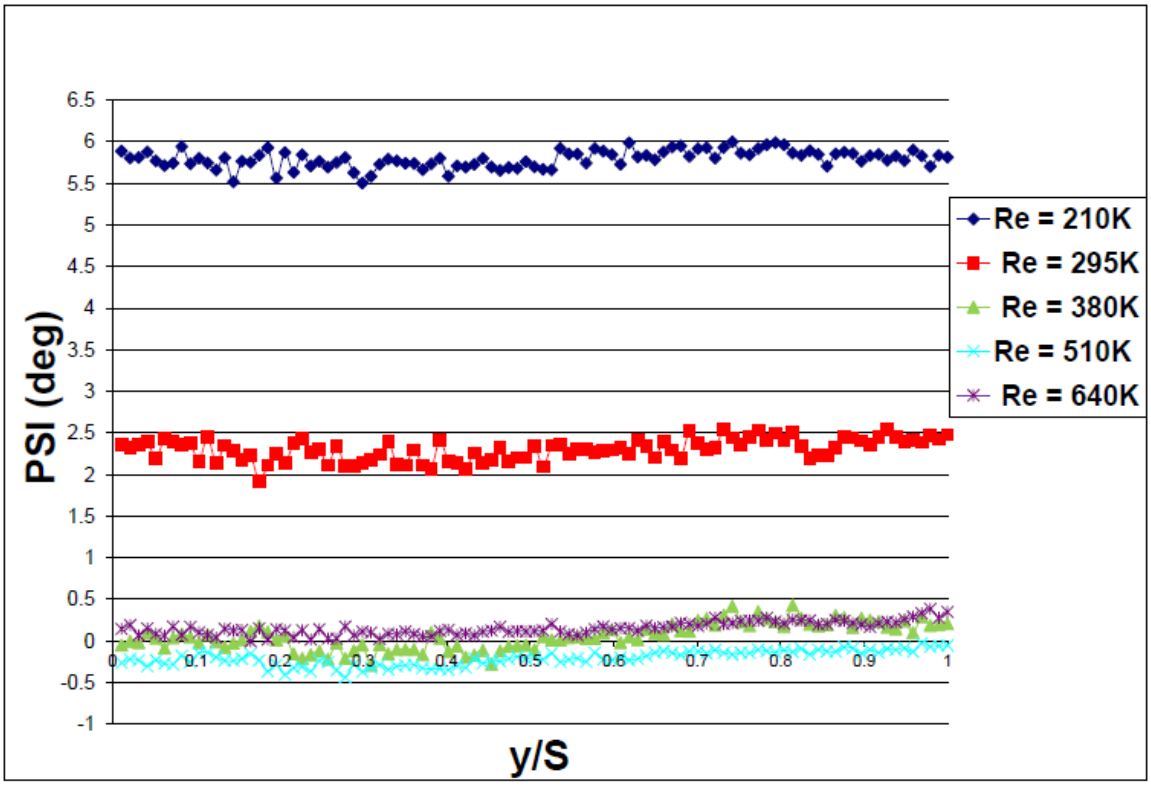

Figure 13. Deviation from design inlet flow angle v. Reynolds number

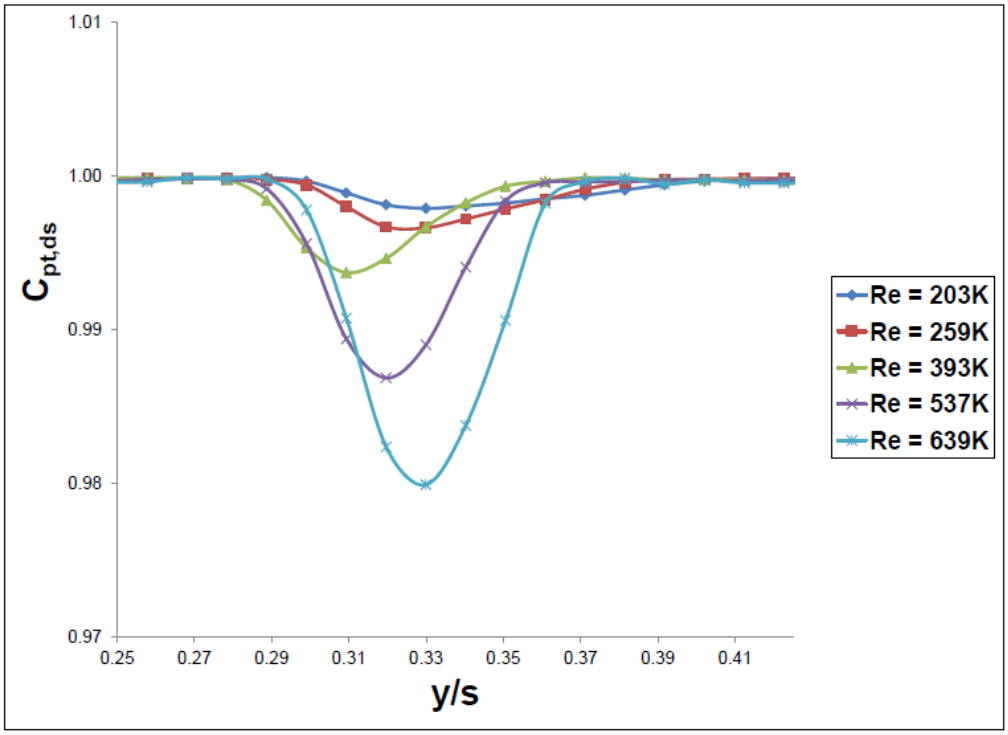

Figure 14. Wake deficit distributions and different Reynolds numbers

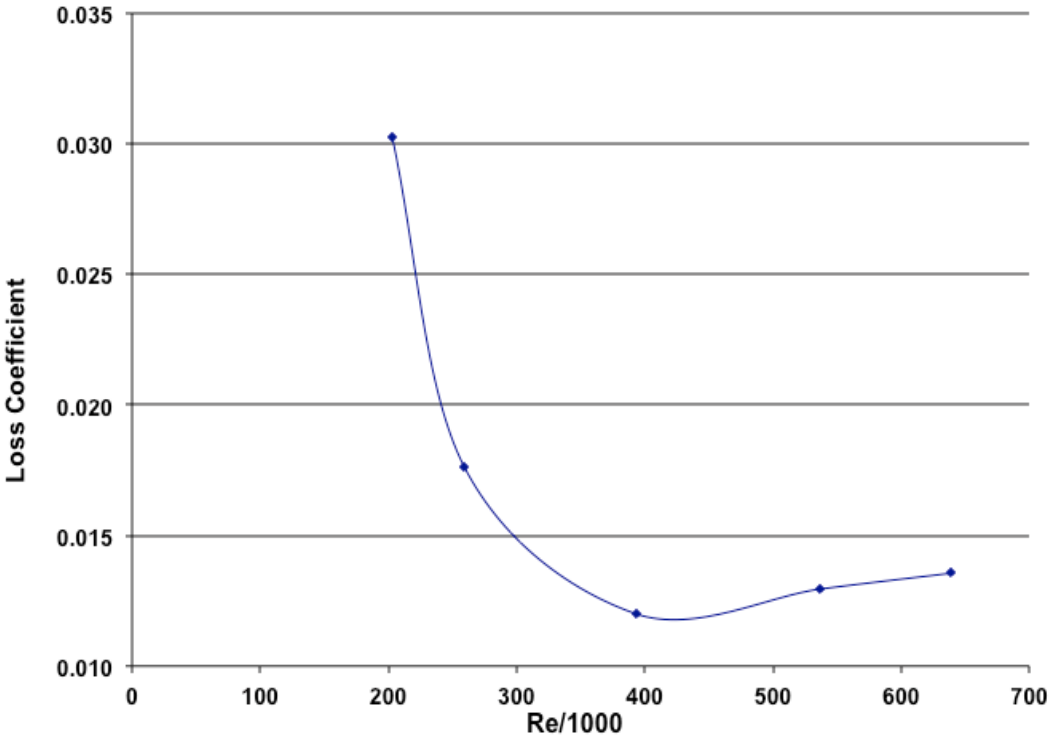

Figure 15. Loss versus Reynolds number

C. LDV RESULTS

1. Inlet and Outlet Flow Measurements

The station 1 surveys showed inlet-flow Turbulence Intensity (Ti) that varied between 2 and 3 percent (Figure 16) and had a positive C_{uv} of 0.2. The LDV and 5-hole probe inlet non-dimensional velocity distribution had an approximately 8 percent error (Figure 17). The deviation from design inlet flow (Figure 18) peaked at 3.5 degrees, which is 2.5 degrees less than the peak deviation as measured by the 5-hole probe. The LDV inlet flow angle had a strong sinusoidal distribution, which was a result of the upstream influence of the blades due to their potential effect.

The station 13 wake surveys (Figure 19) showed a free-stream Ti of 2.5 percent, which then peaked inside the wake at y/S = 0.24 at a value of 20 percent. Comparison of the LDV and 5-hole probe non-dimensional velocities (Figure 20) showed a 7.5 percent

error in the free-stream and a large deviation in wake deficit. However, the width of the wake was adequately captured by both measurement techniques.

2. Boundary Layer Measurements

The velocity profiles at station 6.75 indicated a laminar, attached boundary layer. The turbulence intensities at this station maintained free-stream turbulence values as close to the wall as d/c = 0.005, which also indicated laminar flow (Figure 21). At station 7.0 the velocity profiles still indicated a laminar boundary layer. However, the large increase in turbulence intensities (Figure 22) in the boundary layer was due to the presence of the inflection of the mean velocity profile indicating the onset of separation. Station 7.25 proved to be inside the separation bubble as a region of reverse flow was evident on the velocity-ratio plot from the wall to d/c < 0.008 (Figure 23). Turbulence intensity peaked at stations 7.5 (Figure 24) and the velocity-ratio plot indicates the boundary layer had begun to reattach. Also, the positive increase in the correlation coefficient indicated that the turbulence was oscillating between the first and fourth quadrant. The Station 7.75 velocity-ratio plot indicated a reattached boundary layer (Figure 25) and a reduction in the peak Ti to 25 percent had occurred. At station 8.0 the velocity ratios indicated a turbulent, re-attached boundary layer (Figure 26).

Figure 27 shows the distribution displacement thickness, momentum thickness and shape factor for the boundary layer measurements at stations 6.75 to 8.0. Table 5 presents a listing of δ, θ and H for those stations. A large rise in shape factor to a peak value of 10 occurred between stations 7.00 and 7.25, which is similar to the shape factor as measured by Fitzgerald and Mueller on a NACA-66 series air foil at low Re with a laminar separation bubble [13].

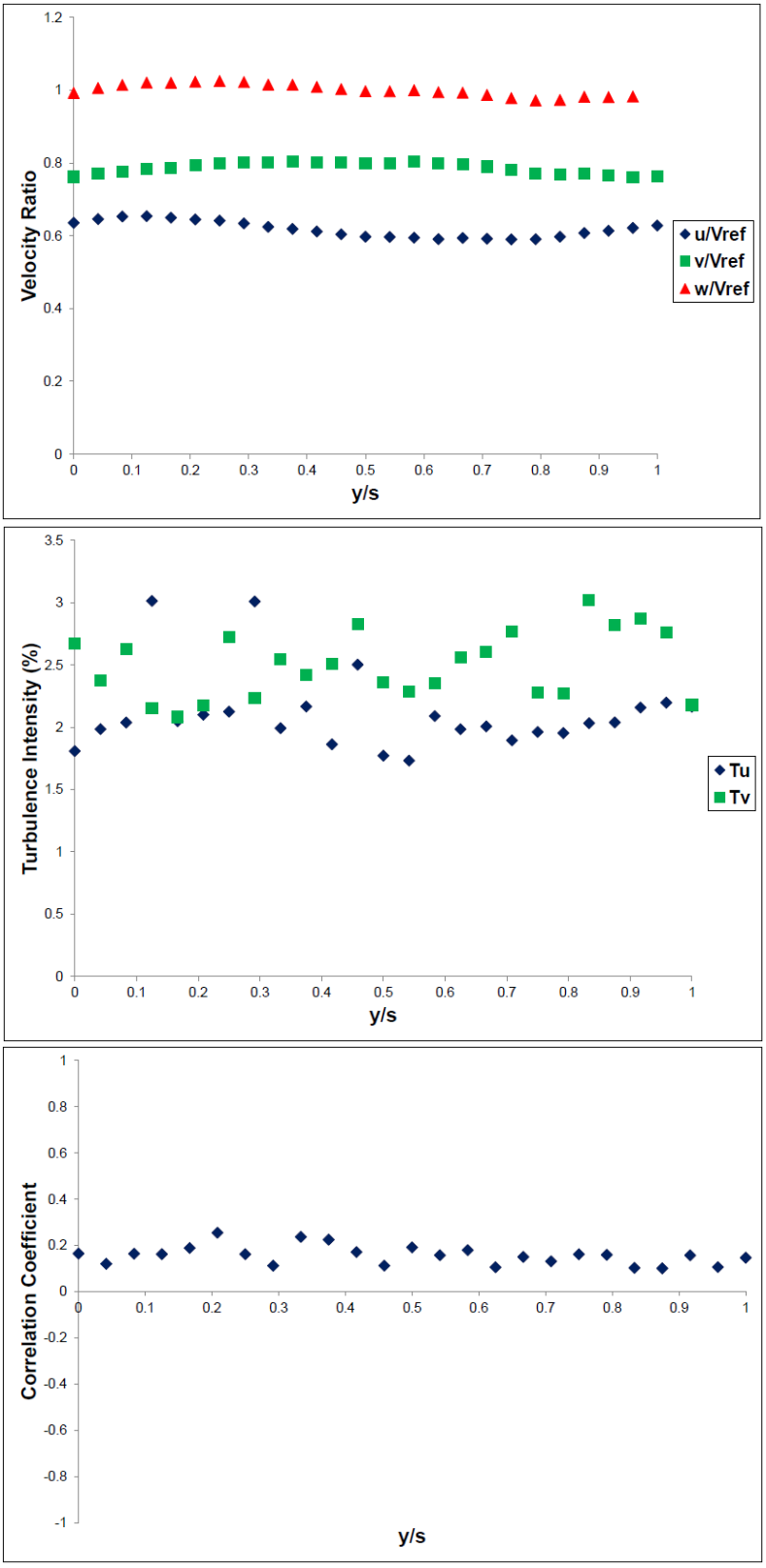

Figure 16. Station 1 inlet survey at Re = 203K

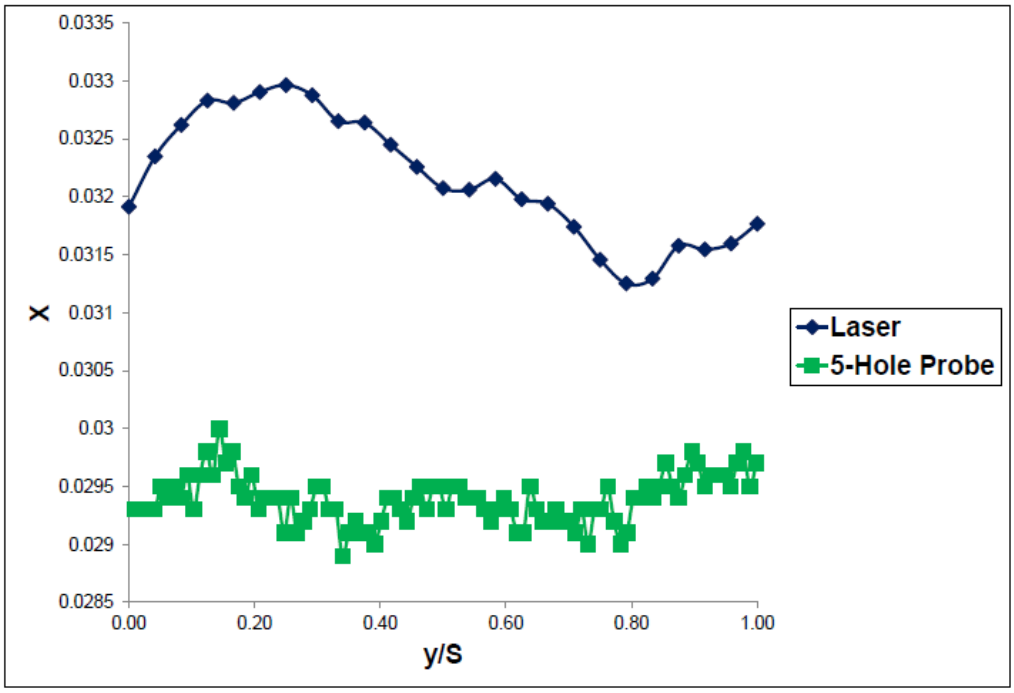

Figure 17. Inlet flow LDV and 5-hole probe comparison at Re = 203K

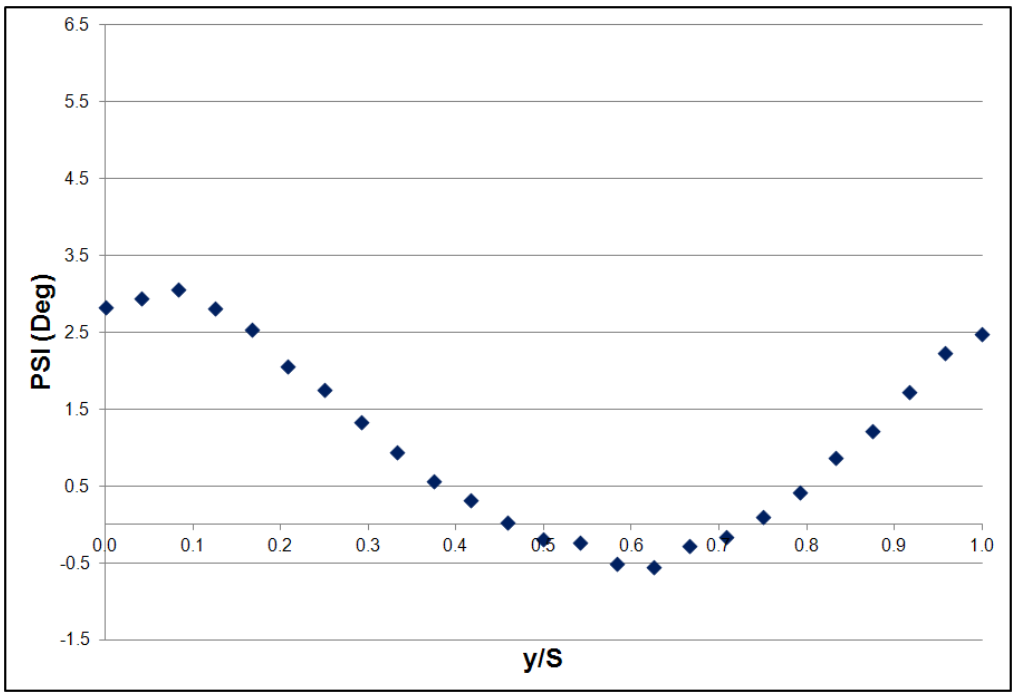

Figure 18. Station 1 LDV deviation from design inlet flow angle at Re = 203K

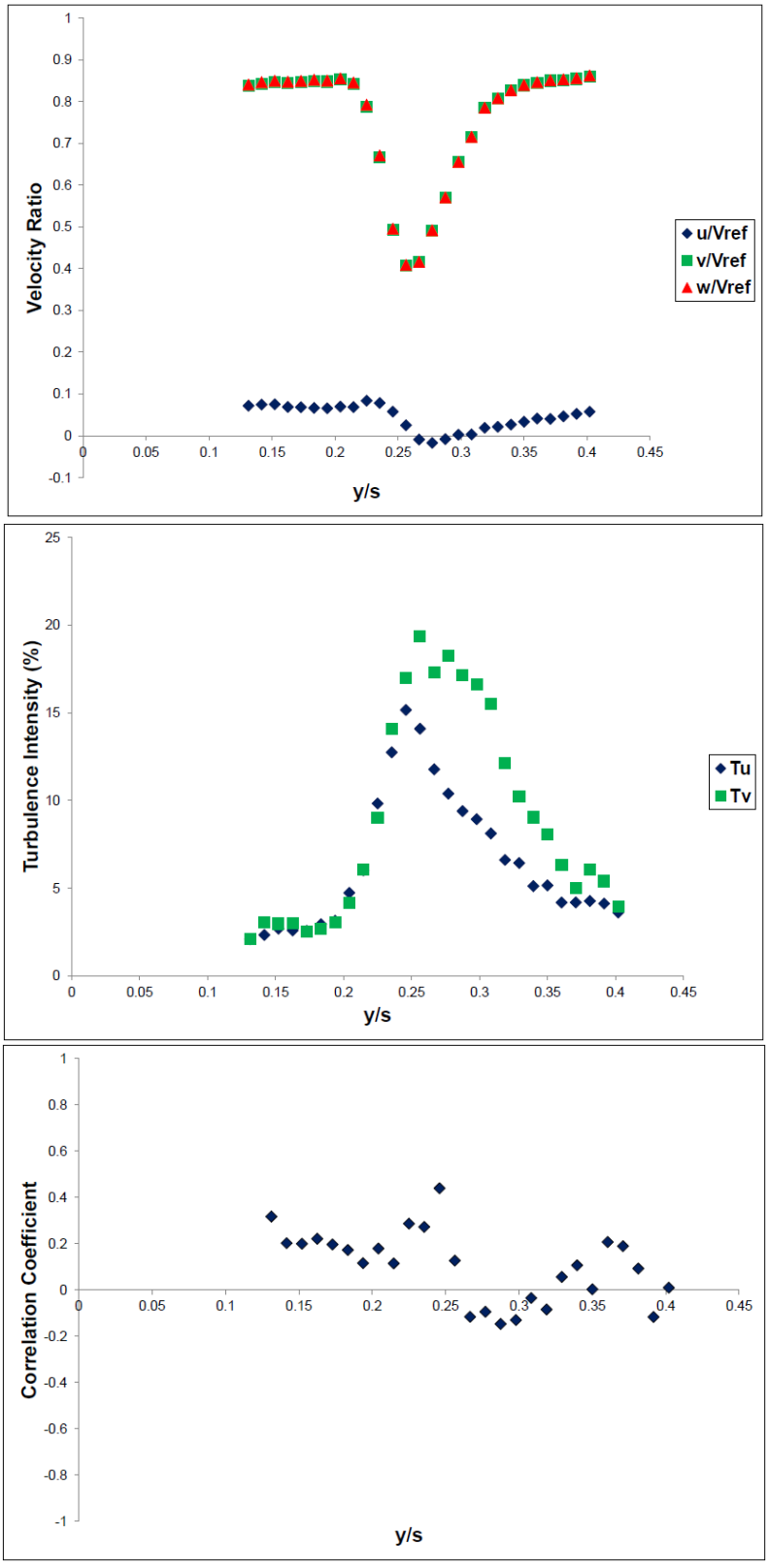

Figure 19. Station 13 blade 3 wake surveys at Re = 203K

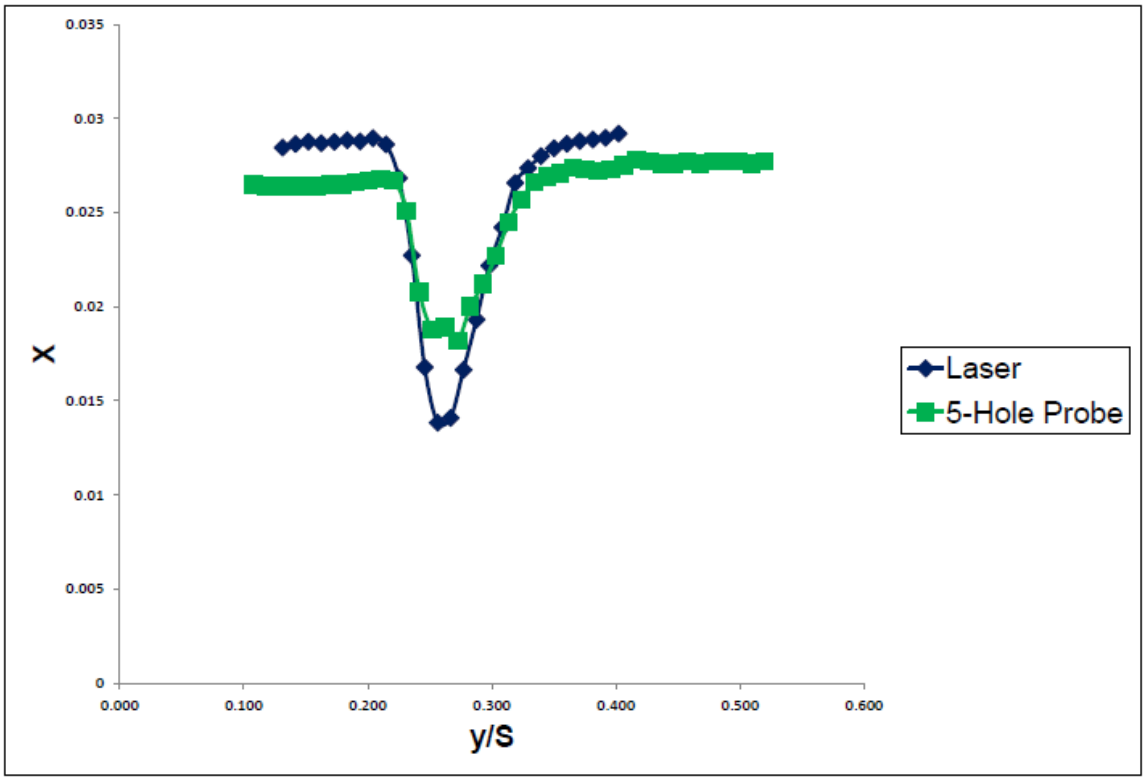

Figure 20. Blade 3 LDV and 5-hole probe wake survey comparison at Re = 203K

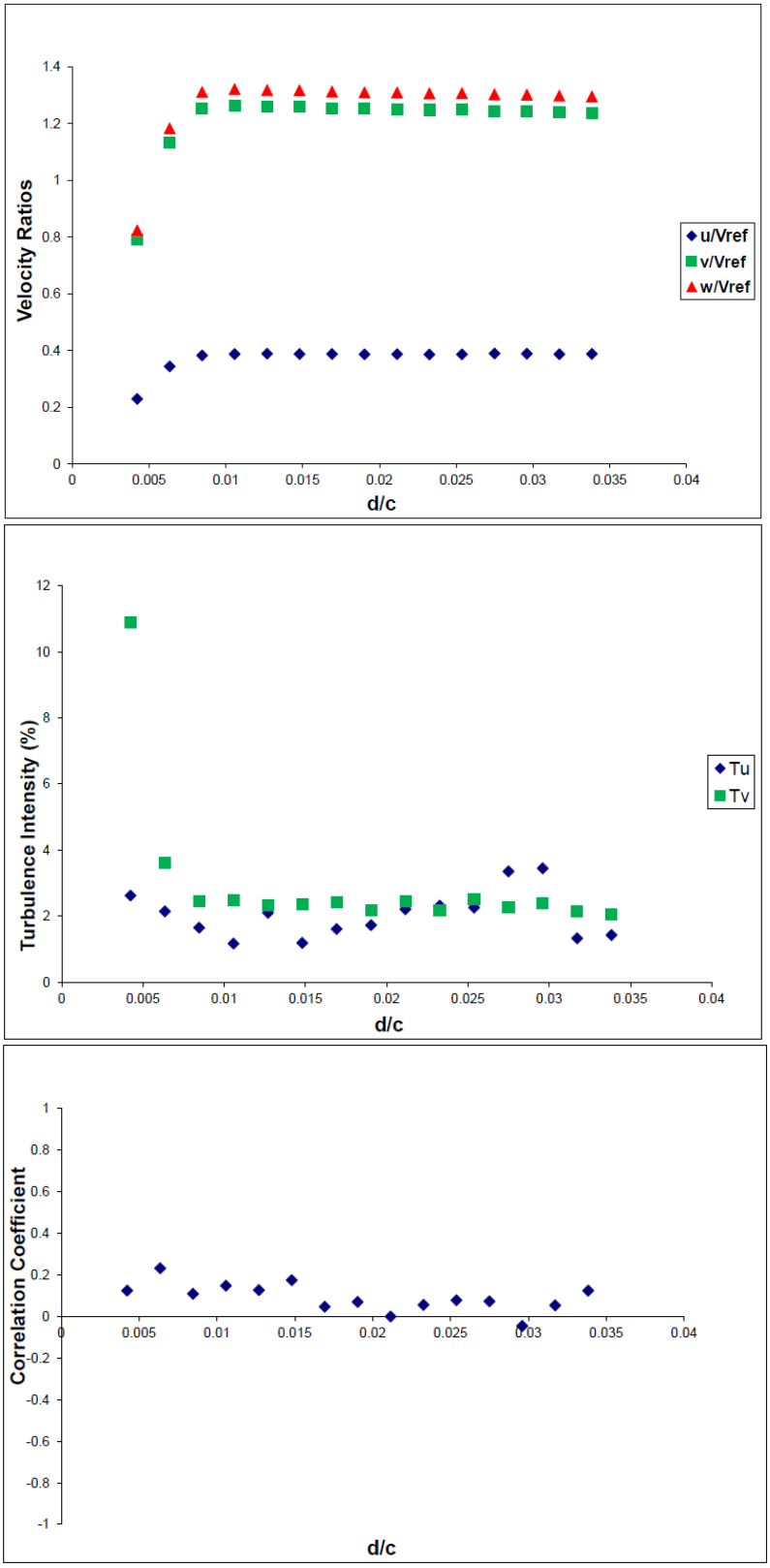

Figure 21. Station 6.75 boundary layer surveys

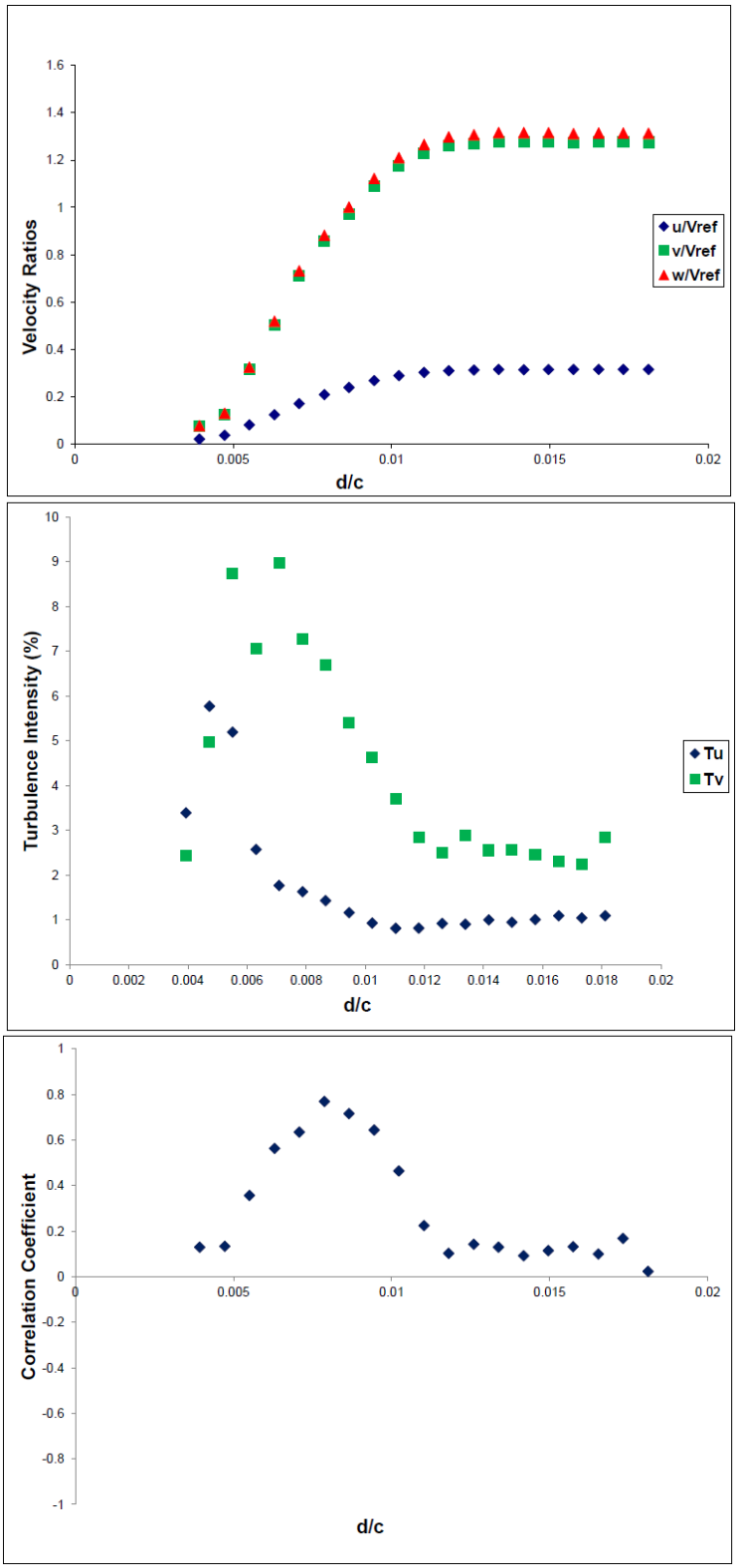

Figure 22. Station 7 boundary layer surveys

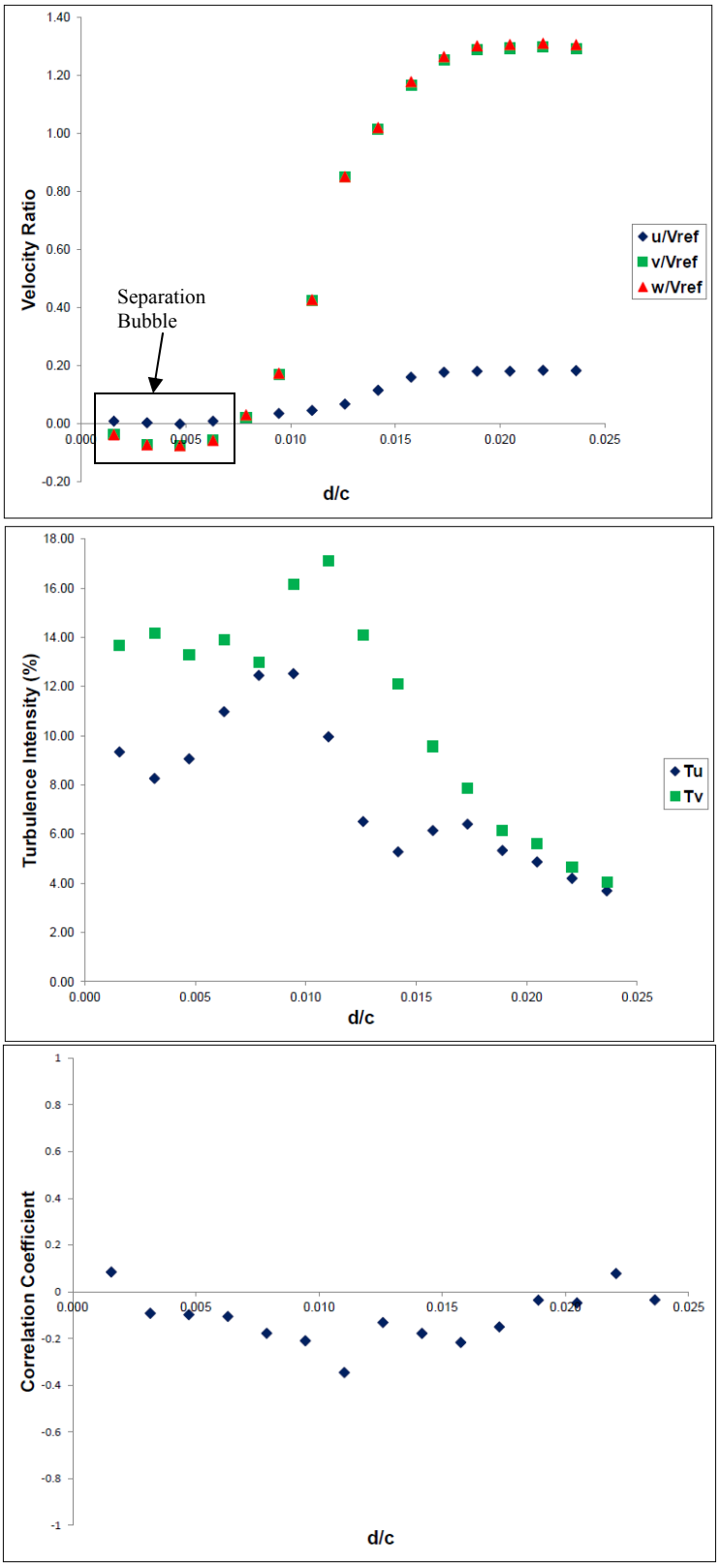

Figure 23. Station 7.25 boundary layer surveys

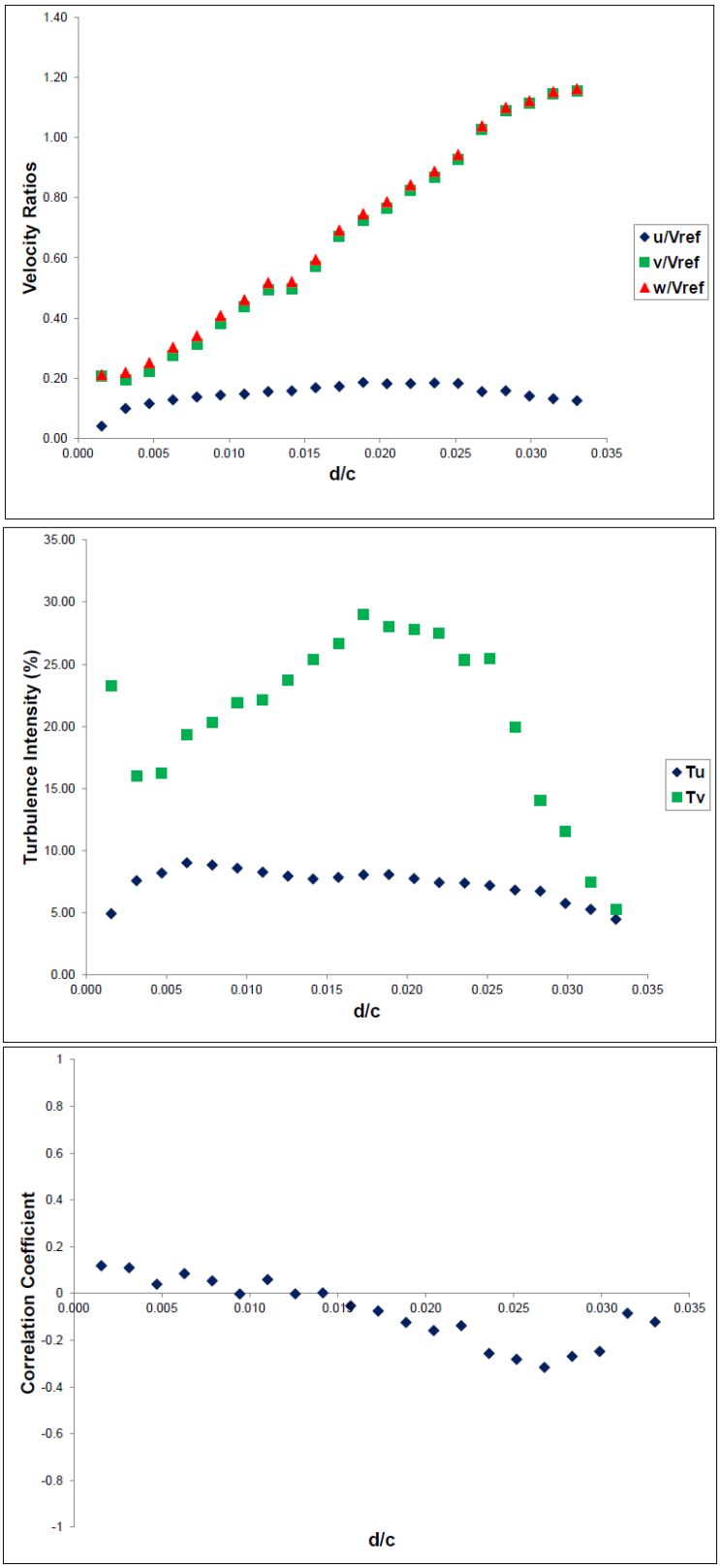

Figure 24. Station 7.5 boundary layer survey

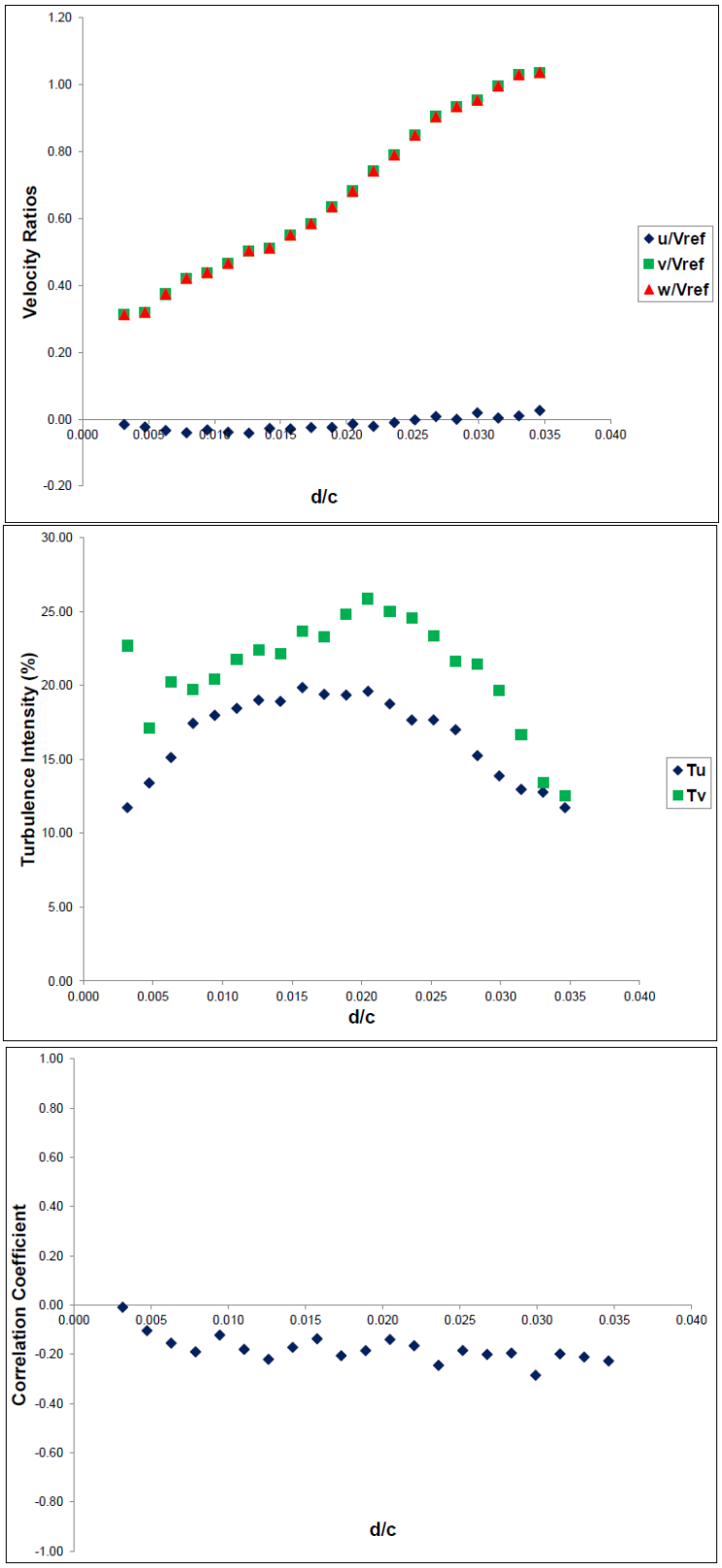

Figure 25. Station 7.75 boundary layer surveys

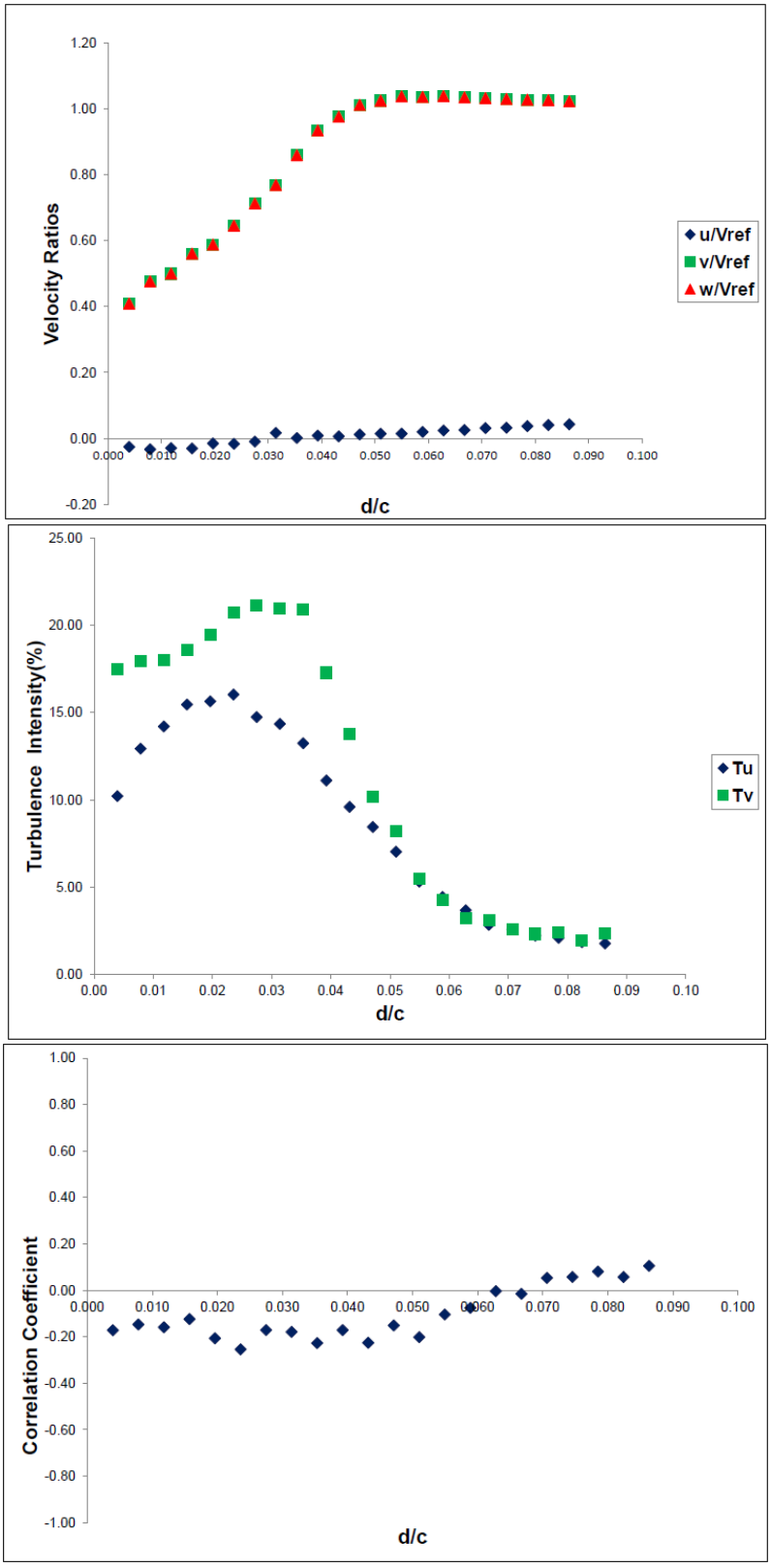

Figure 26. Station 8 boundary layer surveys

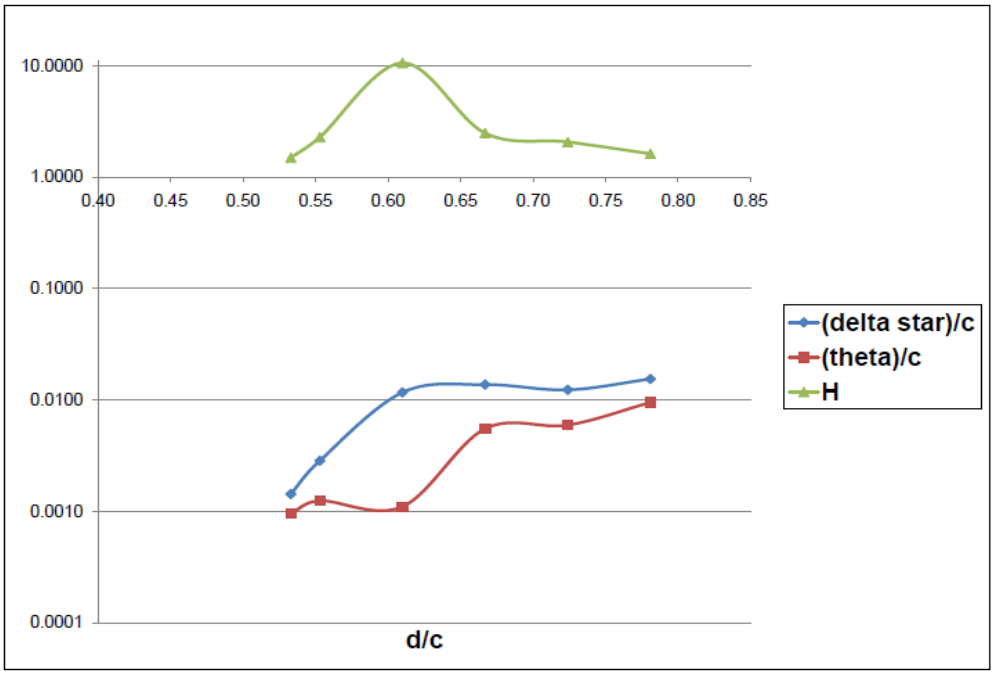

Figure 27. Boundary layer integral approximations

Survey Station	C_{ac} (mm)	(Displacement Thickness)/C	(Momentum Thickness)/C	H
6.75	0.5330	0.0014	0.0010	1.4946
7.00	0.5530	0.0028	0.0012	2.2819
7.25	0.6100	0.0117	0.0011	10.5743
7.50	0.6670	0.0137	0.0055	2.4843
7.75	0.7240	0.0123	0.0060	2.0684
8.00	0.7810	0.0154	0.0095	1.6224

Table 5. Boundary layer integral approximation chart

D. CFD RESULTS

The computational model successfully predicted the mid-span surface pressure distribution (Figure 28). There is a slight over prediction in the pressure side but the suction side was accurately modeled, including the separation bubble. The turbulent kinetic energy (TKE) distribution was plotted (Figure 29) and showed no variation in TKE in the free-stream. Examination of the TKE superimposed on recirculating streamlines within the predicted separation bubble (Figure 30) showed a large increase in the TKE in the recirculation region, which showed boundary layer transition occurred there.

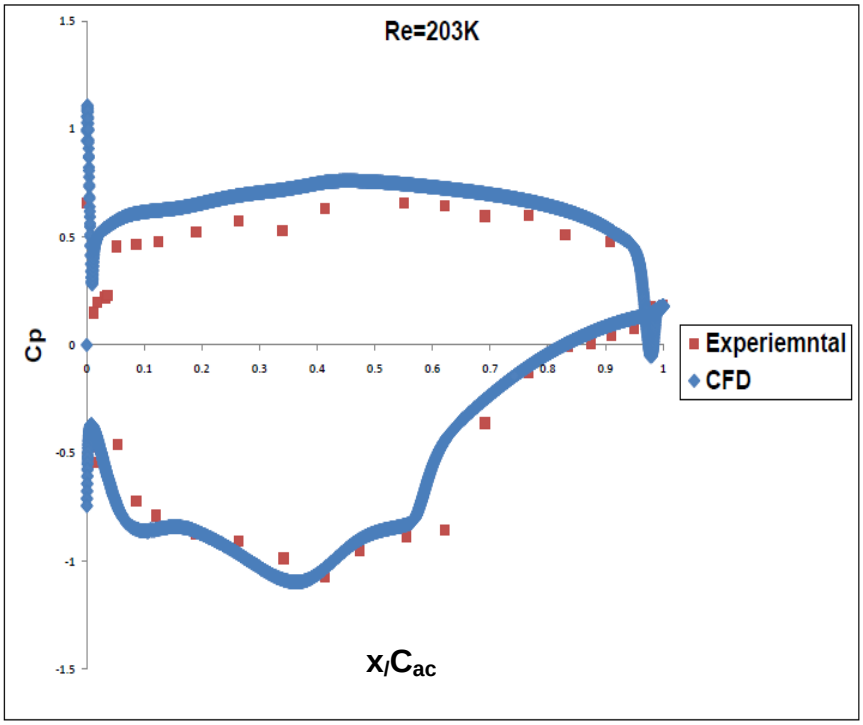

Figure 28. CFD and experimental surface pressure distribution

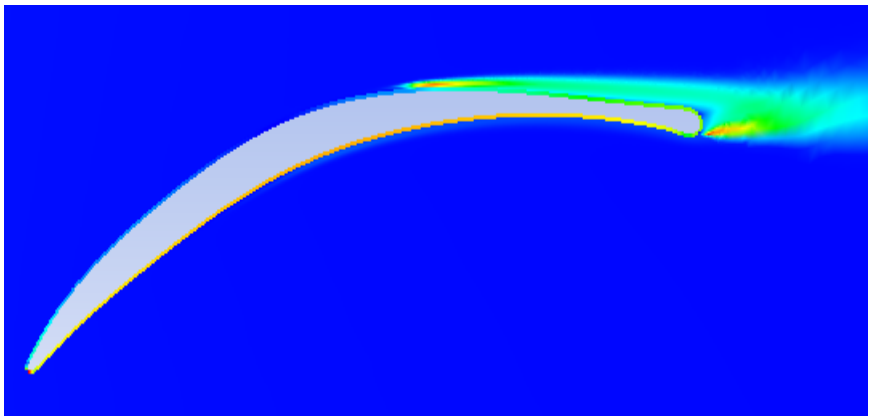

Figure 29. Turbulent kinetic energy distribution

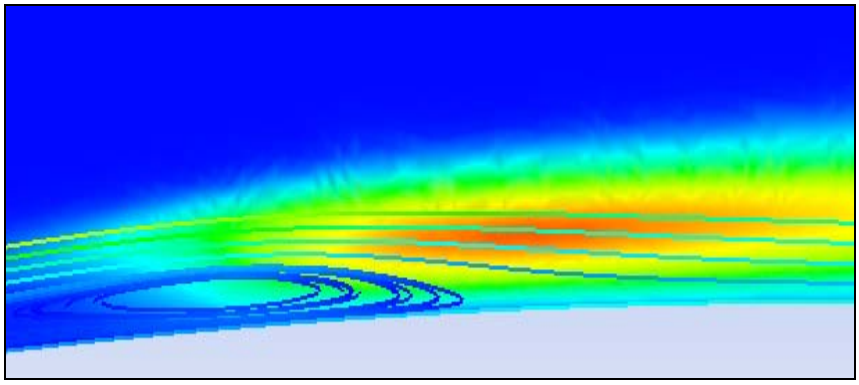

Figure 30. Turbulent kinetic superimposed on the streamlines

E. FLOW VISUALIZATION RESULTS

Flow visualization (Flow Viz) corroborated the flow characteristics measured during the LDV boundary layer surveys and provided insight into the time dependence of the separation bubble. The separation point was a smooth, stable line, which indicated laminar, time-invariant separation. The re-attachment region was turbulent, transient and three-dimensional and is depicted by Figure 31. Three-dimensional corner separation was evident at Re = 203K and illustrated the three dimensionality of the flow. The influence of the AVDR was evident in mid-span stream tube contraction (Figure 32).

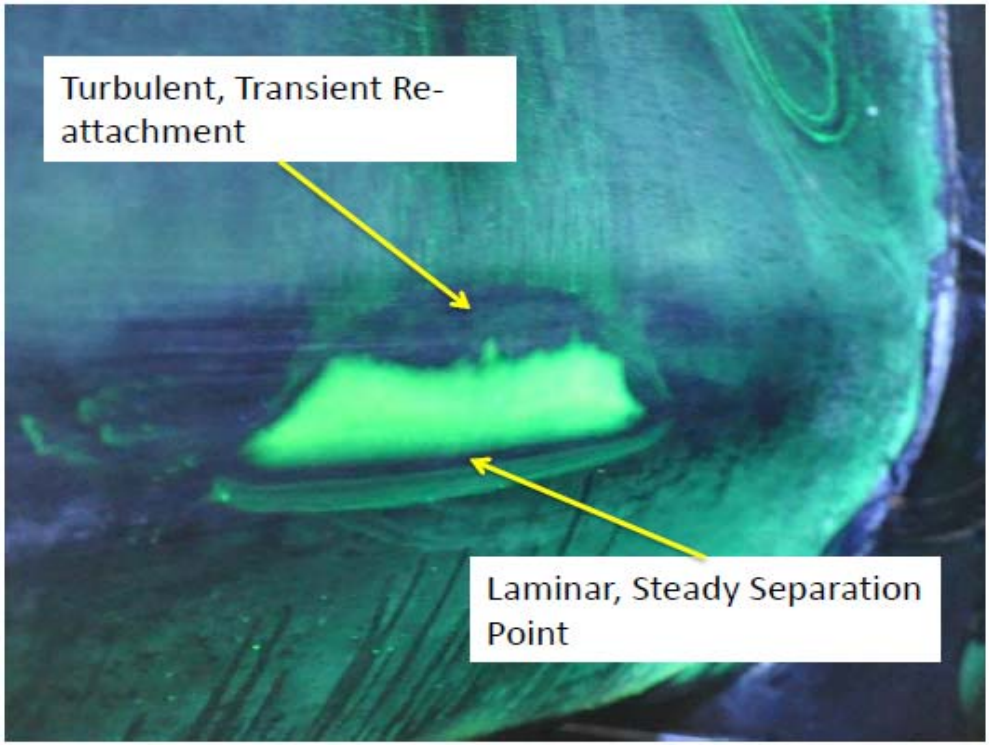

Figure 31. Suction-side separation bubble

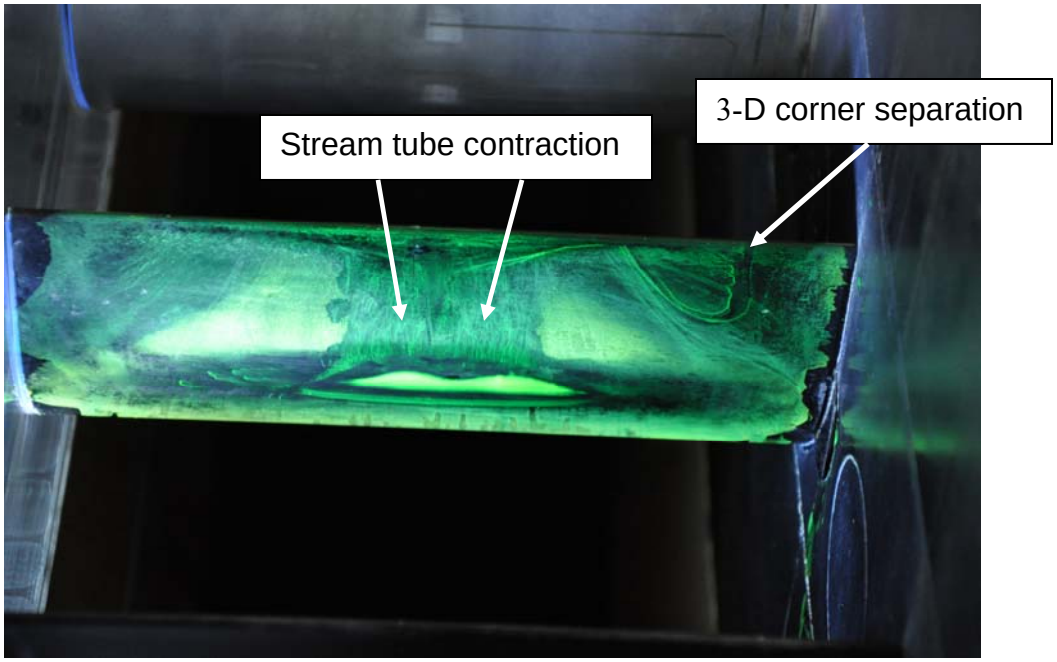

Figure 32. Blade 3 suction-side flow visualization

THIS PAGE INTENTIONALLY LEFT BLANK

VI. CONCLUSIONS AND RECOMMENDATIONS

A. CONCLUSIONS

The trailing edges of the NPS LSCWT IGVs were machined down to uniform trailing edge thickness, refurbished and reinstalled. Ten second-generation controlled-diffusion compressor-stator mid-span sections were polished to Ra < 0.38 μm, re-installed and set to the design inlet flow angle of 36 degrees. The IGVs and downstream tail boards were independently adjusted to attain inlet and outlet flow uniformity of 124 Pa (0.5 inches of water) as read by the water manometers. The instrumentation was upgraded to four DSAs and the data acquisition process was automated.

Blade 5 experimental midspan surface pressure measurements were obtained over the transitional range of flow. A suction side separation bubble and lower suction peak was evident at the lower Re. As the Re increased the bubble collapsed and the suction peak was recovered.

Five-hole probe inlet flow angle measurements showed a significant deviation from design at Re = 203K that contributed to the formation of the separation bubble. By Re = 400K the inlet flow had returned to design. Superimposed plots of blade 3 and 4 wakes show that by Re = 400K periodicity began to breakdown as the flow became fully three-dimensional. The loss was a maximum at Re = 203K, experienced a minimum value of 0.012 at Re = 400K and then moderately rose to a value of 0.014 as the design Re was approached. Therefore, the polished blades have an optimal Re = 400K.

Inlet and outlet flow was also characterized with two-component LDV at Re = 203K. The IFA variation was less severe than that measured by the 5-hole probe, but had a strong sinusoidal distribution. The outlet non-dimensional velocity distribution was calculated and differed by 8 percent from the 5-hole probe in the free-stream. The separation bubble at Re = 203K was fully documented by LDV measurements. At 53% C_{ac} the boundary layer was laminar and fully attached. At 61% C_{ac} the boundary layer had separated. By 67% C_{ac} the boundary layer was turbulent and re-attached.

A quasi-three-dimensional CFD model successfully predicted the low Re test case using a Reynolds-Averaged Navier Stokes solver. The surface pressure distribution suction-side separation bubble was predicted as evidenced by comparison to experimental data. Analysis of the turbulent kinetic energy distribution and stream lines showed that the boundary layer entered the separation bubble laminar and transitioned to turbulence inside the bubble, which was corroborated by LDV data. A transient analysis was done, which produced a movie that showed pulsing of the separation bubble, which was seen during flow visualization experiments.

B. RECOMMENDATIONS

This was the first study to be performed on the NPS LSCWT since the IGVs have been refurbished and the test blades polished. Therefore, the tunnel should be treated as a new tunnel and off mid span flow features should be investigated to determine end wall effects.

LDV surveys should be performed for the 5 higher Re not done in this study. LDV data and span-wise flow distribution information can be used as parameters for a three-dimensional computational model.

While the quasi-3-dimensional CFD model successfully predicted the flow features at mid-span determined by the experimental methods of this study, the flow field is unquestionably three-dimensional. Therefore, a fully three-dimensional computational model should be developed.

High Re, off design IFA testing should be performed to evaluate the stall characteristics of the polished blades.

APPENDIX A: DSA AND TRAVERSE INITIALIZATION

For the DSAs to work they must have the same IP addresses as the host computer with the exception of the last group of numbers. Figure 20 shows the front panel of the VEE pro program used to change the IP addresses of the DSAs. The IP address to be changed was entered in the "DSA Address" field. The desired IP Address was entered in the "Text" field. All four DSAs and the PC had "172.20.121.XXX" in their IP addresses, where "XXX" was selected by the user and uniquely identified the DSAs.

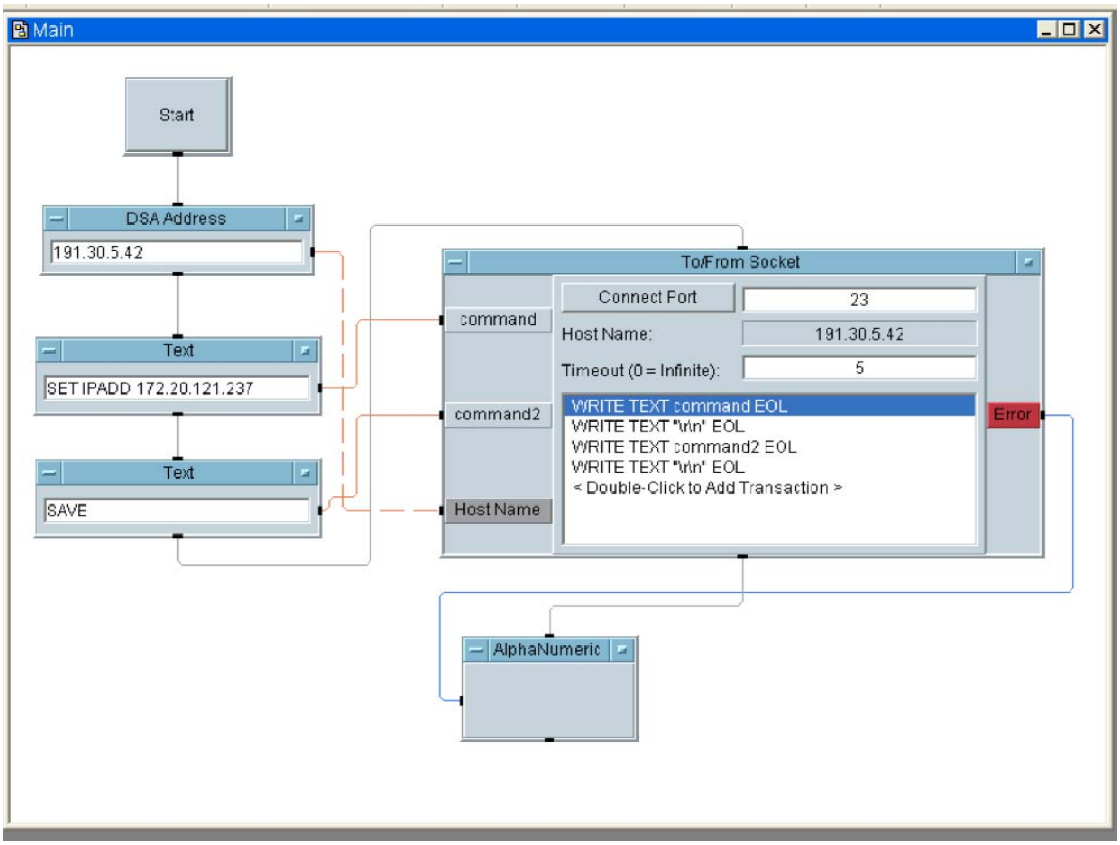

Figure 33. DSA IP addressing program

The text command in Figure 34 will initialize the traverse if it has been de-energized.

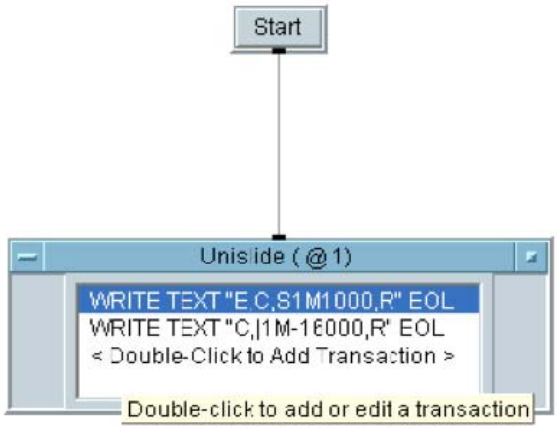

Figure 34. Traverse initialization script

APPENDIX B: MATLAB SCRIPT S9.M

```
% LT J. Carlson
% Modified by Dr. Anthony Gannon and LT Michael Holihan
% to automatically read the size of the beta, gamma and delta
% taxt files
% 5 Hole Probe Data Conversion
% s9.m
% This program reads the calibration coefficients obtained
% from calibration.m and uses them along with user inputs
% for beta, gamma and delta from SURVEY1 to determine X, Phi and Psi.


clear
clf

RESULT  = dlmread('s9bgd.txt','\t',1,0);
beta(:,1) = RESULT(:,1);
gamma(:,1)= RESULT(:,2);
delta(:,1)= RESULT(:,3);


%Set Parameters
L=7;
M=7;
N=6;

c=zeros(1,294);
d=zeros(1,294);
e=zeros(1,294);

C=wk1read('C');
D=wk1read('D');
E=wk1read('E');

z=size(RESULT,1); %number of measurements recorded
LOC=zeros(z,1);
X=zeros(z,1);
PHI=zeros(z,1);
PSI=zeros(z,1);
R=zeros(z,4);

%load s9bgd.dat
%beta(:,1)=s9bgd(:,1);
%gamma(:,1)=s9bgd(:,2);
%delta(:,1)=s9bgd(:,3);

%Probe location
count=.25;
for q=1:z
   LOC(q)=count;
```

```
   count=count+.25;
end

%solve for X, PHI, PSI

for l=1:z

%Mach Number

count=1;
  for i=1:L
      for j=1:M
          for k=1:N
              term1(l)=beta(l)^(k-1);
              term2(l)=gamma(l)^(j-1);
              term3(l)=delta(l)^(i-1);
              c(count)=term1(l)*term2(l)*term3(l);
              count=count+1;
          end
      end
  end
  X(l,1)=c*C;
%Phi
count=1;
  for i=1:L
      for j=1:M
          for k=1:N
              term1(l)=beta(l)^(k-1);
              term2(l)=gamma(l)^(j-1);
              term3(l)=delta(l)^(i-1);
              d(count)=term1(l)*term2(l)*term3(l);
              count=count+1;
          end
      end
  end
  PHI(l,1)=d*D;
%Psi
count=1;
  for i=1:L
      for j=1:M
          for k=1:N
              term1(l)=beta(l)^(k-1);
              term2(l)=gamma(l)^(j-1);
              term3(l)=delta(l)^(i-1);
              e(count)=term1(l)*term2(l)*term3(l);
              count=count+1;
          end
      end
  end
  PSI(l,1)=e*E;


end
```

```
%disp('This program reads in beta, gamma, and delta information from a
')
%disp('5 hole probe survey and outputs probe location, X, PHI, and
PSI.')
%disp('  ')
%disp('Note: The probe position at the start of this test was at 8.75
inches ')
%disp('on a traverse scale.  This corresponds to the point even with
the ')
%disp('leading edge of the third blade.  Measurements were taken at .25
inch ')
%disp('intervals for a total of twelve inches ending past the trailing
edge ')
%disp('of trailing edge of blade four.')
%disp('  ')

R(:,1)=LOC(:,1);
R(:,2)=X(:,1);
R(:,3)=PHI(:,1);
R(:,4)=PSI(:,1);


%format short
%disp('    Location     X       PHI        PSI   ')

%R
X
PSI

figure(1)
plot(LOC,X)
title('Survey 9in Re=510K')
xlabel('Traverse position')
ylabel('X')
legend
figure(2)
plot(LOC,PHI,'g+',LOC,PSI,'bd')
title('Survey 9in Re=510K')
xlabel('Traverse position')
ylabel('Pitch (PHI) and Yaw (PSI) Sensivity')
legend
figure(3)
plot(LOC,PHI,'c',LOC,PSI,'b')
title('Survey 9in Re=510K')
xlabel('Traverse position')
ylabel('Pitch (PHI) and Yaw (PSI) Sensivity')
legend
```

THIS PAGE INTENTIONALLY LEFT BLANK

APPENDIX C: S9.M OUTPUT

Downstream

X	PSI(deg)	PSI(rad)
0.0245	-6.1175	-0.106770517
0.0246	-5.5038	-0.096059431
0.0247	-6.0958	-0.106391781
0.0246	-6.3466	-0.110769066
0.0248	-4.178	-0.072919856
0.0246	-4.1384	-0.072228706
0.0248	-3.7435	-0.065336401
0.0246	-3.5888	-0.062636376
0.0245	-3.1553	-0.055070374
0.025	-2.8425	-0.049610984
0.0249	-3.1524	-0.055019759
0.0248	-2.2554	-0.039364156
0.0248	-1.6765	-0.029260445
0.0249	-0.8965	-0.015646877
0.0252	-1.0124	-0.017669713
0.0251	-0.4944	-0.008628908
0.0249	0.8161	0.014243632
0.025	0.0683	0.00119206
0.0252	0.402	0.007016224
0.0251	0.527	0.009197885
0.0252	1.8856	0.032909928
0.0255	0.6129	0.010697123
0.0251	2.0097	0.035075882
0.0253	0.3096	0.005403539
0.0252	2.0448	0.035688493
0.0253	2.0723	0.036168458
0.0254	1.8523	0.032328734
0.0256	-0.691	-0.012060225
0.0244	-0.7319	-0.012774065
0.0204	-3.2289	-0.056354936
0.0151	-1.2617	-0.022020819
0.0183	7.5582	0.131915476
0.0162	9.2785	0.161940375
0.0174	8.6521	0.151007632
0.0192	8.0745	0.14092661
0.0201	7.5463	0.131707781
0.0217	7.6078	0.132781159
0.0235	6.9549	0.121385904
0.0248	6.6314	0.115739764
0.0255	6.0355	0.105339347
0.0257	5.6672	0.098911299
0.0261	5.2588	0.091783375
0.026	5.2317	0.09131039
0.0259	4.8617	0.084852672
0.026	4.6589	0.081313145
0.0262	4.3016	0.075077083
0.0261	3.6017	0.062861524

0.0262	3.1635	0.055213491
0.0262	2.8774	0.050220104
0.0261	1.9332	0.033740705
0.0261	0.8503	0.014840535
0.0263	1.1651	0.020334831
0.0263	0.3889	0.006787585
0.0264	0.0663	0.001157153
0.0263	-0.1774	-0.003096214
0.0262	-1.3303	-0.023218115
0.0263	-1.2076	-0.021076596
0.0261	-1.8742	-0.032710961
0.0261	-1.4091	-0.024593434
0.0261	-2.2422	-0.039133772
0.026	-3.1464	-0.05491504
0.026	-2.9268	-0.051082297
0.0259	-3.1789	-0.055482272
0.0259	-4.1689	-0.072761031
0.0258	-4.0935	-0.071445053
0.0257	-4.5457	-0.079337432
0.0257	-5.1828	-0.090456924
0.0255	-4.543	-0.079290308
0.0257	-5.4285	-0.094745198
0.0255	-5.6536	-0.098673935
0.0255	-5.7186	-0.099808399
0.0254	-6.7923	-0.118547999
0.0254	-6.0408	-0.105431849
0.0251	-7.1273	-0.124394852
0.0252	-7.0021	-0.1222097
0.0249	-7.046	-0.122975899
0.0252	-7.289	-0.127217049
0.025	-8.1602	-0.142422358
0.0253	-7.668	-0.133831847
0.025	-7.2895	-0.127225776
0.0249	-6.5997	-0.115186495
0.0248	-7.0289	-0.122677448
0.0252	-8.0083	-0.139771202
0.0247	-7.8993	-0.137868794
0.0248	-8.0213	-0.139998095
0.0251	-7.1316	-0.124469901
0.0251	-7.1586	-0.12494114
0.0252	-7.0294	-0.122686174
0.0253	-6.4517	-0.112603407
0.025	-6.758	-0.117949351
0.025	-6.0902	-0.106294042
0.0251	-6.6546	-0.11614468
0.0252	-5.8284	-0.10172477
0.025	-6.3331	-0.110533447
0.0252	-5.1568	-0.090003139
0.0252	-5.1816	-0.090435981

Upstream

X	PSI(deg)	BETA	BETA (rad)
0.0293	5.8858	42.8858	0.7484984
0.0293	5.8044	42.8044	0.7470777
0.0293	5.81	42.81	0.7471755
0.0293	5.8776	42.8776	0.7483553
0.0295	5.7696	42.7696	0.7464703
0.0294	5.7124	42.7124	0.745472
0.0295	5.7419	42.7419	0.7459869
0.0294	5.9412	42.9412	0.7494653
0.0296	5.7341	42.7341	0.7458507
0.0293	5.8014	42.8014	0.7470254
0.0296	5.7434	42.7434	0.7460131
0.0298	5.6591	42.6591	0.7445418
0.0296	5.8057	42.8057	0.7471004
0.03	5.5171	42.5171	0.7420634
0.0297	5.7647	42.7647	0.7463848
0.0298	5.7516	42.7516	0.7461562
0.0295	5.8358	42.8358	0.7476257
0.0294	5.9267	42.9267	0.7492123
0.0296	5.5627	42.5627	0.7428593
0.0293	5.8686	42.8686	0.7481982
0.0294	5.6312	42.6312	0.7440548
0.0294	5.8429	42.8429	0.7477497
0.0294	5.7082	42.7082	0.7453987
0.0291	5.7636	42.7636	0.7463656
0.0294	5.6936	42.6936	0.7451439
0.0291	5.7498	42.7498	0.7461248
0.0292	5.8083	42.8083	0.7471458
0.0293	5.6267	42.6267	0.7439763
0.0295	5.5011	42.5011	0.7417841
0.0295	5.5847	42.5847	0.7432432
0.0293	5.7274	42.7274	0.7457338
0.0293	5.7896	42.7896	0.7468194
0.0289	5.7696	42.7696	0.7464703
0.0291	5.7403	42.7403	0.745959
0.0292	5.7383	42.7383	0.7459241
0.0291	5.6631	42.6631	0.7446116
0.0291	5.7335	42.7335	0.7458403
0.029	5.8003	42.8003	0.7470062
0.0292	5.5846	42.5846	0.7432415
0.0294	5.7089	42.7089	0.7454109
0.0294	5.6944	42.6944	0.7451579
0.0293	5.7259	42.7259	0.7457076
0.0292	5.7996	42.7996	0.7469939
0.0294	5.6944	42.6944	0.7451579
0.0295	5.6543	42.6543	0.744458
0.0293	5.6887	42.6887	0.7450584
0.0295	5.6788	42.6788	0.7448856
0.0295	5.7584	42.7584	0.7462749

0.0293	5.6976	42.6976	0.7452137
0.0295	5.6672	42.6672	0.7446831
0.0295	5.6604	42.6604	0.7445644
0.0294	5.9195	42.9195	0.7490866
0.0294	5.8522	42.8522	0.747912
0.0294	5.8512	42.8512	0.7478945
0.0293	5.742	42.742	0.7459886
0.0292	5.9186	42.9186	0.7490709
0.0293	5.8859	42.8859	0.7485002
0.0294	5.8451	42.8451	0.7477881
0.0293	5.7287	42.7287	0.7457565
0.0291	5.9852	42.9852	0.7502333
0.0291	5.8171	42.8171	0.7472994
0.0295	5.8351	42.8351	0.7476135
0.0293	5.7833	42.7833	0.7467094
0.0292	5.876	42.876	0.7483274
0.0292	5.9359	42.9359	0.7493728
0.0293	5.9487	42.9487	0.7495962
0.0292	5.8231	42.8231	0.7474041
0.0292	5.9163	42.9163	0.7490307
0.0291	5.9276	42.9276	0.749228
0.0293	5.8026	42.8026	0.7470463
0.029	5.93	42.93	0.7492698
0.0293	5.9992	42.9992	0.7504776
0.0293	5.8608	42.8608	0.7480621
0.0295	5.8424	42.8424	0.7477409
0.0292	5.9158	42.9158	0.749022
0.029	5.9635	42.9635	0.7498545
0.0291	5.9882	42.9882	0.7502856
0.0294	5.963	42.963	0.7498458
0.0294	5.8644	42.8644	0.7481249
0.0295	5.8351	42.8351	0.7476135
0.0294	5.891	42.891	0.7485892
0.0295	5.8469	42.8469	0.7478195
0.0297	5.7052	42.7052	0.7453463
0.0295	5.8527	42.8527	0.7479207
0.0294	5.8736	42.8736	0.7482855
0.0296	5.8584	42.8584	0.7480202
0.0298	5.7639	42.7639	0.7463709
0.0297	5.8321	42.8321	0.7475612
0.0295	5.8475	42.8475	0.74783
0.0296	5.7754	42.7754	0.7465716
0.0296	5.8272	42.8272	0.7474756
0.0296	5.7702	42.7702	0.7464808
0.0295	5.8993	42.8993	0.748734
0.0297	5.8287	42.8287	0.7475018
0.0298	5.7017	42.7017	0.7452853
0.0295	5.8351	42.8351	0.7476135
0.0297	5.8117	42.8117	0.7472051

Table 6. Re = 203,000 S9.M output

Downstream

X	PSI(deg)	PSI(rad)
0.0352	-5.5503	-0.09687
0.0354	-5.6528	-0.09866
0.0356	-5.1027	-0.08906
0.0353	-5.294	-0.0924
0.0356	-5.1341	-0.08961
0.0353	-4.9819	-0.08695
0.0354	-5.0873	-0.08879
0.0352	-4.608	-0.08042
0.0354	-4.6264	-0.08075
0.0352	-3.826	-0.06678
0.0351	-3.7137	-0.06482
0.0349	-3.2552	-0.05681
0.0353	-2.8242	-0.04929
0.0353	-2.3767	-0.04148
0.0354	-2.4182	-0.04221
0.035	-2.1248	-0.03708
0.0352	-1.8511	-0.03231
0.0353	-1.3216	-0.02307
0.0352	-1.0664	-0.01861
0.0354	-0.6378	-0.01113
0.0353	-0.1949	-0.0034
0.0354	-0.1808	-0.00316
0.0353	0.1772	0.003093
0.0351	0.1556	0.002716
0.0355	0.4994	0.008716
0.0355	0.4962	0.00866
0.0357	0.5141	0.008973
0.0357	0.2149	0.003751
0.0341	-0.5773	-0.01008
0.0277	0.0257	0.000449
0.0217	3.4274	0.059819
0.0223	7.9196	0.138223
0.0244	7.5037	0.130964
0.0269	6.4048	0.111785
0.0299	5.8845	0.102704
0.033	4.8884	0.085319
0.0352	4.1367	0.072199
0.0359	3.7472	0.065401
0.0364	3.2706	0.057083
0.0366	2.9257	0.051063
0.0365	2.7452	0.047913
0.0366	2.317	0.040439
0.0368	2.1765	0.037987
0.0368	1.6968	0.029615
0.0371	1.5463	0.026988
0.037	1.2744	0.022242
0.0371	1.0262	0.017911

0.037	0.7241	0.012638
0.0372	0.5918	0.010329
0.0373	0.1609	0.002808
0.0375	-0.1335	-0.00233
0.0375	-0.4551	-0.00794
0.0377	-0.7715	-0.01347
0.0375	-1.125	-0.01963
0.0373	-1.554	-0.02712
0.0375	-1.6694	-0.02914
0.0373	-1.9496	-0.03403
0.0373	-2.1149	-0.03691
0.0374	-2.7319	-0.04768
0.0372	-3.0773	-0.05371
0.0372	-2.8719	-0.05012
0.0371	-3.5182	-0.0614
0.0373	-3.5829	-0.06253
0.0368	-3.5762	-0.06242
0.037	-4.3363	-0.07568
0.0369	-4.2847	-0.07478
0.0372	-4.9763	-0.08685
0.0366	-5.2205	-0.09111
0.0369	-5.2329	-0.09133
0.0369	-5.1451	-0.0898
0.0366	-5.7753	-0.1008
0.0367	-5.9582	-0.10399
0.0367	-6.3235	-0.11037
0.0365	-6.2853	-0.1097
0.0363	-5.9481	-0.10381
0.0363	-6.5029	-0.1135
0.0359	-6.5807	-0.11485
0.0358	-6.9424	-0.12117
0.0355	-6.4581	-0.11272
0.0358	-6.9391	-0.12111
0.0359	-6.7223	-0.11733
0.0357	-6.8943	-0.12033
0.0359	-6.6741	-0.11649
0.0357	-6.4764	-0.11303
0.0356	-6.4857	-0.1132
0.0359	-6.3175	-0.11026
0.0358	-6.3115	-0.11016
0.0358	-6.0129	-0.10494
0.036	-5.892	-0.10283
0.0357	-5.8983	-0.10294
0.0359	-5.729	-0.09999
0.0358	-5.362	-0.09358
0.0355	-5.5603	-0.09705
0.0355	-5.5138	-0.09623
0.0356	-5.3242	-0.09292
0.0355	-4.9274	-0.086

Upstream

X	PSI(deg)	BETA	BETA (rad)
0.0434	2.365	39.365	0.6870489
0.0438	2.3179	39.3179	0.6862268
0.0437	2.3628	39.3628	0.6870105
0.0434	2.3983	39.3983	0.6876301
0.0432	2.1888	39.1888	0.6839736
0.0432	2.4336	39.4336	0.6882462
0.043	2.3936	39.3936	0.687548
0.0432	2.3601	39.3601	0.6869633
0.0434	2.3727	39.3727	0.6871833
0.0434	2.1571	39.1571	0.6834203
0.0432	2.449	39.449	0.6885149
0.0437	2.1364	39.1364	0.683059
0.0432	2.3476	39.3476	0.6867452
0.0433	2.2894	39.2894	0.6857294
0.0434	2.1756	39.1756	0.6837432
0.0433	2.2304	39.2304	0.6846996
0.0433	1.9243	38.9243	0.6793572
0.0432	2.1085	39.1085	0.6825721
0.0432	2.2451	39.2451	0.6849562
0.0433	2.1324	39.1324	0.6829892
0.0433	2.3699	39.3699	0.6871344
0.0432	2.4291	39.4291	0.6881676
0.0432	2.2662	39.2662	0.6853245
0.0434	2.3034	39.3034	0.6859737
0.0438	2.1115	39.1115	0.6826245
0.0433	2.3464	39.3464	0.6867242
0.0437	2.0955	39.0955	0.6823452
0.044	2.0962	39.0962	0.6823574
0.0437	2.1334	39.1334	0.6830067
0.0438	2.1689	39.1689	0.6836263
0.0437	2.2373	39.2373	0.6848201
0.0435	2.3977	39.3977	0.6876196
0.0436	2.1166	39.1166	0.6827135
0.0437	2.1112	39.1112	0.6826192
0.044	2.2926	39.2926	0.6857852
0.0437	2.1085	39.1085	0.6825721
0.0442	2.0618	39.0618	0.681757
0.0436	2.4113	39.4113	0.6878569
0.0438	2.1519	39.1519	0.6833296
0.0437	2.1387	39.1387	0.6830992
0.0441	2.0608	39.0608	0.6817396
0.0436	2.2587	39.2587	0.6851936
0.0439	2.1371	39.1371	0.6830713
0.044	2.1717	39.1717	0.6836751
0.0437	2.3259	39.3259	0.6863664
0.0439	2.1604	39.1604	0.6834779
0.0441	2.2025	39.2025	0.6842127
0.0442	2.2012	39.2012	0.68419

0.0441	2.3422	39.3422	0.6866509
0.0443	2.0916	39.0916	0.6822771
0.0442	2.3513	39.3513	0.6868097
0.0437	2.353	39.353	0.6868394
0.0439	2.2419	39.2419	0.6849004
0.0437	2.3043	39.3043	0.6859894
0.0436	2.3048	39.3048	0.6859982
0.0436	2.2719	39.2719	0.685424
0.0437	2.2875	39.2875	0.6856962
0.0438	2.2962	39.2962	0.6858481
0.0437	2.3188	39.3188	0.6862425
0.0439	2.2482	39.2482	0.6850103
0.0439	2.4173	39.4173	0.6879617
0.0439	2.3463	39.3463	0.6867225
0.0441	2.2026	39.2026	0.6842144
0.044	2.3988	39.3988	0.6876388
0.0443	2.2946	39.2946	0.6858201
0.044	2.1953	39.1953	0.684087
0.0439	2.5181	39.5181	0.689721
0.044	2.3829	39.3829	0.6873613
0.0438	2.3048	39.3048	0.6859982
0.0439	2.3216	39.3216	0.6862914
0.0433	2.5406	39.5406	0.6901137
0.0434	2.439	39.439	0.6883404
0.0435	2.3584	39.3584	0.6869337
0.0435	2.4523	39.4523	0.6885725
0.0435	2.5304	39.5304	0.6899356
0.0439	2.4162	39.4162	0.6879425
0.0436	2.4976	39.4976	0.6893632
0.0439	2.4118	39.4118	0.6878657
0.0438	2.5078	39.5078	0.6895412
0.0439	2.3399	39.3399	0.6866108
0.044	2.1939	39.1939	0.6840626
0.0447	2.2348	39.2348	0.6847764
0.0443	2.2267	39.2267	0.6846351
0.0444	2.3201	39.3201	0.6862652
0.044	2.4556	39.4556	0.6886301
0.0441	2.4419	39.4419	0.688391
0.0442	2.4025	39.4025	0.6877034
0.0443	2.355	39.355	0.6868743
0.0442	2.4464	39.4464	0.6884696
0.044	2.5435	39.5435	0.6901643
0.0441	2.4486	39.4486	0.688508
0.0445	2.4008	39.4008	0.6876737
0.0444	2.4072	39.4072	0.6877854
0.0446	2.3868	39.3868	0.6874293
0.0444	2.4717	39.4717	0.6889111
0.0447	2.423	39.423	0.6880612
0.0444	2.4757	39.4757	0.6889809

Table 7. Re = 259,000 S9.M output

Downstream

X	PSI(deg)	PSI(rad)
0.0515	-5.344	-0.09327
0.0512	-5.5223	-0.09638
0.0508	-5.1231	-0.08941
0.0508	-5.2256	-0.0912
0.0509	-4.7471	-0.08285
0.0509	-4.7893	-0.08359
0.0509	-4.6648	-0.08142
0.0508	-4.3767	-0.07639
0.0507	-4.1967	-0.07325
0.0508	-4.0282	-0.07031
0.051	-3.8344	-0.06692
0.0506	-3.5799	-0.06248
0.05	-3.4442	-0.06011
0.0507	-3.0936	-0.05399
0.0504	-2.869	-0.05007
0.0502	-2.849	-0.04972
0.0504	-2.5479	-0.04447
0.0507	-2.3889	-0.04169
0.0505	-2.0032	-0.03496
0.0505	-1.8502	-0.03229
0.0507	-1.7068	-0.02979
0.0508	-1.5157	-0.02645
0.0503	-1.452	-0.02534
0.0509	-1.5084	-0.02633
0.0517	-1.4015	-0.02446
0.0508	-1.3626	-0.02378
0.0509	-1.8792	-0.0328
0.0465	-2.3345	-0.04074
0.0345	-1.3758	-0.02401
0.0287	4.2414	0.074026
0.0315	5.662	0.098821
0.0395	4.0769	0.071155
0.0451	2.8392	0.049553
0.0492	1.8026	0.031461
0.0513	1.2043	0.021019
0.0518	0.6752	0.011784
0.0524	0.3885	0.006781
0.0522	0.1453	0.002536
0.0525	-0.1021	-0.00178
0.0523	-0.1655	-0.00289
0.0525	-0.3095	-0.0054
0.0529	-0.9582	-0.01672
0.0529	-1.0227	-0.01785
0.0529	-0.9888	-0.01726
0.053	-1.2724	-0.02221
0.0532	-1.4291	-0.02494
0.0536	-1.5657	-0.02733

0.0534	-1.9974	-0.03486
0.0536	-2.0296	-0.03542
0.0535	-2.06	-0.03595
0.0537	-2.2595	-0.03944
0.0535	-2.6855	-0.04687
0.0537	-2.852	-0.04978
0.0538	-2.9432	-0.05137
0.0536	-2.9916	-0.05221
0.0534	-3.2228	-0.05625
0.0534	-3.2835	-0.05731
0.0536	-3.5414	-0.06181
0.0537	-3.8554	-0.06729
0.0535	-3.9908	-0.06965
0.0532	-4.1112	-0.07175
0.0532	-4.1674	-0.07273
0.0532	-4.4665	-0.07796
0.0535	-4.6484	-0.08113
0.0533	-4.7367	-0.08267
0.053	-4.8608	-0.08484
0.0531	-4.8828	-0.08522
0.0534	-5.2431	-0.09151
0.0529	-4.917	-0.08582
0.0528	-5.4444	-0.09502
0.0529	-5.3972	-0.0942
0.0528	-5.597	-0.09769
0.0525	-5.6034	-0.0978
0.0523	-5.5829	-0.09744
0.0518	-5.7563	-0.10047
0.0519	-5.7683	-0.10068
0.0515	-5.9729	-0.10425
0.0516	-5.9163	-0.10326
0.0516	-5.8818	-0.10266
0.052	-5.9973	-0.10467
0.052	-6.0742	-0.10601
0.0519	-5.8957	-0.1029
0.0516	-5.9448	-0.10376
0.0515	-5.8301	-0.10175
0.0516	-5.7666	-0.10065
0.0517	-5.5534	-0.09693
0.0517	-5.8644	-0.10235
0.0519	-5.5255	-0.09644
0.0518	-5.4255	-0.09469
0.0516	-5.5527	-0.09691
0.0515	-5.3233	-0.09291
0.0515	-5.4067	-0.09436
0.0517	-5.2143	-0.09101
0.0514	-5.1022	-0.08905
0.0516	-4.9875	-0.08705
0.0516	-4.948	-0.08636

Upstream

X	PSI(deg)	BETA	BETA (rad)
0.0625	-0.0513	36.9487	0.6448765
0.0618	-0.0055	36.9945	0.6456758
0.0615	-0.0214	36.9786	0.6453983
0.0617	0.0907	37.0907	0.6473548
0.0612	0.0325	37.0325	0.6463391
0.0611	-0.0893	36.9107	0.6442132
0.0611	0.0352	37.0352	0.6463862
0.061	0.0815	37.0815	0.6471943
0.0611	0.0427	37.0427	0.6465171
0.0615	-0.0236	36.9764	0.6453599
0.0611	0.0752	37.0752	0.6470843
0.0622	-0.0122	36.9878	0.6455589
0.0615	-0.0785	36.9215	0.6444017
0.0614	-0.0302	36.9698	0.6452447
0.0617	0.0111	37.0111	0.6459656
0.0624	0.1143	37.1143	0.6477667
0.062	0.1779	37.1779	0.6488768
0.0622	0.1058	37.1058	0.6476184
0.0618	0.0109	37.0109	0.6459621
0.0616	0.0563	37.0563	0.6467544
0.0611	-0.1577	36.8423	0.6430194
0.0615	-0.2124	36.7876	0.6420647
0.0618	-0.1683	36.8317	0.6428344
0.0622	-0.1251	36.8749	0.6435884
0.062	-0.2219	36.7781	0.6418989
0.0623	-0.0259	36.9741	0.6453198
0.0618	-0.2134	36.7866	0.6420473
0.0622	-0.1196	36.8804	0.6436844
0.062	-0.052	36.948	0.6448643
0.0626	-0.2947	36.7053	0.6406283
0.0624	-0.0462	36.9538	0.6449655
0.0623	-0.1568	36.8432	0.6430351
0.0624	-0.1043	36.8957	0.6439514
0.062	-0.1048	36.8952	0.6439427
0.0621	-0.1048	36.8952	0.6439427
0.0616	-0.1668	36.8332	0.6428606
0.0619	0.1007	37.1007	0.6475294
0.0616	0.0297	37.0297	0.6462902
0.0614	-0.1284	36.8716	0.6435308
0.0618	-0.0667	36.9333	0.6446077
0.0617	-0.1982	36.8018	0.6423126
0.0617	-0.1726	36.8274	0.6427594
0.0621	-0.1157	36.8843	0.6437525
0.0622	-0.2805	36.7195	0.6408762
0.0621	-0.1232	36.8768	0.6436216
0.0625	-0.0698	36.9302	0.6445536
0.0625	-0.0608	36.9392	0.6447107
0.0625	-0.0546	36.9454	0.6448189

0.0617	-0.1083	36.8917	0.6438816
0.0624	0.0513	37.0513	0.6466672
0.0616	0.0105	37.0105	0.6459551
0.0613	0.0065	37.0065	0.6458853
0.0614	0.0371	37.0371	0.6464193
0.0613	0.0459	37.0459	0.6465729
0.0616	0.0267	37.0267	0.6462378
0.0615	0.0272	37.0272	0.6462466
0.0615	0.0921	37.0921	0.6473793
0.061	0.1312	37.1312	0.6480617
0.0621	-0.0212	36.9788	0.6454018
0.0618	0.0479	37.0479	0.6466078
0.0618	0.0126	37.0126	0.6459917
0.0623	0.1408	37.1408	0.6482292
0.0621	0.0872	37.0872	0.6472938
0.0618	0.0794	37.0794	0.6471576
0.0616	0.2011	37.2011	0.6492817
0.0615	0.1209	37.1209	0.6478819
0.062	0.1128	37.1128	0.6477406
0.0616	0.2458	37.2458	0.6500618
0.0614	0.2668	37.2668	0.6504284
0.0616	0.1868	37.1868	0.6490321
0.0612	0.3076	37.3076	0.6511405
0.0609	0.4159	37.4159	0.6530306
0.0612	0.226	37.226	0.6497163
0.0611	0.1811	37.1811	0.6489326
0.061	0.3473	37.3473	0.6518334
0.0608	0.2631	37.2631	0.6503638
0.0614	0.2276	37.2276	0.6497442
0.0617	0.1706	37.1706	0.6487494
0.0613	0.4243	37.4243	0.6531773
0.0619	0.2728	37.2728	0.6505331
0.0618	0.2004	37.2004	0.6492695
0.0618	0.1798	37.1798	0.6489099
0.0621	0.1903	37.1903	0.6490932
0.0618	0.3041	37.3041	0.6510794
0.0614	0.2812	37.2812	0.6506797
0.0618	0.1622	37.1622	0.6486027
0.0616	0.2707	37.2707	0.6504964
0.062	0.2484	37.2484	0.6501072
0.0617	0.2321	37.2321	0.6498227
0.0619	0.1637	37.1637	0.6486289
0.0623	0.1432	37.1432	0.6482711
0.0619	0.2374	37.2374	0.6499152
0.0624	0.0979	37.0979	0.6474805
0.0623	0.2887	37.2887	0.6508106
0.0629	0.1838	37.1838	0.6489797
0.0626	0.1952	37.1952	0.6491787
0.0624	0.2041	37.2041	0.649334

Table 8. Re = 393,000 S9.M output

Downstream

X	PSI(deg)	PSI(rad)
0.0718	-4.4579	-0.07781
0.0712	-4.55	-0.07941
0.0711	-4.4595	-0.07783
0.0716	-4.2766	-0.07464
0.0715	-4.3548	-0.07601
0.0711	-4.2214	-0.07368
0.0712	-4.2149	-0.07356
0.0722	-4.0214	-0.07019
0.0709	-3.9818	-0.0695
0.0717	-3.9274	-0.06855
0.0714	-3.8613	-0.06739
0.071	-3.7782	-0.06594
0.0713	-3.6545	-0.06378
0.0713	-3.596	-0.06276
0.0712	-3.4498	-0.06021
0.0712	-3.3656	-0.05874
0.0712	-3.2921	-0.05746
0.0708	-3.0981	-0.05407
0.0715	-3.044	-0.05313
0.0711	-2.9163	-0.0509
0.0718	-2.8707	-0.0501
0.0718	-2.8106	-0.04905
0.072	-2.8197	-0.04921
0.0714	-2.6757	-0.0467
0.0722	-2.6617	-0.04646
0.0725	-2.7317	-0.04768
0.0716	-2.9367	-0.05126
0.0708	-3.528	-0.06158
0.0616	-4.9012	-0.08554
0.0411	-7.2179	-0.12598
0.0324	1.6124	0.028142
0.0399	4.5636	0.07965
0.0559	2.234	0.038991
0.0688	0.6612	0.01154
0.0725	0.0608	0.001061
0.0725	-0.3705	-0.00647
0.0726	-0.5941	-0.01037
0.0732	-0.8487	-0.01481
0.074	-0.9978	-0.01741
0.074	-1.1776	-0.02055
0.0736	-1.3485	-0.02354
0.0742	-1.4561	-0.02541
0.0742	-1.5871	-0.0277
0.0742	-1.7149	-0.02993
0.0749	-1.8021	-0.03145
0.0746	-1.9957	-0.03483
0.0743	-2.137	-0.0373

0.0747	-2.2483	-0.03924
0.0746	-2.2958	-0.04007
0.075	-2.403	-0.04194
0.075	-2.5509	-0.04452
0.0752	-2.6326	-0.04595
0.075	-2.7332	-0.0477
0.0748	-2.8219	-0.04925
0.0748	-2.8879	-0.0504
0.0749	-3.0606	-0.05342
0.0749	-3.0766	-0.0537
0.075	-3.1743	-0.0554
0.0748	-3.304	-0.05767
0.0746	-3.3867	-0.05911
0.0741	-3.5069	-0.06121
0.0745	-3.5026	-0.06113
0.0743	-3.643	-0.06358
0.0742	-3.7392	-0.06526
0.0744	-3.7309	-0.06512
0.0743	-3.8304	-0.06685
0.0742	-4.0468	-0.07063
0.074	-3.9866	-0.06958
0.0739	-4.0022	-0.06985
0.0739	-4.1797	-0.07295
0.0736	-4.311	-0.07524
0.0739	-4.222	-0.07369
0.0738	-4.1995	-0.0733
0.0734	-4.4131	-0.07702
0.0731	-4.3456	-0.07585
0.073	-4.4342	-0.07739
0.0726	-4.428	-0.07728
0.0726	-4.4556	-0.07776
0.0724	-4.4557	-0.07777
0.0721	-4.4104	-0.07698
0.072	-4.4963	-0.07848
0.0722	-4.477	-0.07814
0.0721	-4.4998	-0.07854
0.072	-4.4918	-0.0784
0.072	-4.498	-0.0785
0.0723	-4.4397	-0.07749
0.0721	-4.3949	-0.07671
0.072	-4.3869	-0.07657
0.072	-4.3681	-0.07624
0.0719	-4.3661	-0.0762
0.072	-4.3435	-0.07581
0.072	-4.2229	-0.0737
0.0719	-4.1764	-0.07289
0.0722	-4.1424	-0.0723
0.0717	-4.1697	-0.07277
0.0722	-4.0372	-0.07046

Upstream

X	PSI(deg)	BETA	BETA (rad)
0.0845	-0.2652	36.7348	0.6411432
0.0844	-0.2228	36.7772	0.6418832
0.0845	-0.2343	36.7657	0.6416825
0.0837	-0.3065	36.6935	0.6404224
0.0841	-0.2324	36.7676	0.6417157
0.0839	-0.2745	36.7255	0.6409809
0.0839	-0.2853	36.7147	0.6407924
0.0845	-0.1806	36.8194	0.6426198
0.0843	-0.2541	36.7459	0.6413369
0.0846	-0.1478	36.8522	0.6431922
0.0848	-0.1404	36.8596	0.6433214
0.085	-0.1963	36.8037	0.6423457
0.0844	-0.2383	36.7617	0.6416127
0.0843	-0.2394	36.7606	0.6415935
0.0848	-0.2159	36.7841	0.6420037
0.0847	-0.1575	36.8425	0.6430229
0.0843	-0.2341	36.7659	0.641686
0.0841	-0.3688	36.6312	0.639335
0.0843	-0.2874	36.7126	0.6407557
0.0841	-0.4076	36.5924	0.6386579
0.0845	-0.3258	36.6742	0.6400855
0.0846	-0.3118	36.6882	0.6403299
0.0847	-0.3699	36.6301	0.6393159
0.085	-0.2387	36.7613	0.6416057
0.0845	-0.2575	36.7425	0.6412776
0.0854	-0.3544	36.6456	0.6395864
0.0854	-0.4401	36.5599	0.6380906
0.0846	-0.2877	36.7123	0.6407505
0.0849	-0.3722	36.6278	0.6392757
0.0855	-0.3237	36.6763	0.6401222
0.085	-0.2888	36.7112	0.6407313
0.085	-0.3451	36.6549	0.6397487
0.0851	-0.3068	36.6932	0.6404172
0.0853	-0.2964	36.7036	0.6405987
0.0853	-0.29	36.71	0.6407104
0.0848	-0.3277	36.6723	0.6400524
0.0844	-0.3405	36.6595	0.639829
0.0848	-0.3364	36.6636	0.6399005
0.0842	-0.3488	36.6512	0.6396841
0.0849	-0.3024	36.6976	0.6404939
0.0846	-0.3244	36.6756	0.64011
0.085	-0.2122	36.7878	0.6420682
0.0853	-0.2685	36.7315	0.6410856
0.0857	-0.2376	36.7624	0.6416249
0.0855	-0.2473	36.7527	0.6414556
0.0851	-0.2154	36.7846	0.6420124
0.0851	-0.1908	36.8092	0.6424417
0.0852	-0.2119	36.7881	0.6420735

0.0851	-0.1995	36.8005	0.6422899
0.0852	-0.2251	36.7749	0.6418431
0.0846	-0.1512	36.8488	0.6431329
0.0844	-0.255	36.745	0.6413212
0.0846	-0.2258	36.7742	0.6418309
0.0845	-0.2097	36.7903	0.6421119
0.0842	-0.2529	36.7471	0.6413579
0.0847	-0.1447	36.8553	0.6432463
0.0844	-0.2258	36.7742	0.6418309
0.0849	-0.2315	36.7685	0.6417314
0.0846	-0.2035	36.7965	0.6422201
0.085	-0.2339	36.7661	0.6416895
0.085	-0.2164	36.7836	0.6419949
0.0847	-0.1809	36.8191	0.6426145
0.0852	-0.1447	36.8553	0.6432463
0.0851	-0.1231	36.8769	0.6436233
0.0852	-0.1456	36.8544	0.6432306
0.0847	-0.1716	36.8284	0.6427768
0.0849	-0.1301	36.8699	0.6435011
0.0844	-0.1275	36.8725	0.6435465
0.0845	-0.1504	36.8496	0.6431468
0.0841	-0.1122	36.8878	0.6438136
0.0846	-0.1458	36.8542	0.6432271
0.0842	-0.167	36.833	0.6428571
0.0838	-0.1417	36.8583	0.6432987
0.0841	-0.1487	36.8513	0.6431765
0.0841	-0.107	36.893	0.6439043
0.0846	-0.1225	36.8775	0.6436338
0.0844	-0.1395	36.8605	0.6433371
0.0847	-0.113	36.887	0.6437996
0.0849	-0.1337	36.8663	0.6434383
0.085	-0.0951	36.9049	0.644112
0.0854	-0.1637	36.8363	0.6429147
0.085	-0.1065	36.8935	0.643913
0.0853	-0.1271	36.8729	0.6435535
0.0852	-0.1313	36.8687	0.6434802
0.0854	-0.0767	36.9233	0.6444332
0.0848	-0.0914	36.9086	0.6441766
0.0851	-0.1503	36.8497	0.6431486
0.0847	-0.1063	36.8937	0.6439165
0.0848	-0.1416	36.8584	0.6433004
0.0853	-0.0965	36.9035	0.6440876
0.086	-0.1107	36.8893	0.6438397
0.0856	-0.0877	36.9123	0.6442412
0.0862	-0.1314	36.8686	0.6434785
0.086	-0.0303	36.9697	0.645243
0.0865	-0.0714	36.9286	0.6445257
0.086	-0.0606	36.9394	0.6447142
0.0859	-0.0559	36.9441	0.6447962

Table 9. Re = 537,000 S9.M output

Downstream

X	PSI(deg)	PSI(rad)
0.0845	-3.6827	-0.06428
0.0849	-3.655	-0.06379
0.0846	-3.5636	-0.0622
0.0849	-3.5373	-0.06174
0.085	-3.4992	-0.06107
0.0847	-3.374	-0.05889
0.0848	-3.2867	-0.05736
0.0853	-3.2385	-0.05652
0.0853	-3.2333	-0.05643
0.0851	-3.1021	-0.05414
0.0846	-3.0953	-0.05402
0.0853	-2.9446	-0.05139
0.0846	-2.9466	-0.05143
0.0845	-2.8475	-0.0497
0.0848	-2.7925	-0.04874
0.0847	-2.747	-0.04794
0.084	-2.6668	-0.04654
0.085	-2.573	-0.04491
0.0845	-2.5502	-0.04451
0.0843	-2.5751	-0.04494
0.0848	-2.3937	-0.04178
0.0854	-2.3367	-0.04078
0.0855	-2.3197	-0.04049
0.0853	-2.3045	-0.04022
0.0859	-2.2325	-0.03896
0.0862	-2.2332	-0.03898
0.0854	-2.3501	-0.04102
0.0862	-2.7483	-0.04797
0.0823	-3.6317	-0.06339
0.067	-5.3134	-0.09274
0.0402	-11.2213	-0.19585
0.0334	2.1976	0.038355
0.0443	5.2303	0.091286
0.0657	1.7027	0.029718
0.0833	0.5415	0.009451
0.0869	0.1955	0.003412
0.0869	-0.1638	-0.00286
0.0869	-0.3501	-0.00611
0.0881	-0.4495	-0.00785
0.0874	-0.6306	-0.01101
0.0878	-0.7287	-0.01272
0.088	-0.8049	-0.01405
0.0886	-0.8684	-0.01516
0.0885	-1.0057	-0.01755
0.0884	-1.1258	-0.01965
0.0885	-1.1945	-0.02085
0.0884	-1.327	-0.02316

0.0891	-1.3639	-0.0238
0.0885	-1.4687	-0.02563
0.0889	-1.569	-0.02738
0.0893	-1.6149	-0.02819
0.0894	-1.6972	-0.02962
0.0894	-1.7953	-0.03133
0.0893	-1.8823	-0.03285
0.0891	-2.0066	-0.03502
0.0893	-2.0268	-0.03537
0.0887	-2.1413	-0.03737
0.0888	-2.2536	-0.03933
0.0885	-2.3465	-0.04095
0.0887	-2.4165	-0.04218
0.0886	-2.551	-0.04452
0.0888	-2.6176	-0.04569
0.0884	-2.721	-0.04749
0.0877	-2.8227	-0.04927
0.0883	-2.8429	-0.04962
0.0874	-2.958	-0.05163
0.0881	-2.996	-0.05229
0.0881	-3.0222	-0.05275
0.0878	-3.1563	-0.05509
0.0877	-3.2636	-0.05696
0.0879	-3.2889	-0.0574
0.0873	-3.4059	-0.05944
0.0873	-3.4015	-0.05937
0.0871	-3.5467	-0.0619
0.0865	-3.4948	-0.061
0.0869	-3.6036	-0.06289
0.0861	-3.7309	-0.06512
0.0863	-3.7113	-0.06477
0.086	-3.7414	-0.0653
0.0853	-3.7191	-0.06491
0.0859	-3.6895	-0.06439
0.0857	-3.7046	-0.06466
0.0854	-3.7303	-0.06511
0.0853	-3.6719	-0.06409
0.0855	-3.6218	-0.06321
0.085	-3.6459	-0.06363
0.0851	-3.6557	-0.0638
0.0858	-3.5025	-0.06113
0.0852	-3.5427	-0.06183
0.0853	-3.4772	-0.06069
0.0855	-3.4244	-0.05977
0.0854	-3.4064	-0.05945
0.0853	-3.3712	-0.05884
0.0859	-3.3098	-0.05777
0.0855	-3.2817	-0.05728
0.0858	-3.2197	-0.05619

Upstream

X	PSI(deg)	BETA	BETA (rad)
0.0998	0.1433	37.1433	0.6482729
0.1002	0.1881	37.1881	0.6490548
0.0994	0.0662	37.0662	0.6469272
0.0998	0.1493	37.1493	0.6483776
0.0997	0.0833	37.0833	0.6472257
0.0993	0.062	37.062	0.6468539
0.0995	0.1695	37.1695	0.6487302
0.0996	0.069	37.069	0.6469761
0.0999	0.1668	37.1668	0.648683
0.0999	0.1008	37.1008	0.6475311
0.1005	0.0707	37.0707	0.6470058
0.0999	0.0396	37.0396	0.646463
0.1001	0.1427	37.1427	0.6482624
0.1	0.1225	37.1225	0.6479099
0.1001	0.1303	37.1303	0.648046
0.0998	-0.0072	36.9928	0.6456462
0.1	0.1501	37.1501	0.6483916
0.0996	0.0154	37.0154	0.6460406
0.0999	0.1393	37.1393	0.6482031
0.0999	0.1241	37.1241	0.6479378
0.1001	0.0417	37.0417	0.6464996
0.1002	0.1254	37.1254	0.6479605
0.1002	0.0144	37.0144	0.6460232
0.1	0.1378	37.1378	0.6481769
0.1004	0.0274	37.0274	0.64625
0.1007	0.0246	37.0246	0.6462012
0.1002	0.1709	37.1709	0.6487546
0.1009	0.0651	37.0651	0.646908
0.1004	0.1083	37.1083	0.647662
0.1008	0.0983	37.0983	0.6474875
0.1003	0.0236	37.0236	0.6461837
0.1006	0.085	37.085	0.6472554
0.1002	0.0763	37.0763	0.6471035
0.1005	0.1129	37.1129	0.6477423
0.1003	0.0811	37.0811	0.6471873
0.0998	0.0518	37.0518	0.6466759
0.0999	0.0527	37.0527	0.6466916
0.1002	0.1186	37.1186	0.6478418
0.1004	0.1308	37.1308	0.6480547
0.1002	0.0702	37.0702	0.646997
0.1007	0.0892	37.0892	0.6473287
0.1005	0.066	37.066	0.6469237
0.1008	0.1062	37.1062	0.6476254
0.101	0.1231	37.1231	0.6479203
0.1009	0.167	37.167	0.6486865
0.1009	0.1058	37.1058	0.6476184
0.1008	0.1173	37.1173	0.6478191
0.1001	0.1117	37.1117	0.6477214

0.1004	0.1152	37.1152	0.6477824
0.1001	0.1232	37.1232	0.6479221
0.1002	0.2002	37.2002	0.649266
0.0998	0.1099	37.1099	0.6476899
0.0995	0.0799	37.0799	0.6471663
0.0995	0.0645	37.0645	0.6468976
0.1001	0.0981	37.0981	0.647484
0.0996	0.1398	37.1398	0.6482118
0.0996	0.1723	37.1723	0.648779
0.1007	0.1362	37.1362	0.648149
0.1007	0.1526	37.1526	0.6484352
0.1008	0.1528	37.1528	0.6484387
0.1011	0.121	37.121	0.6478837
0.1009	0.1819	37.1819	0.6489466
0.1007	0.1528	37.1528	0.6484387
0.101	0.1626	37.1626	0.6486097
0.1004	0.1709	37.1709	0.6487546
0.1006	0.2151	37.2151	0.649526
0.0997	0.2009	37.2009	0.6492782
0.1	0.1786	37.1786	0.648889
0.1002	0.2035	37.2035	0.6493236
0.0997	0.2763	37.2763	0.6505942
0.0995	0.2011	37.2011	0.6492817
0.0995	0.2127	37.2127	0.6494841
0.0996	0.2353	37.2353	0.6498786
0.0993	0.2429	37.2429	0.6500112
0.0995	0.2419	37.2419	0.6499938
0.0996	0.2767	37.2767	0.6506011
0.1002	0.2301	37.2301	0.6497878
0.1002	0.2072	37.2072	0.6493881
0.1003	0.252	37.252	0.6501701
0.1001	0.2454	37.2454	0.6500549
0.1003	0.2435	37.2435	0.6500217
0.1005	0.1944	37.1944	0.6491647
0.1009	0.201	37.201	0.6492799
0.1006	0.2479	37.2479	0.6500985
0.1005	0.2403	37.2403	0.6499658
0.1	0.2146	37.2146	0.6495173
0.1008	0.1943	37.1943	0.649163
0.1008	0.1663	37.1663	0.6486743
0.1011	0.2097	37.2097	0.6494318
0.1009	0.2291	37.2291	0.6497704
0.1016	0.2182	37.2182	0.6495801
0.1015	0.2579	37.2579	0.650273
0.1016	0.2903	37.2903	0.6508385
0.1015	0.332	37.332	0.6515663
0.1016	0.3821	37.3821	0.6524407
0.1017	0.2759	37.2759	0.6505872
0.1022	0.3454	37.3454	0.6518002

Table 10. Re = 639,000 S9.M output

APPENDIX D: 5-HOLE PROBE PLOTS

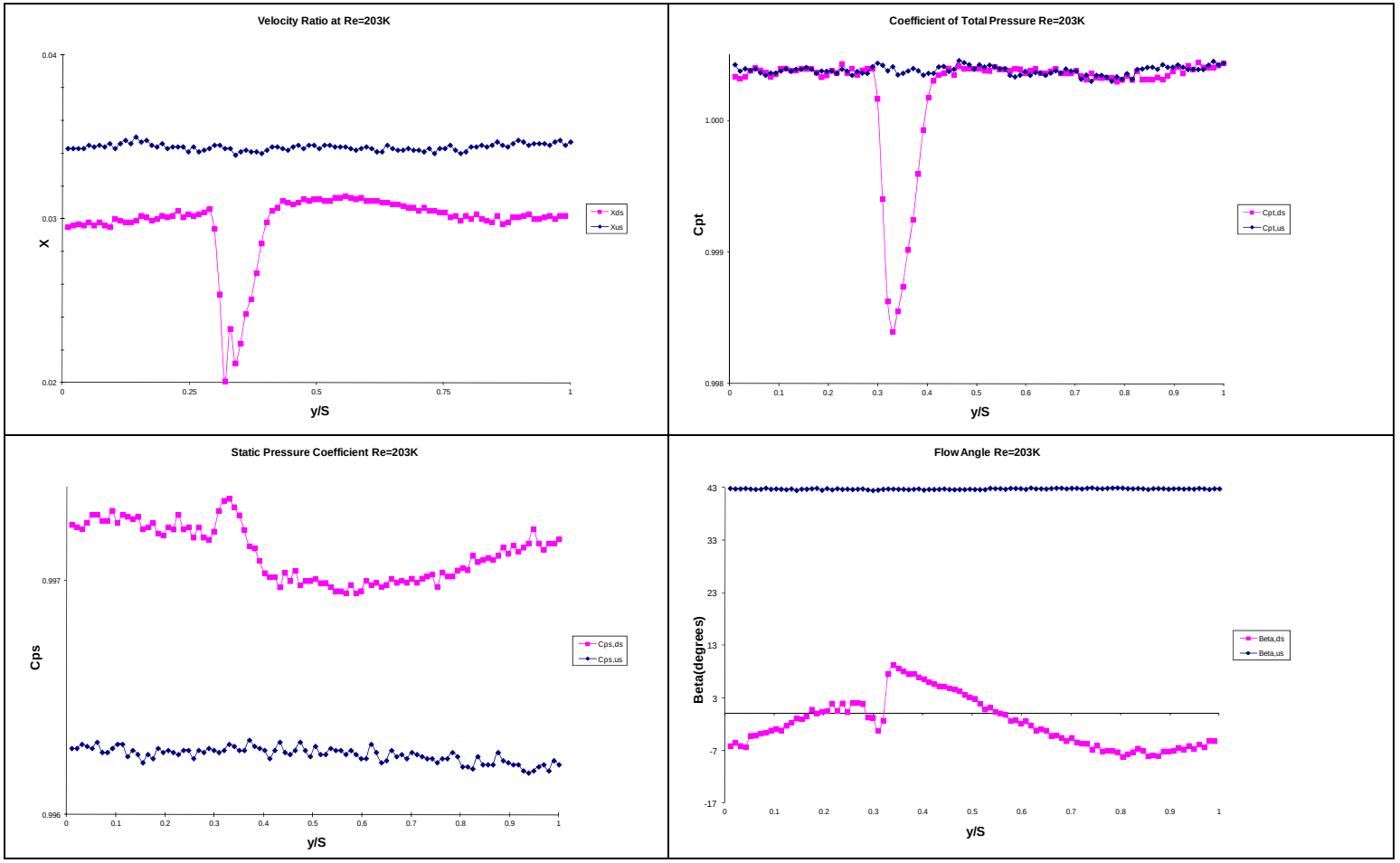

Figure 35. Re = 203,000 5-hole probe plots

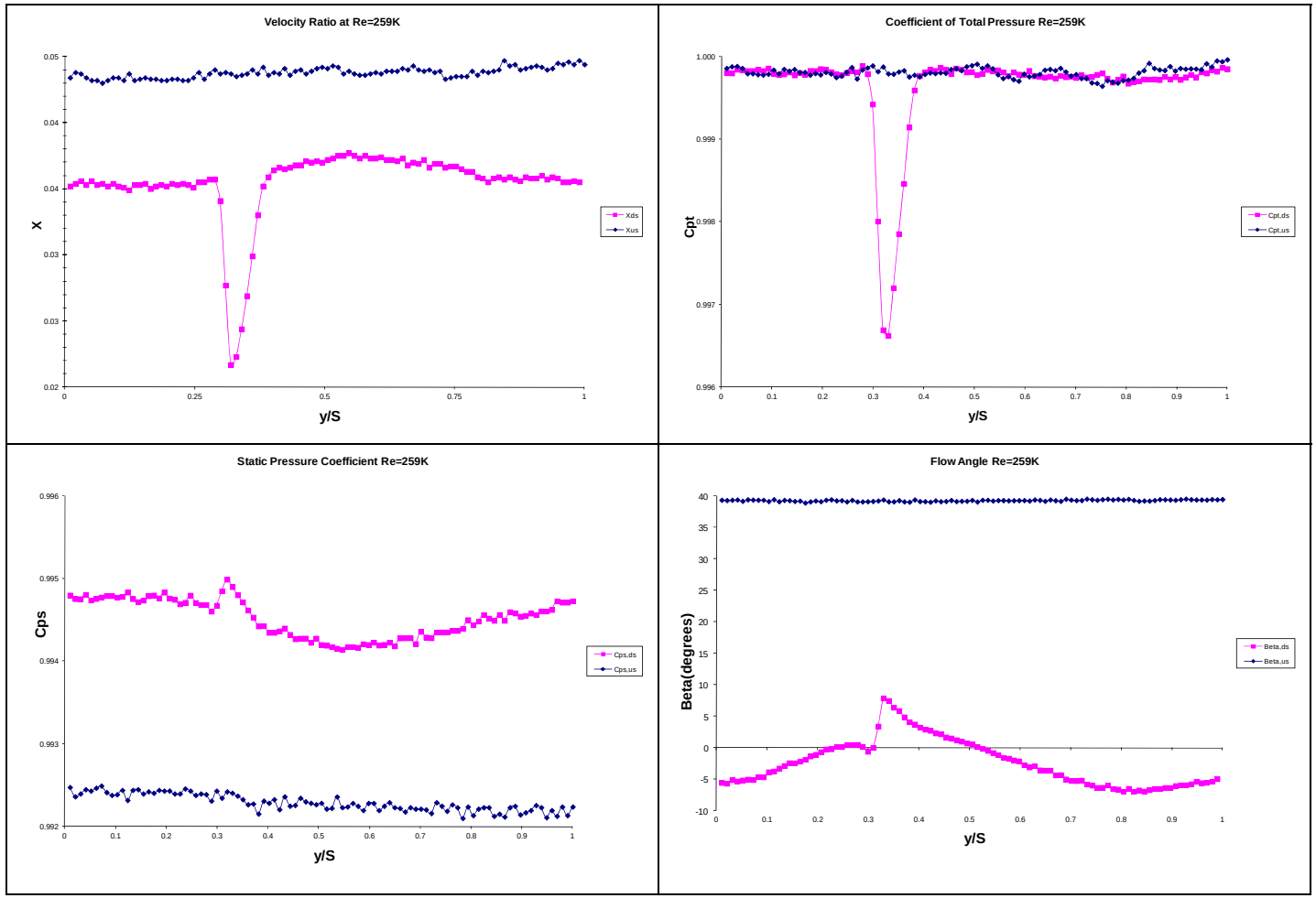

Figure 36. Re = 259,000 5-hole probe plots

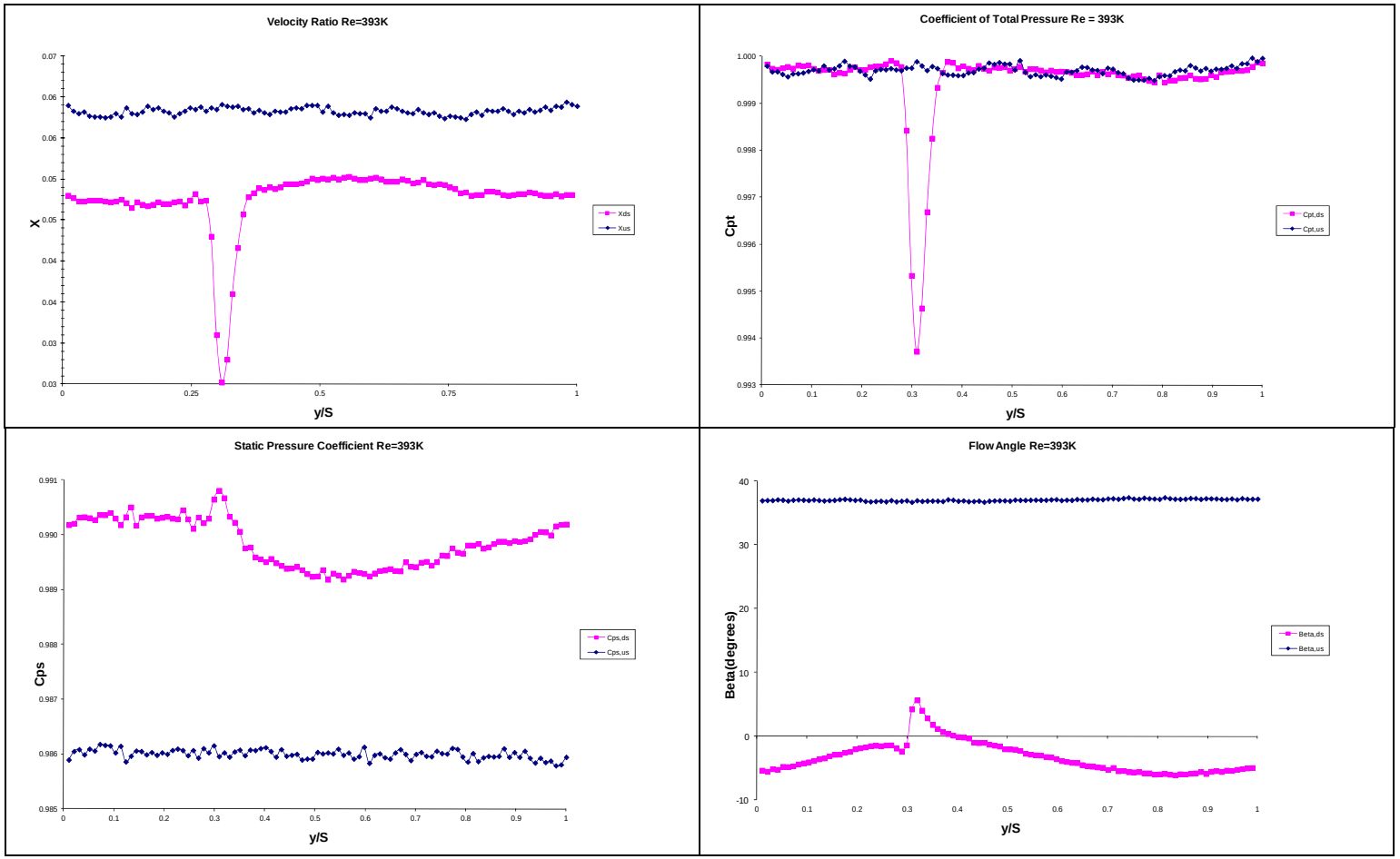

Figure 37. Re = 393,000 5-hole probe plots

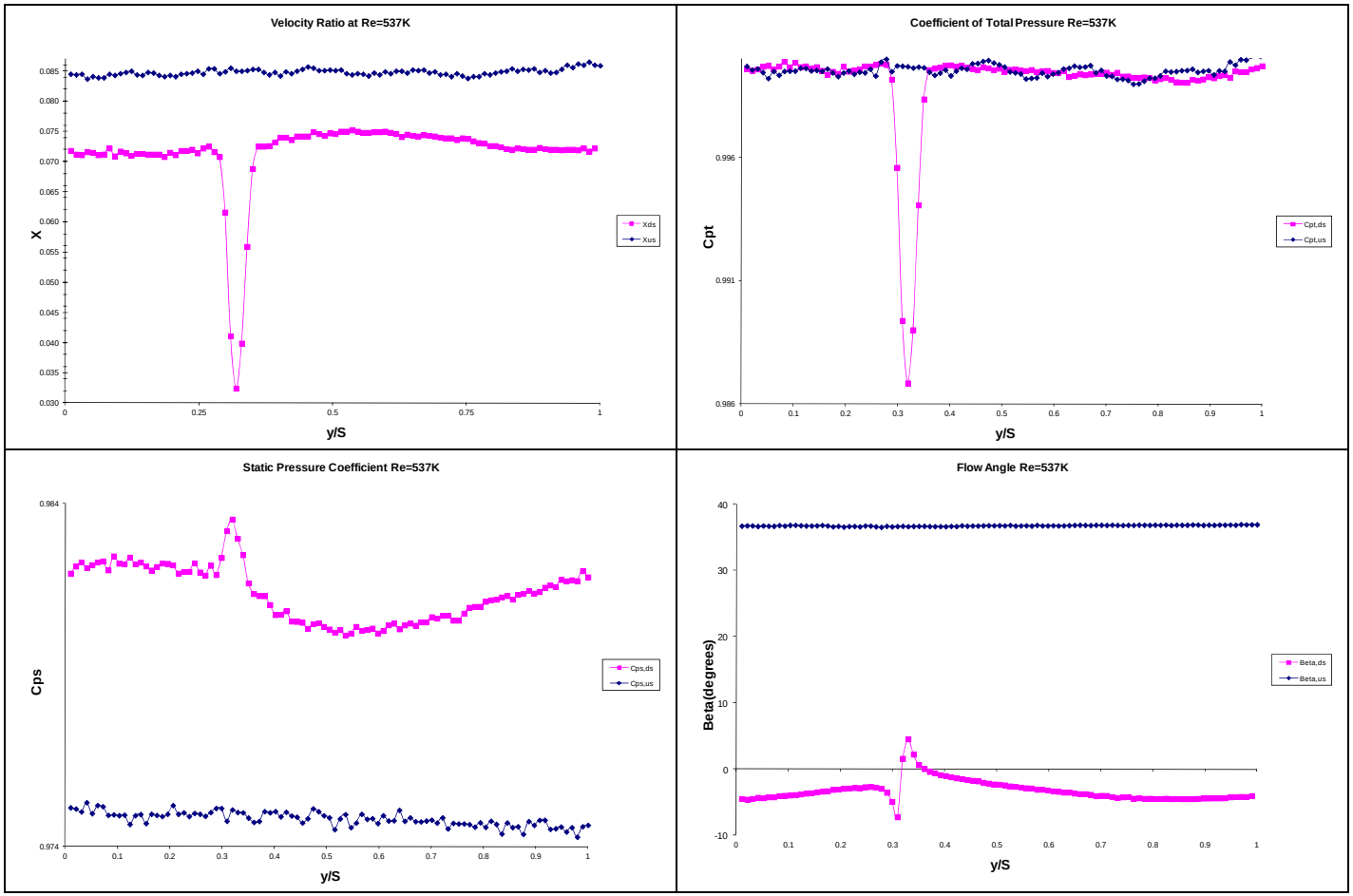

Figure 38. Re = 537,000 5-hole probe plots

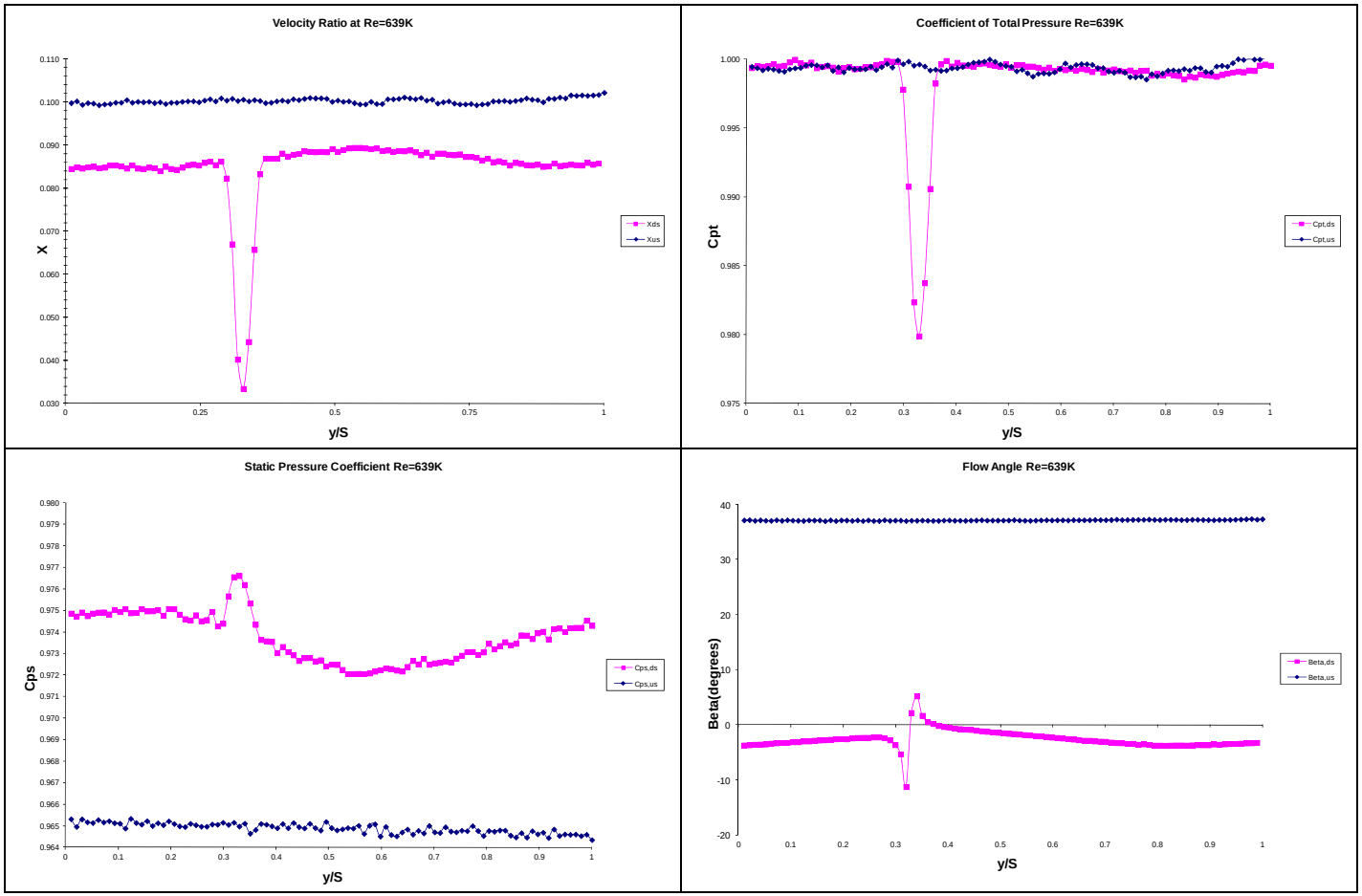

Figure 39. Re = 639,000 5-hole probe plots

THIS PAGE INTENTIONALLY LEFT BLANK

APPENDIX E: LASER ALIGNMENT TOOL AND COORDINATES

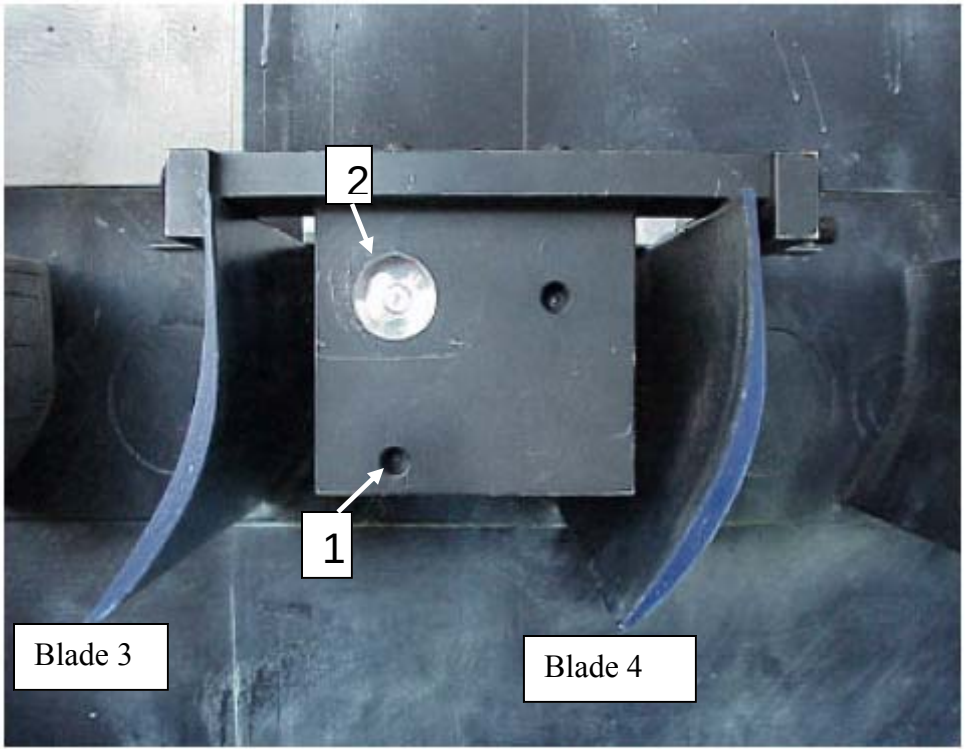

Figure 40. Laser alignment tool

Hole	x (mm)	y(mm)
1	42.95	87.653
2	93.75	87.653
3	93.75	138.453

Table 11. Hole coordinates relative to blade 3 leading edge

THIS PAGE INTENTIONALLY LEFT BLANK

APPENDIX F: LDV SURVEY TABLES

y(mm)	x(mm)	d/c	u/Vref	v/Vref	w/Vref	Tu	Tv	Re stress	Cuv
39.721	53.661	0.422	1.617	2.184	0.017	2.619	10.892	0.215	0.125
39.982	53.595	0.422	1.627	2.182	0.017	2.141	3.622	0.109	0.232
40.242	53.530	0.421	1.638	2.179	0.017	1.648	2.445	0.027	0.109
40.503	53.464	0.421	1.649	2.176	0.017	1.166	2.491	0.026	0.148
40.764	53.398	0.420	1.659	2.174	0.017	2.097	2.318	0.037	0.127
41.024	53.333	0.419	1.670	2.171	0.017	1.185	2.343	0.029	0.175
41.285	53.267	0.419	1.681	2.168	0.017	1.607	2.418	0.011	0.047
41.546	53.201	0.418	1.691	2.166	0.017	1.724	2.172	0.016	0.070
41.807	53.135	0.418	1.702	2.163	0.017	2.206	2.446	0.000	0.000
42.067	53.070	0.417	1.712	2.160	0.017	2.314	2.161	0.017	0.056
42.328	53.004	0.417	1.723	2.158	0.017	2.255	2.502	0.027	0.078
42.589	52.938	0.416	1.734	2.155	0.017	3.350	2.267	0.033	0.073
42.849	52.873	0.416	1.744	2.152	0.017	3.444	2.389	-0.023	-0.046
43.110	52.807	0.415	1.755	2.150	0.017	1.325	2.152	0.009	0.054
43.371	52.741	0.415	1.765	2.147	0.017	1.424	2.059	0.022	0.124

Figure 41. Station 6.75 boundary layer survey

X (mm)	Z (mm)	d/c	u/Vref	v/Vref	w/Vref	Tu	Tv	Re stress	Cuv
42.957	60.465	0.018	1.777	2.501	0.001	1.094	2.846	0.004	0.023
42.857	60.479	0.017	1.773	2.502	0.001	1.044	2.242	0.023	0.168
42.759	60.494	0.017	1.769	2.503	0.001	1.093	2.315	0.015	0.100
42.659	60.509	0.016	1.765	2.503	0.001	1.008	2.457	0.019	0.132
42.560	60.524	0.015	1.761	2.504	0.001	0.948	2.556	0.016	0.115
42.462	60.539	0.014	1.757	2.504	0.001	1.001	2.555	0.014	0.092
42.362	60.554	0.013	1.752	2.505	0.001	0.904	2.883	0.020	0.130
42.264	60.570	0.013	1.748	2.506	0.001	0.921	2.492	0.019	0.143
42.164	60.585	0.012	1.744	2.506	0.000	0.817	2.854	0.014	0.103
42.066	60.600	0.011	1.740	2.507	0.000	0.813	3.712	0.040	0.224
41.966	60.615	0.010	1.736	2.508	0.000	0.930	4.638	0.117	0.464
41.868	60.630	0.009	1.732	2.508	0.000	1.163	5.396	0.236	0.644
41.768	60.645	0.009	1.728	2.509	0.000	1.430	6.697	0.401	0.716
41.670	60.659	0.008	1.724	2.509	0.000	1.630	7.270	0.533	0.770
41.570	60.674	0.007	1.720	2.510	0.000	1.769	8.967	0.589	0.635
41.472	60.689	0.006	1.716	2.511	0.000	2.574	7.061	0.598	0.563
41.372	60.704	0.006	1.711	2.511	0.000	5.194	8.732	0.946	0.357
41.274	60.719	0.005	1.707	2.512	0.000	5.772	4.977	0.224	0.133
41.174	60.734	0.004	1.703	2.512	0.000	3.391	2.439	0.063	0.130

Figure 42. Station 7.0 boundary layer survey

X	Z	d/c	u/Vref	v/Vref	w/Vref	Tu	Tv	Re Stress	Cuv
42.399	68.560	0.002	0.010	-0.036	-0.037	9.344	13.665	0.669	0.085
42.600	68.549	0.003	0.004	-0.072	-0.072	8.267	14.175	-0.668	-0.092
42.799	68.540	0.005	0.000	-0.075	-0.075	9.065	13.309	-0.734	-0.098
43.000	68.530	0.006	0.010	-0.056	-0.057	10.982	13.898	-0.999	-0.106
43.200	68.519	0.008	0.023	0.022	0.032	12.458	12.975	-1.781	-0.178
43.399	68.510	0.009	0.036	0.171	0.175	12.529	16.159	-2.632	-0.210
43.600	68.500	0.011	0.047	0.426	0.428	9.962	17.110	-3.651	-0.346
43.799	68.489	0.013	0.069	0.850	0.853	6.514	14.090	-0.749	-0.132
44.000	68.480	0.014	0.116	1.015	1.021	5.280	12.107	-0.705	-0.178
44.200	68.469	0.016	0.161	1.169	1.180	6.147	9.572	-0.791	-0.217
44.399	68.459	0.017	0.178	1.254	1.266	6.408	7.883	-0.470	-0.150
44.600	68.450	0.019	0.181	1.290	1.303	5.338	6.135	-0.072	-0.036
44.799	68.439	0.020	0.182	1.295	1.308	4.871	5.622	-0.081	-0.048
45.000	68.430	0.022	0.185	1.299	1.312	4.203	4.678	0.095	0.078
45.200	68.420	0.024	0.184	1.294	1.307	3.693	4.045	-0.032	-0.035

Figure 43. Station 7.25 boundary layer survey

y(mm)	x(mm)	d/c	u/Vref	v/Vref	w/Vref	Tu	Tv	Re Stress	Cuv
45.994	76.241	0.033	0.124	1.157	1.163	4.468	5.291	-0.177	-0.122
45.795	76.239	0.031	0.131	1.146	1.154	5.265	7.423	-0.204	-0.085
45.594	76.237	0.030	0.140	1.114	1.123	5.746	11.558	-1.016	-0.248
45.395	76.235	0.028	0.157	1.090	1.101	6.735	14.009	-1.565	-0.269
45.195	76.233	0.027	0.155	1.028	1.040	6.822	19.953	-2.656	-0.316
44.994	76.231	0.025	0.182	0.927	0.944	7.187	25.429	-3.175	-0.282
44.795	76.229	0.024	0.184	0.869	0.889	7.383	25.347	-2.961	-0.257
44.594	76.227	0.022	0.182	0.824	0.843	7.422	27.518	-1.734	-0.138
44.395	76.225	0.020	0.181	0.766	0.787	7.748	27.782	-2.104	-0.158
44.195	76.223	0.019	0.185	0.724	0.747	8.067	28.022	-1.727	-0.124
43.994	76.221	0.017	0.172	0.671	0.692	8.052	29.037	-1.082	-0.075
43.795	76.219	0.016	0.168	0.571	0.595	7.842	26.656	-0.682	-0.053
43.594	76.217	0.014	0.157	0.497	0.521	7.710	25.418	0.030	0.002
43.395	76.215	0.013	0.155	0.494	0.518	7.938	23.735	-0.019	-0.002
43.195	76.213	0.011	0.146	0.437	0.461	8.260	22.121	0.669	0.059
42.994	76.211	0.009	0.143	0.382	0.408	8.579	21.886	-0.025	-0.002
42.795	76.209	0.008	0.137	0.312	0.340	8.833	20.287	0.596	0.054
42.594	76.207	0.006	0.127	0.274	0.303	9.018	19.319	0.910	0.085
42.395	76.205	0.005	0.115	0.223	0.251	8.191	16.226	0.325	0.040
42.195	76.203	0.003	0.099	0.195	0.219	7.575	15.980	0.820	0.110
41.994	76.201	0.002	0.040	0.207	0.211	4.923	23.283	0.839	0.119
41.795	76.199	0.000	0.120	1.107	1.113	2.616	3.862	0.272	0.436

Figure 44. Station 7.5 boundary layer survey

X(mm)	Z(mm)	d/c	u/Vref	v/Vref	w/Vref	Tu	Tv	Re Stress	Cuv
45.954	83.968	0.035	0.026	1.037	1.037	11.737	12.535	-2.082	-0.227
45.753	83.962	0.033	0.010	1.031	1.031	12.789	13.442	-2.263	-0.211
45.554	83.956	0.031	0.004	0.997	0.997	12.975	16.705	-2.684	-0.199
45.353	83.950	0.030	0.019	0.954	0.954	13.888	19.688	-4.859	-0.285
45.154	83.944	0.028	0.000	0.935	0.935	15.259	21.463	-3.985	-0.195
44.954	83.938	0.027	0.008	0.905	0.905	17.013	21.635	-4.606	-0.201
44.753	83.932	0.025	-0.002	0.850	0.850	17.678	23.392	-4.753	-0.184
44.554	83.926	0.024	-0.010	0.790	0.790	17.669	24.557	-6.629	-0.245
44.353	83.920	0.022	-0.021	0.742	0.742	18.762	25.053	-4.842	-0.165
44.154	83.914	0.020	-0.014	0.682	0.682	19.619	25.887	-4.430	-0.140
43.954	83.908	0.019	-0.024	0.635	0.635	19.361	24.812	-5.546	-0.185
43.753	83.902	0.017	-0.025	0.585	0.585	19.418	23.299	-5.800	-0.206
43.554	83.896	0.016	-0.029	0.550	0.551	19.869	23.660	-4.015	-0.137
43.353	83.890	0.014	-0.028	0.512	0.512	18.932	22.188	-4.507	-0.172
43.154	83.884	0.013	-0.042	0.502	0.504	19.020	22.424	-5.859	-0.220
42.954	83.878	0.011	-0.039	0.465	0.466	18.462	21.773	-4.509	-0.180
42.753	83.871	0.009	-0.032	0.438	0.439	17.990	20.457	-2.798	-0.122
42.554	83.865	0.008	-0.040	0.420	0.422	17.447	19.746	-4.077	-0.190
42.353	83.859	0.006	-0.034	0.374	0.376	15.134	20.222	-2.950	-0.155
42.154	83.853	0.005	-0.023	0.319	0.320	13.412	17.143	-1.491	-0.104
41.954	83.847	0.003	-0.016	0.312	0.313	11.741	22.703	-0.144	-0.009

Figure 45. Station 7.75 boundary layer survey

X(mm)	Z(mm)	d/c	u/Vref	v/Vref	w/Vref	Tu	Tv	Re Stress	Cuv
52.155	92.141	0.086	0.043	1.023	1.023	1.781	2.351	0.027	0.105
51.658	92.109	0.082	0.040	1.026	1.027	1.859	1.972	0.013	0.057
51.159	92.078	0.078	0.037	1.028	1.028	2.103	2.438	0.026	0.081
50.661	92.046	0.075	0.032	1.030	1.031	2.233	2.332	0.019	0.058
50.164	92.013	0.071	0.031	1.033	1.033	2.584	2.602	0.022	0.053
49.665	91.981	0.067	0.025	1.035	1.035	2.849	3.131	-0.008	-0.015
49.167	91.950	0.063	0.024	1.039	1.039	3.684	3.246	-0.003	-0.004
48.670	91.918	0.059	0.020	1.037	1.037	4.442	4.274	-0.089	-0.076
48.171	91.885	0.055	0.014	1.038	1.038	5.323	5.516	-0.190	-0.104
47.673	91.853	0.051	0.014	1.025	1.025	7.038	8.209	-0.723	-0.202
47.176	91.822	0.047	0.012	1.013	1.013	8.454	10.197	-0.808	-0.151
46.677	91.790	0.043	0.006	0.976	0.977	9.605	13.788	-1.856	-0.226
46.179	91.757	0.039	0.008	0.935	0.935	11.116	17.289	-2.041	-0.171
45.682	91.725	0.035	0.001	0.860	0.860	13.249	20.901	-3.904	-0.227
45.183	91.694	0.031	0.017	0.769	0.769	14.356	20.974	-3.343	-0.179
44.685	91.662	0.027	-0.010	0.713	0.713	14.748	21.131	-3.306	-0.171
44.188	91.629	0.024	-0.017	0.645	0.646	16.038	20.740	-5.246	-0.254
43.689	91.597	0.020	-0.015	0.588	0.589	15.650	19.446	-3.901	-0.207
43.192	91.566	0.016	-0.031	0.560	0.561	15.465	18.580	-2.206	-0.124
42.694	91.534	0.012	-0.029	0.500	0.500	14.209	18.034	-2.530	-0.159
42.195	91.501	0.008	-0.033	0.475	0.476	12.939	17.949	-2.119	-0.147
41.698	91.469	0.004	-0.026	0.409	0.409	10.223	17.484	-1.905	-0.172

Figure 46. Station 8.0 boundary layer survey

X	Z	y/s	u/Vref	v/Vref	w/Vref	Tu	Tv	Re Stress	Cuv
20.000	146.304	0.131	0.767	5.613	0.005	2.086	2.121	0.096	0.318
21.587	146.304	0.142	0.828	5.613	0.005	2.329	3.071	0.098	0.203
23.175	146.304	0.152	0.889	5.613	0.006	2.690	2.971	0.109	0.200
24.762	146.304	0.162	0.950	5.613	0.006	2.590	2.985	0.116	0.222
26.350	146.304	0.173	1.011	5.613	0.007	2.560	2.534	0.087	0.197
27.937	146.304	0.183	1.072	5.613	0.007	2.939	2.673	0.092	0.173
29.524	146.304	0.194	1.133	5.613	0.007	3.137	3.060	0.076	0.116
31.112	146.304	0.204	1.194	5.613	0.008	4.728	4.147	0.239	0.180
32.700	146.304	0.215	1.255	5.613	0.008	6.012	6.055	0.285	0.115
34.287	146.304	0.225	1.315	5.613	0.009	9.826	9.036	1.731	0.287
35.875	146.304	0.235	1.376	5.613	0.009	12.744	14.093	3.329	0.273
37.462	146.304	0.246	1.437	5.613	0.009	15.164	16.982	7.695	0.440
39.049	146.304	0.256	1.498	5.613	0.010	14.090	19.347	2.356	0.127
40.637	146.304	0.267	1.559	5.613	0.010	11.778	17.296	-1.600	-0.116
42.225	146.304	0.277	1.620	5.613	0.011	10.387	18.269	-1.210	-0.094
43.812	146.304	0.287	1.681	5.613	0.011	9.392	17.130	-1.602	-0.147
45.399	146.304	0.298	1.742	5.613	0.011	8.935	16.600	-1.306	-0.130
46.987	146.304	0.308	1.803	5.613	0.012	8.119	15.500	-0.293	-0.034
48.575	146.304	0.319	1.864	5.613	0.012	6.606	12.115	-0.456	-0.084
50.162	146.304	0.329	1.924	5.613	0.013	6.432	10.237	0.254	0.057
51.750	146.304	0.340	1.985	5.613	0.013	5.113	9.040	0.336	0.107
53.337	146.304	0.350	2.046	5.613	0.013	5.159	8.050	0.010	0.003
54.924	146.304	0.360	2.107	5.613	0.014	4.179	6.327	0.373	0.208
56.512	146.304	0.371	2.168	5.613	0.014	4.184	4.983	0.269	0.190
58.100	146.304	0.381	2.229	5.613	0.015	4.264	6.044	0.163	0.093
59.687	146.304	0.392	2.290	5.613	0.015	4.120	5.398	-0.176	-0.116
61.274	146.304	0.402	2.351	5.613	0.015	3.607	3.969	0.010	0.011

Figure 47. Station 13 blade 3 wake survey

X	Z	y/s	u/Vref	v/Vref	w/Vref	Tu	Tv	Re Stress	Cuv
0.000	146.304	0.000	0.127	0.833	0.843	2.320	2.360	0.128	0.350
6.349	146.304	0.042	0.120	0.834	0.843	2.578	2.900	0.200	0.400
12.699	146.304	0.083	0.114	0.837	0.845	2.934	2.863	0.224	0.397
19.050	146.304	0.125	0.109	0.844	0.851	3.185	3.187	0.252	0.371
25.399	146.304	0.167	0.103	0.850	0.856	4.356	4.117	0.446	0.372
31.750	146.304	0.208	0.100	0.847	0.853	8.211	7.767	1.948	0.456
38.100	146.304	0.250	0.129	0.451	0.469	19.587	18.521	10.994	0.453
44.450	146.304	0.292	-0.021	0.411	0.411	16.607	21.768	-4.184	-0.173
50.799	146.304	0.333	-0.022	0.634	0.634	12.249	24.396	-0.237	-0.012
57.149	146.304	0.375	-0.004	0.730	0.730	11.590	21.135	4.518	0.275
63.500	146.304	0.417	0.013	0.750	0.750	11.364	20.691	2.174	0.138
69.849	146.304	0.458	0.051	0.795	0.797	10.910	16.972	1.009	0.081
76.200	146.304	0.500	0.077	0.822	0.825	9.166	15.272	-1.410	-0.150
82.549	146.304	0.542	0.113	0.843	0.851	9.282	11.048	-2.082	-0.303
88.900	146.304	0.583	0.125	0.855	0.864	7.542	7.440	-1.275	-0.339
95.250	146.304	0.625	0.124	0.864	0.873	4.213	4.906	-0.202	-0.146
101.599	146.304	0.667	0.132	0.855	0.865	3.316	3.367	0.040	0.054
107.950	146.304	0.708	0.141	0.844	0.856	3.014	3.278	0.060	0.090
114.299	146.304	0.750	0.140	0.836	0.848	2.614	3.140	0.113	0.206
120.650	146.304	0.792	0.138	0.830	0.842	2.492	2.649	0.108	0.243
127.000	146.304	0.833	0.139	0.826	0.837	2.475	2.753	0.085	0.187
133.349	146.304	0.875	0.135	0.829	0.840	2.228	3.695	0.091	0.166
139.699	146.304	0.917	0.133	0.832	0.843	2.253	3.522	0.099	0.187
146.050	146.304	0.958	0.124	0.823	0.833	2.126	2.763	0.118	0.300
152.400	146.304	1.000	0.119	0.826	0.835	2.231	2.321	0.096	0.278

Figure 48. Station 13 outlet survey

X	Z	y/s	u/Vref	v/Vref	w/Vref	Tu	Tv	Re Stress	Cuv
0.000	-36.576	0.000	0.636	0.762	0.993	1.808	2.669	0.048	0.164
6.349	-36.576	0.042	0.646	0.771	1.006	1.985	2.372	0.034	0.120
12.699	-36.576	0.083	0.653	0.777	1.015	2.037	2.624	0.053	0.164
19.050	-36.576	0.125	0.654	0.784	1.021	3.014	2.155	0.064	0.162
25.399	-36.576	0.167	0.650	0.787	1.021	2.049	2.082	0.049	0.189
31.750	-36.576	0.208	0.645	0.795	1.024	2.100	2.176	0.071	0.255
38.100	-36.576	0.250	0.642	0.800	1.025	2.125	2.722	0.057	0.162
44.450	-36.576	0.292	0.634	0.802	1.023	3.010	2.237	0.046	0.112
50.799	-36.576	0.333	0.624	0.801	1.016	1.992	2.548	0.073	0.237
57.149	-36.576	0.375	0.619	0.805	1.015	2.166	2.418	0.072	0.225
63.500	-36.576	0.417	0.612	0.803	1.009	1.863	2.508	0.049	0.171
69.849	-36.576	0.458	0.604	0.801	1.003	2.502	2.827	0.048	0.112
76.200	-36.576	0.500	0.598	0.799	0.998	1.772	2.363	0.049	0.191
82.549	-36.576	0.542	0.597	0.799	0.997	1.732	2.287	0.038	0.157
88.900	-36.576	0.583	0.595	0.804	1.000	2.090	2.353	0.054	0.179
95.250	-36.576	0.625	0.591	0.800	0.995	1.984	2.558	0.033	0.105
101.599	-36.576	0.667	0.594	0.796	0.993	2.007	2.604	0.048	0.150
107.950	-36.576	0.708	0.592	0.790	0.987	1.895	2.769	0.042	0.131
114.299	-36.576	0.750	0.590	0.780	0.978	1.962	2.279	0.044	0.161
120.650	-36.576	0.792	0.591	0.772	0.972	1.953	2.270	0.043	0.159
127.000	-36.576	0.833	0.598	0.768	0.973	2.033	3.021	0.038	0.103
133.349	-36.576	0.875	0.608	0.772	0.982	2.039	2.817	0.035	0.100
139.699	-36.576	0.917	0.614	0.766	0.981	2.158	2.871	0.059	0.157
146.050	-36.576	0.958	0.622	0.761	0.983	2.197	2.764	0.039	0.106
152.400	-36.576	1.000	0.628	0.763	0.988	2.165	2.178	0.042	0.146

Figure 49. Station 1 inlet survey

THIS PAGE INTENTIONALLY LEFT BLANK

APPENDIX G: 5-HOLE PROBE PRESSURE PORT NUMBERING AND BETA, GAMMA AND DELTA EQUATIONS

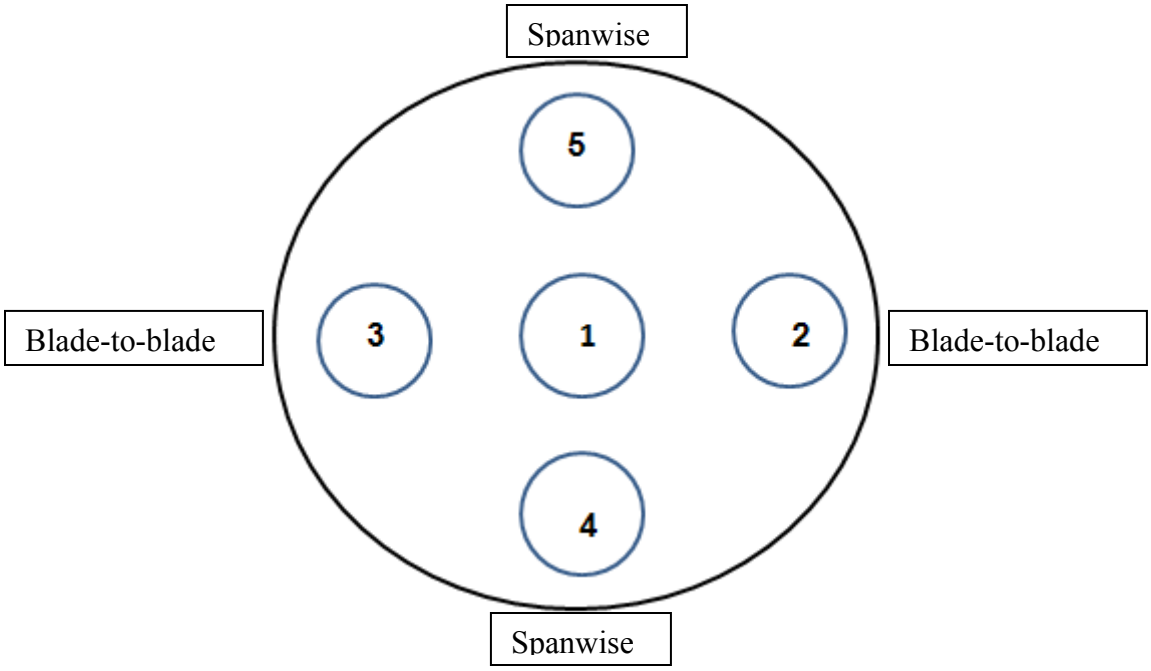

$$P_{avg} = \frac{P_2 + P_3 + P_4 + P_5}{4}$$

$$\beta = \frac{P_1 - P_{avg}}{P_1}$$

$$\gamma = \frac{P_4 - P_5}{P_1 - P_{avg}}$$

$$\delta = \frac{P_2 - P_3}{P_1 - P_{avg}}$$

THIS PAGE INTENTIONALLY LEFT BLANK

LIST OF REFERENCES

[1] G. V. Hobson, D. J. Hansen, D. G. Schnorenberg, and D. V. Grove, "Effect of Reynolds number on separation bubbles on compressor blades in cascade," *Journal of Propulsion and Power,* vol. 17, pp. 154–161, January-February 2001.

[2] J. P. Gostelow, *Cascade Aerodynamics*. New York, Pergamon Press, 1984.

[3] D.J. Hansen, "Investigation of second generation controlled-diffusion compressor Blades in cascade," M.S. thesis, Naval Postgraduate School, Monterey, California, September 1995.

[4] D. G. Schnorenberg, "Investigation of the effect of Reynolds number on laminar separation bubbles on controlled-diffusion compressor blades in cascade," M.S. Thesis, Naval Postgraduate School, Monterey, California, June 1996.

[5] J. L. Nicholls, "Investigation of flow over second generation controlled-diffusion blades in a linear cascade," M.S. Thesis, Naval Postgraduate School, Monterey, California, September 1999.

[6] J. R. Carlson, "Experimental and computational investigation of the endwall flow in a cascade of compressor blades," M.S. Thesis, Naval Postgraduate School, Monterey, California, September 2000.

[7] T. M. Caruso, "Three-component LDV measurements of corner vorticies over second-generation, controlled-diffusion, compressor blades in cascade," M.S. thesis, Naval Postgraduate School, Monterey, California, September 2001.

[8] K. D. Fitzgerald, "Examination of flow around second-generation compressor blades in cascade at stall," M.S. thesis, Naval Postgraduate School, Monterey, California, June 2004.

[9] M. C. Urban, "Loss measurements in the endwall region of a cascade of compressor blades at stall," M.S. thesis, Naval Postgraduate School, Monterey, California, June 2006.

[10] P .J. Brown, "Experimental investigation of vortex shedding in flow over second-generation, controlled-diffusion, compressor blades in cascade," M.S. thesis, Naval Postgraduate School, Monterey, California, March, 2002.

[11] P. L. Choon "Experimental investigation of vortex shedding in high Reynolds number flow over compressor blades in cascade," M.S. thesis, Naval Postgraduate School, Monterey, California, March, 2003.

[12] C. Grubb, L. W. Grubbs, M. D. Neuser, J. Muller, and, J. O'Brien, "Subsonic five-hole probe calibration in non null-yaw mode," AA-3802 Term Project, Naval Postgraduate School, Monterey, California, December 8, 1999.

[13] J. Fitzgerald, T. J. Mueller, "Measurement in a separation bubble on an airfoil using laser velocimetry," *AIAA Journal,* vol. 28, no.4, pp. 584–591, July 1989.

INITIAL DISTRIBUTION LIST

1. Defense Technical Information Center
   Ft. Belvoir, Virginia

2. Dudley Knox Library
   Naval Postgraduate School
   Monterey, California

3. Department Chairman, Code ME
   Department of Mechanical and Aerospace Engineering
   Naval Postgraduate School
   Monterey, California

4. Dr. Garth V. Hobson, Code ME/HG
   Department of Mechanical and Aerospace Engineering
   Naval Postgraduate School
   Monterey, California

5. Dr. Anthony J. Gannon, Code ME/HG
   Department of Mechanical and Aerospace Engineering
   Naval Postgraduate School
   Monterey, California